

# PRG

# Photogrammetrie Fernerkundung Geoinformation

Organ der Deutschen Gesellschaft für Photogrammetrie,  
Fernerkundung und Geoinformation (DGPF) e. V.

Jahrgang 2010, Heft 2

Hauptschriftleiter:  
Prof. Dr.-Ing. Helmut Mayer

Schriftleiter:  
Prof. Dr. rer.nat. Carsten Jürgens, Prof. Dipl.-Ing. Thomas P. Kersten,  
Prof. Dr. rer.nat. Lutz Plümer und Dr.-Ing. Eckhardt Seyfert

**Redaktionsbeirat** (Editorial Board): Clement Atzberger, Andrew Frank,  
Christian Heipke, Joachim Hill, Patrick Hostert, Hans-Gerd Maas, Wolfgang  
Reinhardt, Franz Rottensteiner, Jochen Schiewe



E. Schweizerbart'sche Verlagsbuchhandlung  
(Nägele u. Obermiller) Stuttgart 2010



Deutsche Gesellschaft für Photogrammetrie, Fernerkundung  
und Geoinformation (DGPF) e.V.  
Gegründet 1909

Die *Deutsche Gesellschaft für Photogrammetrie, Fernerkundung und Geoinformation* (DGPF) e.V. unterstützt als Mitglieds- bzw. Trägergesellschaft die folgenden Dachverbände:



International Society  
for Photogrammetry  
and Remote Sensing

**DAGM**

Deutsche Arbeits-  
gemeinschaft für  
Mustererkennung e.V.



Herausgeber:

© 2010 Deutsche Gesellschaft für Photogrammetrie, Fernerkundung und Geoinformation (DGPF) e.V.  
Präsidentin: Prof. Dr. Cornelia Gläßer, Martin-Luther-Universität Halle-Wittenberg, Institut für Geowissenschaften, Von-Seckendorff-Platz 4, D-06120 Halle, Tel.: +49(0)345 55-26020  
Geschäftsstelle: Dr. Klaus-Ulrich Komp, c/o EFTAS Fernerkundung Technologietransfer GmbH, Oststraße 2–18, D-48145 Münster, e-mail: klaus.komp@eftas.com

Published by:

E. Schweizerbart'sche Verlagsbuchhandlung (Nägele u. Obermiller), Johannesstraße 3A,  
D-70176 Stuttgart. Tel.: 0711 351456-0, Fax: 0711 351456-99, e-mail: mail@schweizerbart.de  
Internet: <http://www.schweizerbart.de>

© Gedruckt auf alterungsbeständigem Papier nach ISO 9706-1994

All rights reserved including translation into foreign languages. This journal or parts thereof may not be reproduced in any form without permission from the publishers.

Die Wiedergabe von Gebrauchsnamen, Handelsnamen, Warenbezeichnungen usw. in dieser Zeitschrift berechtigt auch ohne besondere Kennzeichnung nicht zu der Annahme, dass solche Namen im Sinne der Warenzeichen- und Markenschutz-Gesetzgebung als frei zu betrachten wären und daher von jedermann benutzt werden dürften.

Verantwortlich für den Inhalt der Beiträge sind die Autoren.

ISSN 1432-8364

Science Citation Index Expanded (also known as SciSearch®) Journal Citation Reports/Science Edition  
Hauptschriftleiter: Prof. Dr.-Ing. Helmut Mayer, Institut für Angewandte Informatik, Universität der Bundeswehr München, D-85577 Neubiberg, e-mail: Helmut.Mayer@unibw.de  
Schriftleiter: Prof. Dr. rer.nat. Carsten Jürgens, Ruhr-Universität Bochum, Geographisches Institut, Gebäude NA 7/133, D-44780 Bochum, e-mail: carsten.juergens@rub.de, Prof. Dipl.-Ing. Thomas P. Kersten, HafenCity Universität Hamburg, Department Geomatik, Hebebrandstr.1, D-22297 Hamburg, e-mail: thomas.kersten@hcu-hamburg.de, Prof. Dr. rer.nat. Lutz Plümer, Universität Bonn, Institut für Geodäsie und Geoinformation, Meckenheimer Allee 172, D-53115 Bonn, e-mail: Lutz.Pluemer@ikg.uni-bonn.de und Dr.-Ing. Eckhardt Seyfert, Landesvermessung und Geobasisinformation Brandenburg, Heinrich-Mann-Allee 107, D-14473 Potsdam, e-mail: eckhardt.seyfert@geobasis-bb.de

Erscheinungsweise: 6 Hefte pro Jahrgang.

Bezugspreis im Abonnement: € 191,- pro Jahrgang. Mitglieder der DGPF erhalten die Zeitschrift kostenlos. Der Online-Zugang ist im regulären Subskriptionspreis enthalten.

Anzeigenverwaltung: E. Schweizerbart'sche Verlagsbuchhandlung (Nägele u. Obermiller), Johannesstraße 3A, D-70176 Stuttgart, Tel.: 0711 351456-0; Fax: 0711 351456-99.  
e-mail: mail@schweizerbart.de, Internet: <http://www.schweizerbart.de>

Bernhard Harzer Verlag GmbH, Westmarkstraße 59/59a, D-76227 Karlsruhe, Tel.: 0721 944020, Fax: 0721 9440230, e-mail: Info@harzer.de, Internet: [www.harzer.de](http://www.harzer.de)

Printed in Germany by Tutte Druckerei GmbH, D-94121 Salzweg bei Passau

## PFG – Jahrgang 2010, Heft 2

### Inhaltsverzeichnis

---

#### DGPF-Test on Digital Airborne Camera Evaluation

GLÄSSER, C.: Editorial .....	69
CRAMER, M.: The DGPF-Test on Digital Airborne Camera Evaluation – Overview and Test Design. ....	73
JACOBSEN, K., CRAMER, M., LADSTÄDTER, R., RESSL, C. & SPRECKELS, V.: DGPF-Project: Evaluation of Digital Photogrammetric Camera Systems – Geometric Performance. ....	83
HAALA, N., HASTEDT, H., WOLF, K., RESSL, C. & BALTRUSCH, S.: Digital Photogrammetric Camera Evaluation – Generation of Digital Elevation Models .....	99
SPRECKELS, V., SYREK, L. & SCHLIENKAMP, A.: DGPF Project: Evaluation of Digital Photogrammetric Camera Systems – Stereoplotting .....	117
SCHÖNERMARK, M. VON: Status Report on the Evaluation of the Radiometric Properties of Digital Photogrammetric Airborne Cameras .....	131
WASER, L.T., KLONUS, S., EHLERS, M., KÜCHLER, M. & JUNG, A.: Potential of Digital Sensors for Land Cover and Tree Species Classifications – A Case Study in the Framework of the DGPF-Project .....	141

---

#### Berichte und Mitteilungen

Berichte von Veranstaltungen	
ISPRS/COST-Workshop “Quality, Scale and Analysis Aspects of City Models” vom 3.–4. Dezember 2009 in Lund, Schweden .....	157
Neue Mitglieder der DGPF .....	159
Buchbesprechung	
SANDAU, R.: Digital Airborne Camera .....	159
Veranstaltungskalender .....	161
Neuerscheinungen .....	162
Zum Titelbild .....	163
Korporative Mitglieder .....	164
Zusammenfassungen der „Originalbeiträge“ und der Beiträge „Aus Wissenschaft und Technik“ (deutsch und englisch) sind auch verfügbar unter <a href="http://www.dgpf.de/neu/pfg/ausgaben.htm">www.dgpf.de/neu/pfg/ausgaben.htm</a>	





## Editorial: DGPF-Project: Digital Photogrammetric Camera Evaluation

The German Society of Photogrammetry, Remote Sensing and Geoinformation (DGPF) plays an active part in networking science, industry and public institutions and makes this intension evident through its work and annual scientific technical conferences.

In a special way, by this PFG issue we would like to show our philosophy as well as to present the first results of the DGPF-Project: *Digital Photogrammetric Camera Evaluation*.

How did this project come about? How is it organized?

By the rapid development and establishment of digital photogrammetric cameras manifold questions have been posed from users and customers. Flight providers have to make numerous decisions according the suitability of different camera systems for the multiple tasks and commissions.

Application oriented quality parameters are therefore as important as handling routine operations or the specification of data processing. Many clients of photogrammetric services are mainly interested in the advantages of the concrete, application- and project oriented camera system in relation to proven analog camera systems or image products. The expanded usability and applicability of digital image data challenged the different camera systems.

These questions were often posed to the executive committee of DGPF and initiated this unique project. This way the evaluation could be achieved without commercial and industrial lobby.

The project agreement regulates the free data access of all involved institutions and provides the data for the analysis. The participants are obligated to inform the executive committee of DGPF and the leader of the project about

the analysis and to publish the results in PFG and at annual conferences of DGPF.

As a result of a first project meeting at the annual conference 2008 in Oldenburg the organizational and substantive framework and the flight campaigns for 2009 were constituted. The test site of the University Stuttgart at Vaihingen/Enz was found to be an ideal area with its versatile relief and agricultural character containing many signalized and permanent geodetic control marks. The meteorological conditions were unfavourable, that's why the airborne part took longer than expected. This was leading to interpretation limitations for the radiometry working group.

It's the special merit of Dr. Herbert Krauß, Cologne and Dr. Klaus Komp, Münster, that this DGPF-project could be realized as a result of numerous enquiries to the society.

Special thanks are due to Prof. Dieter Fritsch, Stuttgart, and his team, not only for the possibility to use the test area in Vaihingen but also for the complex and time-consuming logistic and data preparation.

Further on a particular thank to Dr. Michael Cramer, Stuttgart, for taking care of the project management including the organisation of project meetings and the finishing of articles for this issue in due time.

Without the involvement of around 100 people from science and technology and in particular the commitment of manufactures and flight providers this project would not have been realizable. Thanks to all of them!

Hopefully all involved persons in this unconventional project will get impetus for their work beyond the precise objectives, whether in research and education or through new contacts.

The first interim results of the project were presented at the annual meeting 2009 on the occasion of the 100<sup>th</sup> anniversary of the society. Manufacturers, users, and scientists at home and abroad showed great interest.

It is the aim of this English special issue of PFG to enable the dissemination of the project results in an international context. After the introducing essay about project design and the involved companies and institutions, results of comparative investigations of geometric pa-

rameters, generation of elevation models and stereo plotting are presented. Supplementing this you will find an introduction to an initial analysis of radiometry and the thematic classification.

We hope you will enjoy reading this issue and are looking forward to many interesting and stimulating publications of the project results.

Prof. CORNELIA GLÄSSER, President of DGPF  
Halle, January 2010



## Editorial: DGPF-Projekt: Evaluierung digitaler photogrammetrischer Luftbildkamarasysteme

Die DGPF versteht sich als Mittler zwischen Wissenschaft, Wirtschaft und öffentlichen Einrichtungen und hat dies zum Credo ihrer Arbeit und ihrer wissenschaftlich-technischen Jahrestagungen erhoben. In einer ganz besonderen Weise möchten wir Ihnen diese Philosophie mit diesem Heft der PFG vorstellen: Die Präsentation der ersten Ergebnisse des DGPF-Projekts „*Evaluierung digitaler photogrammetrischer Luftbildkamarasysteme*“.

Wie kam es zu diesem speziellen DGPF-Projekt? Wie ist es organisiert?

Mit der rasanten Entwicklung und Etablierung digitaler photogrammetrischer Luftbildkamarasysteme auf dem Markt stellten sich zugleich vielfältige Fragen aus Kunden- und Nutzersicht. Die Befliegungsfirmen haben vielfältige Entscheidungen hinsichtlich der Eignung der verschiedenen Kamerasysteme für die unterschiedlichen Aufgaben und Aufträge zu treffen. Die Vorteile der einzelnen Systeme in Bezug auf die spezifischen, anwendungsorientierten Datenqualitätsparameter sind ebenso von Interesse wie die Handhabung der Systeme im Routinebetrieb und die Spezifika der Datenaufbereitung. Viele Auftraggeber photogrammetrischer Leistungen interessieren sich vor allem für die konkreten, anwendungs- und projektbezogenen Vorteile digitaler Bildflüge in Relation zu den bewährten Konzepten analoger Bildflüge und Bilddaten und den sich daraus ergebenden erweiterten Nutzungsmöglichkeiten und anwendungsbezogenen Unterschieden zwischen den einzelnen Kamerasystemen.

Diese Fragen wurden wiederholt an den Vorstand der DGPF gerichtet und so entstand auf Initiative der DGPF dieses einzigartige Projekt, mit dem eine neutrale Beantwortung dieser Fragen frei von kommerziellen Interessen und herstellerunabhängig erfolgt.

Im Rahmen dieses Projektes gibt es eine Vereinbarung, in der alle beteiligten Einrichtungen einen freien Zugang zu den für ihre Untersuchungen notwendigen Daten erhalten. Sie verpflichten sich gleichzeitig, den DGPF-Vorstand und die Projektleitung regelmäßig über die Ergebnisse der Untersuchungen zu informieren und diese Ergebnisse in der PFG und auf den Jahrestagungen der Gesellschaft zu veröffentlichen.

Nach einem ersten Projekttreffen anlässlich der Jahrestagung 2008 in Oldenburg wurden der organisatorisch-rechtliche Rahmen festgelegt und die Befliegungen für 2009 geplant. Das Testgebiet Vaihingen der Universität Stuttgart mit seinen vielfältigen dauerhaft signalisierten Punkten sowie seiner großen Relief- und Nutzungsvielfalt erwies sich als ein ideales Testgebiet für dieses Projekt. Weniger optimal waren die meteorologischen Bedingungen 2009, so dass der Befliegungszeitraum einige Wochen andauerte. Hieraus ergaben sich vor allem für die radiometrischen Auswertungen erhebliche Einschränkungen.

Es ist das besondere Verdienst von Herrn Dr. Herbert Krauß, Köln, und Herrn Dr. Klaus Komp, Münster, dass aus den Anfragen an die DGPF dieses DGPF-Projekt entstehen konnte!

Herrn Prof. Dieter Fritsch, Stuttgart, und seinem Team gebührt besonderer Dank, nicht nur für die Möglichkeit der Nutzung der Testfläche Vaihingen, sondern vor allem für die aufwändige und umfassende Logistik bei der Planung der Befliegungen und der umfassenden Aufbereitung vieler Terrabytes.

Ganz besonderen Dank an Herrn Dr. Michael Cramer, der freundlicherweise die Projektleitung übernommen hat, viele Projektreffen organisierte und letztendlich dafür sorgte, dass die Artikel termingerecht für dieses Heft fertig gestellt werden konnten.

Ohne die Beteiligung von ca. 100 Personen aus Wissenschaft und Technik und vor allem das große Engagement der Hersteller- und Befliegungsfirmen wäre dieses Projekt nicht realisierbar gewesen. Allen sei herzlichst gedankt! Mögen mit diesem unkonventionellen Vorhaben alle Beteiligten auch weit über die engeren Projektziele hinausgehend Impulse für ihre Arbeiten bekommen, sei es in Forschung und Lehre, sei es durch neue Kontakte.

Bereits die ersten Zwischenergebnisse des Projekts, die auf der Jahrestagung 2009 anlässlich des 100jährigen Bestehens der Gesellschaft vorgestellt wurden, riefen ein großes Interesse bei Herstellern, Nutzern und Wissenschaftlern im In- und Ausland hervor. Lebendiger kann sich eine Gesellschaft nicht präsentieren.

Unser Anliegen ist es, mit diesem englischsprachigen Schwerpunktheft der PFG eine

weite Verbreitung der Ergebnisse des Projekts auch im internationalen Kontext zu ermöglichen.

Nach dem einführenden Aufsatz zum Projektdesign und den beteiligten Firmen und Einrichtungen werden vor allem Ergebnisse der vergleichenden Untersuchungen zu den geometrischen Parametern, der Höhenmodellgenerierung und des Stereoplottings präsentiert und ergänzend erste Auswertungen zur Radiometrie und den thematischen Klassifizierungen vorgestellt.

Wir wünschen Ihnen eine spannende Lektüre und uns allen viele weitere anspruchsvolle Veröffentlichungen zu den Projektergebnissen.

Prof. CORNELIA GLÄSSER  
Präsidentin der DGPF  
Halle, 10. Januar 2010



## The DGPF-Test on Digital Airborne Camera Evaluation – Overview and Test Design

MICHAEL CRAMER, Stuttgart

**Keywords:** Digital airborne camera, test sites, sensor evaluation, on-site system validation

**Summary:** This paper focuses on general remarks on the test of the German Society of Photogrammetry, Remote Sensing and Geoinformation (DGPF) on Digital Airborne Camera Evaluation. It should be seen as an introductory paper which explains the test bed itself, the available reference and test data sets and the overall organization and structure of the data evaluation. The more detailed results are published in separate papers, which are also part of this journal issue.

**Zusammenfassung:** Der DGPF-Test zur Evaluation digitaler Luftbildkameras – Überblick und Testdesign. Dieser Artikel konzentriert sich auf grundsätzliche Anmerkungen zum Test von digitalen photogrammetrischen Luftbildkamerasystemen, durchgeführt von der Deutschen Gesellschaft für Photogrammetrie, Fernerkundung und Geoinformation (DGPF). Der Beitrag soll einen Überblick über die Rahmenbedingungen des Tests geben, die verfügbaren Referenz- und Testdaten vorstellen und die Struktur und Organisation der Datenauswertung erläutern. Die detaillierten Ergebnisse der Auswertungen werden in separaten Beiträgen vorgestellt, die ebenfalls Bestandteil dieser Ausgabe der Zeitschrift sind.

### 1 Introduction

Despite the fact, that digital airborne photogrammetric imaging is already widely used for operational projects and sales numbers of digital airborne cameras are much higher than originally expected from the manufacturers' point of view, comprehensive and independent empirical tests on system performance and quality of photogrammetric products based on digital airborne images are only partially available. Tests published by PASSINI & JACOBSEN (2008) or CRAMER (2007) could be mentioned, mainly focussing on the geometric performance of the systems and not covering the latest generation of sensor development. Investigations on the radiometric systems potential and applications can be found in MARTÍNEZ et al. (2007) and HONKAVAARA et al. (2009). Some of these tests also used hyperspectral sensors flown parallel to the digital camera. They are of high importance to evaluate the use of these new imaging sensors in

remote sensing applications. Even though such tests already proved the high potential of digital airborne sensors, at the end of 2007 the German Society of Photogrammetry, Remote Sensing and Geoinformation (DGPF) decided to run a separate and independent test on the evaluation of digital photogrammetric camera systems – not only to confirm results of the earlier tests but also to check the latest generation of digital camera systems and the products derived from them. Not only the camera but the whole process chain is covered and evaluated, as necessary for operational applications. Nevertheless, with digital systems the link to the processing software is much tighter. Many systems do need special software to take care of the individual sensor designs (for example for sensor related image post-processing like virtual image formation or line-scanner image rectification).

The individual and heterogeneous sensor design is another reason why empirical tests in controlled and well established test sites raise

in importance and will become inherent part of future system certification and validation processes. Current calibration of photogrammetric sensors already has changed – for example, looking on the role of calibration certificates from laboratory calibration: The classical calibration of analogue mapping cameras is certified by official metrology organizations, thus the calibration protocol automatically serves as the official certificate. It is internationally accepted through common agreements and typically requested as evidence of correct system functioning for tenders. For the new digital sensors, calibration processes are designed and performed by the manufacturers themselves, but not yet certified by independent metrology institutions. Some parts of the calibration are already exclusively done from real flight data using in-situ calibration approaches. Thus, empirical tests in controlled environments are not only used for quality assessment and system or product validation, they will also be of increased importance in system calibration already, which again underlines the need for current and future test site evaluations.

Today's situation in digital airborne camera evaluation thus underlines the need for empirical and independent tests where in the ideal case all photogrammetric cameras used in practice are involved and all are flown in comparable flight conditions. These tests have to be comprehensive, namely, looking into various aspects of the sensor system (geometry, radiometry) and also cover the product generation domain as well as the associated process chain.

For this purpose several flight campaigns were carried out in the framework of this DGPF camera evaluation test using the Vaihingen/Enz photogrammetric test site. This site is the most used airborne test site for photogrammetric applications in Germany and one of the three to four well established and manufacturer independent photogrammetric airborne sites available in Europe (CRAMER 2005). The test site is maintained by the Institute for Photogrammetry (ifp), Universität Stuttgart – thus, the ifp also served as Pilot Centre during the test, responsible for the project coordination under the umbrella of the DGPF, the request of data from the manufacturers and the

later distribution to the interested parties. The Pilot Centre also prepared reference orientations which were commonly used to derive the sensor products (CRAMER & HAALA 2009). All data was made available for all types of institutions ranging from science, mapping authorities, photogrammetric companies to sensor providers.

The DGPF test can be seen as a benchmark to compare airborne sensor performance. This is often requested from the photogrammetric community and actually was one of the user driven motivations of the test. Still, the main objective of this test is not to directly compare different sensors but to evaluate the sensor specific strengths and weaknesses, which are of relevance when choosing a sensor for specific applications. Since all findings obtained in this test are based on the results of the Vaihingen/Enz test flights only, they have to be confirmed by tests in other sites.

In the next Section the test field Vaihingen/Enz and the available reference data from ground and airborne flights are presented. In Section 3 the test data, as flown by the different camera systems is described. These two sections are of importance for the other reports on this project in this journal issue. Sections 2 and 3 already illustrate many of the boundary conditions during data acquisition, which are of impact for further processing and results. Finally, Section 4 briefly describes the organization of the expert network during data evaluation.

## 2 Reference Test Data

### 2.1 *Permanent Test Field Vaihingen/Enz*

The airborne data was acquired in the Vaihingen/Enz test area. This site covers about  $7.4 \times 4.7 \text{ km}^2$  and is located 25 km north-west of Stuttgart, Germany. Some 200 signalized points are available, marked permanently with white painted squares ( $60 \times 60 \text{ cm}^2$ ). The targets are regularly distributed in the test area. Higher resolution imagery is proposed to be taken in the inner part of the Vaihingen/Enz test site, where additional  $30 \times 30 \text{ cm}^2$  black squares are painted in the centre of each of the

larger white targets to allow for the precise detection of point centres in the images (cf. Fig. 1). The higher resolution flights with ground sampling distance (GSD) of 8 cm presented later were restricted to this part of the test field only.

Assuming flights with a GSD of 20 cm the target size in image space will be in the range of (at least)  $3 \times 3$  pixel, which is sufficient for manual measurements. Effectively, due to blooming effects the imaged points appear much larger (about  $6 \times 6$  pixel for 20 cm GSD). Still, measurements of image points have shown that especially for scanned analogue images, the clear identification of signals caused problems for some points in lower contrast areas and for operators not familiar with the test field and point locations. Fig. 1 exemplarily shows a signalized point located in the inner part of the test site and how this point is imaged in analogue RMK and digital DMC images. These two systems were flown simultaneously with an airplane equipped for two cameras (almost parallel image recording from the same flying heights and in same environmental conditions). Thus the images of the two systems can be compared directly. Both, the images from 20 cm GSD and 8 cm GSD are shown. Modest contrast enhance-

ment was applied to the given image samples. The differences in the quality of point identification are obvious, mainly for the 20 cm GSD image samples. Here the superior radiometric image quality of DMC and digital cameras in general is obvious. For the 8 cm GSD flight the target is clearly identified in both data sets. One should mention that in this case the RMK 8 cm GSD images seem to be sharper than the large-format RGB DMC 8 cm GSD images, which is not the case for the pan-chromatic virtual DMC image. The geometric resolution of different sensors and their image products are currently quantified from the analysis of the Siemens star resolution target (see Fig. 2).

Correct identification and measuring of the signalized targets during manual image mensuration is essential for highly accurate results. In JACOBSEN et al. (2010) manually obtained image coordinates provided by different operators from different institutions are compared and analysed to estimate the variance of manual image point observations.

The object coordinates of the signalized points were determined from static differential phase GPS base line observations in ETRS89/UTM coordinates (using ellipsoidal heights). This coordinate frame is also used in later evaluations. The obtained accuracy of

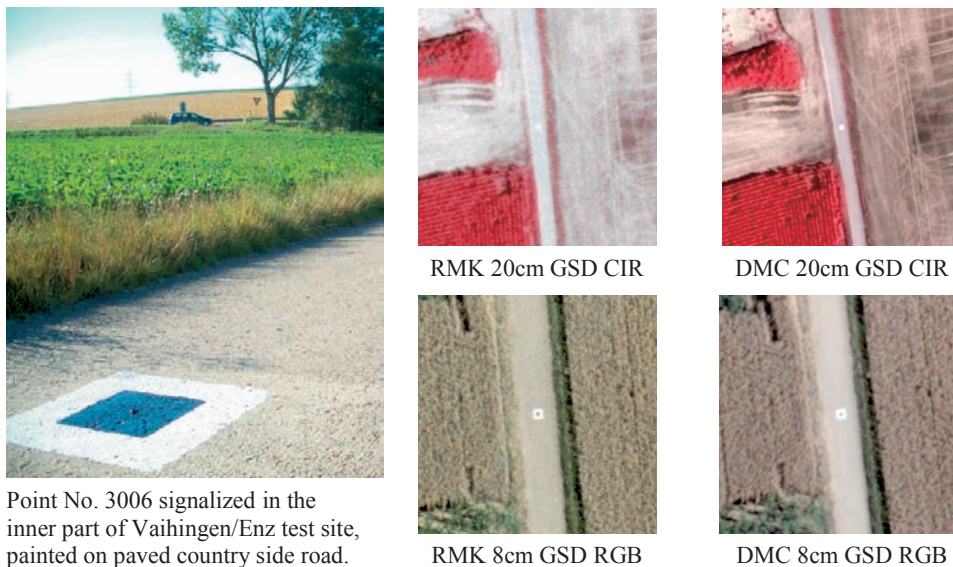


**Fig. 1:** Signalized point in the Vaihingen/Enz test site and the corresponding image points in simultaneously recorded scanned analogue RMK and digital DMC images.

the object points (coordinate error) is in the range (Std.Dev.) of 1cm (horizontal) and 2 cm (vertical). The accuracy was verified from repetitive base line measurements. It has to be kept in mind when the absolute quality of point determination (or surface model generation) from images is assessed from check point differences. Especially for the high resolution flights (8 cm GSD) the absolute accuracy of signalized points is not sufficient to comprehensively serve as reference, as long as sub-pixel accuracy is expected. Assuming high image resolution (which typically comes together with high demands in accuracy) the accuracy of the reference points is thus not of superior quality. This in principle is a general problem which is created by the increasing need for highly resolved images with sub-decimeter resolutions. This automatically increases the demands on the quality of the reference data itself.

For the empirical processing of the test data object space coordinates of 111 signalized points were delivered to the test participants. Most participants used a sub-set of these as control points and the remaining ones as check points for absolute accuracy assessment. Besides, another 78 points were only made available with reduced accuracy, their full coordinate information stayed with the Pilot Centre. In this way fully independent accuracy evaluation is possible, in order to cross-check results obtained from other participants.

System providers had access to 19 ground control points to check whether their data sets

were consistent and comparable to other flights, before data was sent to the Pilot Centre for further dissemination. Apparently, some of the sensor providers used these reference points to already go into deeper analysis of the sensor data. Thus not all finally delivered data sets may fully reflect the standard quality (status of pre-processing) of data which is typically obtained in operational survey mission scenarios.

## 2.2 Geometric and Radiometric Resolution Test Site

In addition to the permanently signalized control points, the test field was amended with temporal targets for the estimation of geometric and radiometric sensor resolution. Fig. 2 shows geometric and radiometric test targets which were installed for each of the different flight days. The colour targets and different resolution test targets (Siemens star) can be seen. The large Siemens star is of 8 m in diameter; all other targets are of  $2 \times 2 \text{ m}^2$  in size. It should be mentioned that the relatively small colour targets were only sufficient for the higher resolution 8 cm GSD flights. This was especially the case when the colour information was captured with coarser spatial resolution compared to panchromatic images as the case for the DMC and Ultracam-X frame based sensor systems. Additionally the colour targets suffered from strong directional reflection effects. This fact later prevented parts of



**Fig. 2:** Vaihingen/Enz radiometric test field from the air (left) and ground team members performing spectrometer measurements parallel to sensor flights (right).

the originally planned absolute radiometric sensor calibration (SCHÖNERMARK 2010).

The relatively small resolution site is located in the inner part of test field Vaihingen/Enz and thus covered by both the 8 cm GSD and 20 cm GSD flights. Additionally, a separate north-south flight line (so-called radiometry flight line) was planned for each flying height, with these targets located in its centre, fulfilling a pre-condition for the later radiometric sensor analysis. Thus, this radiometric and geometric resolution test site was always flown in cross-pattern.

Parallel to the flights, spectrometer and sun photometer measurements were done on the ground to independently measure the spectral characteristic of natural and artificial targets and the optical thickness of the atmosphere. These reference measurements are essential for the later radiometric performance analyses (SCHÖNERMARK 2010). Additional field surveys were carried out to map the land use in parts of the Vaihingen/Enz test site (WASER et al. 2010).

### 2.3 Reference Data from Airborne Sensors

In addition to the previously described reference measurements on the ground additional reference data were recorded from separate sensor flights (see lower part of Tab. 1). Two different hyper-spectral sensors were flown, namely the specim AISA+ and the DLR ROSIS system, both only covered parts of the test field. The AISA+ flight was done as a double-hole flight together with a DMC camera. Unfortunately, this valuable data has not yet been fully investigated in the performance evaluation tests (SCHÖNERMARK 2010).

In order to obtain dense reference data for the evaluation of photogrammetrically derived surface models an ALS50 LiDAR flight was done in August 2008. In order to provide a sufficiently dense reference point distribution on the ground for the later evaluation of the very dense point clouds from image matching a LiDAR point density of 5 pts/m<sup>2</sup> was chosen.

The data from hyper-spectral and LiDAR reference flights was processed by the system

providers and then delivered to the project participants via the Pilot Centre. In case of the ALS50 LiDAR data later analysis showed, that there was some potential to refine provided data at first. This issue is more deeply discussed by HAALA et al. (2010).

## 3 Digital Camera Test Flights

The digital camera flights were flown at six different flight days during a ten weeks time window from the beginning of July till the middle of September 2008 (cf. Tab. 1). Originally a much shorter time period of only two weeks was planned for the photogrammetric data acquisition, which could not be realized due to weather conditions. Most sensors were flown in two different flying heights, resulting in two blocks with the previously defined different ground sampling distances 20 cm GSD and 8 cm GSD (nominal values). The 20 cm GSD blocks covered the whole test area; the GSD 8 cm blocks were limited to the centre part.

The 20 cm GSD blocks were flown with a forward overlap of  $p = 60\%$ , whereas a higher forward overlap of  $p = 80\%$  was aimed at the 8 cm GSD blocks. The side overlap between image strips was consistently defined with  $q = 60\%$ , all this agreed in the project definition phase. Due to the fixed test site extensions and different sensor formats slight adaptations of the block geometry were necessary (mainly influencing side overlap) which potentially influences the later comparison of sensor performance. Additionally, not all test data finally fulfilled the defined overlap requirements.

Some of the sensors were only flown in one flying height (namely the AIC-x1 and 3K-camera), other data sets were influenced by technical problems. This is why AIC-x4 images finally were not made available. One of the Quattro DigiCAM camera heads was slightly defocused during the flight. However, this did not affect the later aerial triangulation. The DMC and RMK-Top15 flights were done as true double-hole flights, where the flight trajectory was fixed to the DMC sensor geometry. Since analogue RMK images were scanned with 14  $\mu\text{m}$  resolution the requested 20 cm GSD and 8 cm GSD images are obtained. The

**Tab. 1:** Participating sensor systems and involved flying companies.

System	System provider / manufacturer	System flyer	Day(s) of flight	Remark
DMC	Intergraph/ZI	RWE Power	24.07.2008 & 06.08.2008	double-hole flight with RMK-Top15 8cm GSD with p=60%
ADS40, SH52	Leica Geosystems	Leica Geosystems	06.08.2008	
JAS-150	Jenaoptronik	RWE Power	09.09.2008	
Ultracam-X	Vexcel Imaging Graz	bsf Swissphoto	11.09.2008	
RMK-Top15	Intergraph/ZI	RWE Power	24.07.2008 & 06.08.2008	double-hole flight with DMC 8cm GSD with p=60%
Quattro DigiCAM	IGI	Geoplana	06.08.2008	
AIC-x1	Rolleimetric	Alpha Luftbild	11.09.2008	only 8cm GSD, no cross strips
AIC-x4	Rolleimetric	Vulcan Air	19.09.2008	data not made available for project
DLR 3K-camera	DLR Munich	DLR Munich	15.07.2008	only 20cm GSD, no cross strips
AISA+ hyper-spectral	specim FH Anhalt	RWE Power	02.07.2008	double-hole flight with DMC
ROSIS hyper-spectral	DLR München	DLR Munich	15.07.2008	
ALS 50 LiDAR	Leica Geosystems	Leica Geosystems	21.08.2008	

Zeiss/ZI-Imaging scanners SCAI (20 cm GSD, Kodak MS 1443 CIR film) and PhotoScan2001 (8 cm GSD, Agfa X-100 CN film) were used to digitize the analogue RMK images. More detailed block configurations and flight parameters for RMK-Top15, DMC, Ultracam-X, Quattro DigiCAM and ADS40 can be seen in (CRAMER 2009). More detailed additional information can also be found in the project web site (DGPF 2009, in German).

The overlap conditions for DMC and Ultracam-X blocks 20 cm GSD and 8 cm GSD are depicted in Fig. 3. Notice the different scaling of the legend colours. The red colour always depicts areas with 2 folded image overlap only, whereas the maximum overlap varies from 12 folded (for 20 cm GSD blocks) to 30 folded images (for 8 cm GSD Ultracam-X block). The DMC 8 cm GSD block only has 14 folded overlap maximum. Even though there are

slight differences in the side overlap parameters for the two 20 cm GSD blocks, the overlap conditions are quite close to the pre-defined values. The larger differences for the 8 cm GSD blocks are due to the much higher forward overlap ( $p = 80\%$ ) for the Ultracam-X flight compared to 60% for the DMC block. This definitely impacts the geometric block layout and the quality of object points.

As already described in other papers discussing the evaluation of the DGPF test flight data, the long flight period not only leads to strong changes in the sun illumination conditions (decrease in maximum sun angle) and vegetation (vegetation period from midsummer till early fall was covered, including the complete harvesting period), the weather changes and the quite in-stable weather conditions during this flight season were of real influence on the data acquisition. The originally

defined conditions on cloud free sky and flights at maximum sun angle (during noon time) could not be realized in several flights. Concessions had to be made, especially with progressing flight season. Unfortunately, no direct link to official weather recordings could be established, nevertheless, cloud coverage has been recorded and documented on an hourly basis by a web cam located in Vaihingen/Enz city centre. Additionally, the sun photometer measurements recording the transmission of atmosphere also indicate the cloud coverage in that part of the test site, where the radiometric and geometric resolution test area is located (see Fig. 2 and SCHÖNERMARK 2010).

The weather situation is exemplarily shown by the web cam images for the flight day August 6 (cf. Fig. 4). As can be seen from Tab. 1, DMC (with RMK in the same plane), Quattro DigiCAM and ADS40 were flown on that day. The DMC flight was performed in almost perfect cloud conditions from UTC 7:50 h – 8:30 h (only 8 cm GSD was flown). The ADS40 and Quattro DigiCAM flights were partially done in parallel. As one can see, the cloud situation significantly changed during the data acquisition period from UTC 9:30 h (start of Quattro DigiCAM flight) till UTC 12:00 h (end of ADS40 image recording). This change in illumination directly influences the radiometric

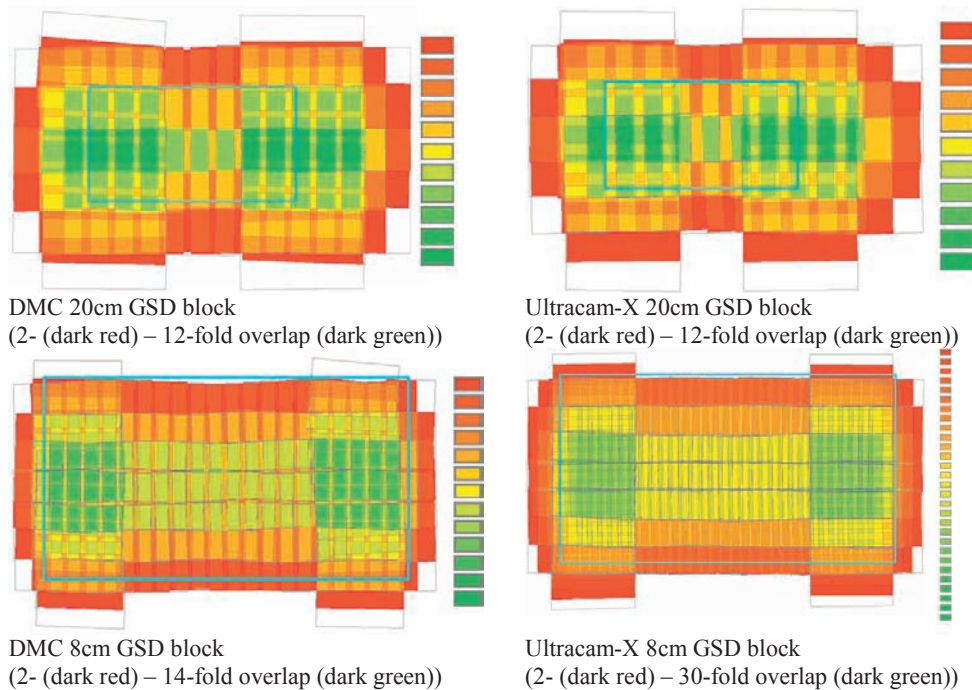


**Fig. 3:** Block configurations / image overlap conditions (colour-coded) for DMC and Ultracam-X blocks.



**Fig. 4:** Cloud situation in western part of test site during flight day August 6, 2008 as recorded by an on-site web cam.

sensor performance and also has to be considered for automatic and manual image measurements. As described by SPRECKELS et al. (2010), different shadow conditions are also of impact on the manual stereoplotting.

#### 4 Competence Teams and Data Evaluation

The outlines of the project were officially presented during the DGPF annual meeting in Oldenburg in spring 2008. Since then interested people mainly from the German speaking countries were invited to actively participate in this project. More than 100 different people showed interest and became part of the project mailing list. About 35 institutions signed the official project agreement fixing the common topics of analysis and a rough working schedule. An almost complete list of the test participants can be found in CRAMER (2009) and on the project web site DGPF (2009). All these participants received the requested data sets. Fig. 5 shows the structure of the project group (only active members), separated in research institutions, national mapping agencies or other organizations and companies, the later also separated into system providers / manufacturers and other commercial companies. As expected about 50 % of the participants are members of the scientific sector. About one third of the participating institutions represent the commercial field. The remaining 15 % are representatives from mapping organizations, representing one of the main later user groups of digital airborne sensor data and products.

The data from the different imaging sensors were altogether delivered 110 times. It is interesting to see that the major interest is on the frame based sensor systems, less than 20 % of delivered data sets were from JAS-150 and ADS40. If the DMC, Ultracam-X and Quattro DigiCAM are regarded as large frame digital sensors, they together cover about 60 % of all data requests. The remaining about 20 % of requests was focused on the smaller format systems AIC-x1 and 3K-camera and the RMK data. The scanned analogue RMK image data mainly serve as direct comparison between analogue and digital image data quality.

In order to structure the data evaluation process and to stimulate intensive discussions between different participating institutions working on the same topics, four competence teams were established, which individually focus on one of the following topics: Geometry, radiometry, digital surface models and manual stereo plotting. Each group is headed by an expert in the corresponding field: Karsten Jacobsen, Leibniz Universität Hannover (team geometry), Maria von Schönermark, former Universität Stuttgart now DLR Oberpfaffenhofen (team radiometry), Norbert Haala, Universität Stuttgart (team surface model) and Volker Spreckels RAG Deutsche Steinkohle (team stereo plotting). Many of the active participants have photogrammetric background, thus the test topics geometry and surface model generation were covered in more detail than for example the analysis of radiometric aspects of digital sensors. Therefore, the test results available so far not in all parts are as comprehensive as originally expected and consequently the publications within this

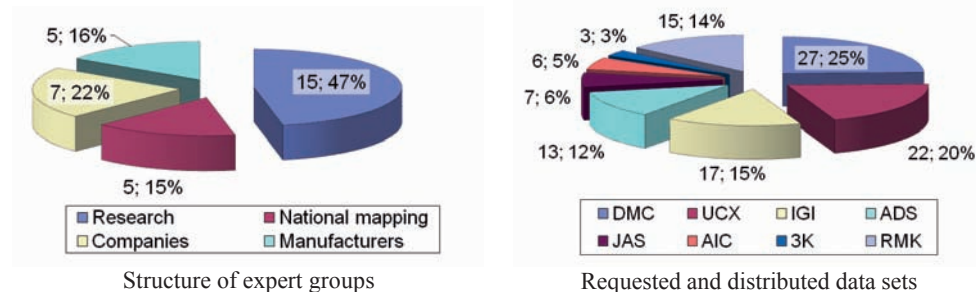


Fig. 5: Participating user groups (left) and distributed data sets (right) – status as of October 1, 2009.

PFG issue partially only reflect the current status of data evaluation.

The fact, that not all analyses could be done with such intensity as aspired is also underlined by the number of delivered results. Apparently, many of those participants, who originally requested data were finally not able to finish or even fully start the processing of the data sets. One of the main reasons was unexpected time limitations, changes in priorities and also lack of sufficient human resources. More than 80 % of the participating commercial companies did not return results to any of the competence teams. From universities and national mapping agencies only 40 % and 20 % did not deliver any processing results.

The available results, however, already illustrate the high potential of digital imaging. The main analysis aspects and the current status of the investigations of the four competence teams are highlighted in the papers (JACOBSEN et al. 2010, HAALA et al. 2010, SPRECKELS et al. 2010). Since the radiometry team focused on the two different topics radiometric sensor calibration and land use classification two separate papers have been submitted from this group (SCHÖNERMARK 2010, WASER et al. 2010). These papers also have to be seen in combination with previous publications, mainly in the frame of the DGPF annual meeting 2009 in Jena. These papers can also be found on the project web site (DGPF 2009). It is obvious, however, that the evaluation of this complex data needs to and will continue.

## 5 Summary

The DGPF project on the comprehensive empirical evaluation of digital airborne sensors and derived products is a very important milestone in the complex field of new digital sensor and product evaluation and validation. As pointed out such in-situ tests using defined processes will become one standard approach in future system certification and quality assessment of sensor products. Even though the active contributions were not as broad as hoped from the number of distributed data sets, the outcomes of this test confirm the high potential of digital sensor data recording and

product processing. It is obvious that there is still a need to complete the data evaluation in the next months.

The DGPF project will officially be closed during the upcoming Dreiländertagung in Vienna in July 2010. This of course will not conclude the deeper scientific evaluations which are still pending. Topics which may be of lesser interest to participants from the operational practice, like development and testing of new image matching concepts, are seen as very valuable from a researchers' perspective. Since the high scientific value of this reference and empirical data sets is generally accepted it was already decided to make the data available for international and other research projects, too. Interested persons are cordially invited to contact the DGPF executive team members directly. We thus hope that this valuable and comprehensive data will become one of the standard empirical data sets used and cited for the next years.

## Acknowledgements

The author would like to acknowledge all people involved in the project preparation, the project organization and the data acquisition as well as the data processing. This especially includes the coordinators of the four competence groups. Special thanks are also expressed to Mr. Werner Schneider from ifp, who not only cares for everything regarding the Vaihingen/Enz test site but also was in charge for data preparation and the final transfer between the Pilot Centre and the project participants. Special thanks are expressed to all the companies who performed the flights and to the system providers, who strongly supported this DGPF activity from the very beginning and who made all these test flights available. Thanks also to the members of the DGPF executive committee, namely Herbert Krauß and Cornelia Gläßer for all their continuous support and activities related to the project!

## References

- CRAMER, M. & HAALA, N., 2009: DGPF project: Evaluation of digital photogrammetric aerial based imaging systems – overview and results from the Pilot Centre. – ISPRS Workshop on High Resolution Earth Imaging for Geospatial Information, on CD.
- CRAMER, M., 2005: 10 Years ifp Test Site Vaihingen/Enz: An Independent Performance Study. – Photogrammetric Week '05, Wichmann Verlag, Heidelberg, 79–92.
- CRAMER, M., 2007: The EuroSDR performance test for digital aerial camera systems. – Photogrammetric Week '07, Wichmann, Heidelberg, 89–106.
- CRAMER, M., 2009: Digital Airborne Camera Performance – The DGPF Test. – Photogrammetric Week '09, Wichmann, Heidelberg, 51–68.
- DGPF, 2009: project web site (in German). – [www.ifp.uni-stuttgart.de/dgpf/](http://www.ifp.uni-stuttgart.de/dgpf/) or [www.dgpf.de](http://www.dgpf.de) (December 2009).
- HAALA, N., HASTEDT, H., WOLFF, K., RESSL, C. & BALTRUSCH, S., 2010: Digital Photogrammetric Camera Evaluation – Generation of Digital Elevation Models. – this issue.
- HONKAVAARA, E., ARBIOL, R., MARKELIN, L., MARTINEZ, L., CRAMER, M., BOVET, S., CHANDELIER, L., ILVES, R., KLONUS, S., MARSHAL, P., SCHLÄPFER, D., TABOR, M., THOM, C. & VEJE, N., 2009: Digital airborne photogrammetry – A new tool for quantitative remote sensing? – A state-of-the-art review on radiometric aspects of digital photogrammetric images. – *Remote Sensing* **2009/1** (3): 577–605.
- JACOBSEN, K., CRAMER, M., LADSTÄDTER, R., RESSL, C. & SPRECKELS, V., 2010: DGPF-Project: Evaluation of Digital Photogrammetric Camera Systems – Geometric Performance. – this issue.
- PASSINI, R. & JACOBSEN, K., 2008: Accuracy analysis of large size digital aerial cameras. – *International Archives of Photogrammetry, Remote Sensing and Spatial Information Sciences* **37** (B1): 507–513.
- MARTÍNEZ, L., ARBIOL, R., PALÀ, V. & PÉREZ, F., 2007: Digital Metric Camera radiometric and colorimetric calibration with simultaneous CASI imagery to a CIE Standard Observer based colour space. – *IEEE International Geoscience and Remote Sensing Symposium*.
- SCHÖNERMARK VON, M., 2010: Status Report on the Evaluation of the Radiometric Properties of Digital Photogrammetric Airborne Cameras. – this issue.
- SPRECKELS, V., SYREK, L. & SCHLIENKAMP, A., 2010: DGPF-Project: Evaluation of Digital Photogrammetric Camera Systems – Stereoplotting. – this issue.
- WASER, L. T., KLONUS, S., EHLERS, M., KÜCHLER, M. & JUNG, A., 2010: Potential of Digital Sensors for Land Cover and Tree Species Classifications – A Case Study in the Framework of the DGPF-Project. – this issue.

### Address of the Author:

Dr.-Ing. MICHAEL CRAMER, Universität Stuttgart, Institut für Photogrammetrie (ifp), Geschwister-Scholl-Straße 24 D, D-70174 Stuttgart, Tel.: +49(0)711/685-84118, [michael.cramer@ifp.uni-stuttgart.de](mailto:michael.cramer@ifp.uni-stuttgart.de).

Manuskript eingereicht: Dezember 2009

Angenommen: Januar 2010



## DGPF-Project: Evaluation of Digital Photogrammetric Camera Systems – Geometric Performance

KARSTEN JACOBSEN, Hannover, MICHAEL CRAMER, Stuttgart, RICHARD LADSTÄDTER, Graz, Austria, CAMILLO RESSL, Vienna, Austria & VOLKER SPRECKELS, Herne

**Keywords:** Digital cameras, geometry, block adjustment, integrated sensor orientation, Self-calibration

**Summary:** The geometric performance of digital airborne cameras also including the impact of direct sensor orientation has been evaluated by a test of the German Society of Photogrammetry, Remote Sensing and Geoinformation (DGPF). This test includes following airborne photogrammetric cameras: the large format frame cameras Z/I Imaging DMC, Vexcel Imaging UltraCamX and the line scanning camera system Leica Geosystems ADS40 (2<sup>nd</sup> generation) and Jena Optronik JAS-150 as well as the mid-format camera Rolleimetric AIC-x1 and the combination of four mid-format cameras Quattro-DigiCAM. The results presented in this paper were achieved by a group of researchers from different institutions, working independently from each other and with different programs for data acquisition and bundle block adjustment. Moreover, different adjustment configurations (i. e. with/without use of perspective centre coordinates and/or attitude information from GPS/inertial systems), and also different control point configurations have been used in the test; this results in a wide range of solutions and accuracy results which are not easy to compare, on the other hand this just shows the spectrum of possible solutions in operational applications.

**Zusammenfassung:** *DGPF-Projekt: Evaluierung digitaler Kamerasysteme – geometrisches Potential.* Das geometrische Potential digitaler Luftbildkameras, auch unter Berücksichtigung der direkten Sensororientierung, wurde im Rahmen eines Tests der Deutschen Gesellschaft für Photogrammetrie, Fernerkundung und Geoinformation (DGPF) untersucht. Dieser Test schließt folgende Kameras ein: die großformatigen Kameras Z/I Imaging DMC, Vexcel Imaging UltraCamX und Zeilenkameras Leica Geosystems ADS40 (2. Generation) und Jena Optronik JAS-150, sowie die Mittelformatkamera Rolleimetric AIC-x1 und die Kombination von vier Mittelformatkameras Quattro-DigiCAM. Die in diesem Bericht präsentierten Ergebnisse wurden von einer Gruppe wissenschaftlicher Mitarbeiter verschiedener Universitäten mit unterschiedlichen Datenerfassungsprogrammen, unterschiedlichen Bündelblockausgleichungsprogrammen, unterschiedlichen Konfigurationen der Ausgleichungen (z. B. mit/ohne Verwendung von Projektionszentrumskoordinaten und Richtungsinformation aus GPS/inertial Systemen) und unterschiedlicher Passpunktconfiguration erzeugt. Diese Ergebnisse geben einen Überblick über die Variation der Lösungen und Genauigkeiten, die auch in operationeller Anwendung gegeben ist.

### 1 Introduction

Digital cameras are replacing more and more the analogue. The first large format photogrammetric cameras introduced into market were the line scanning camera Leica Geosystems ADS40 and the frame cameras Z/I Imaging DMC and Vexcel Imaging UltraCam, where current systems have already been

modified compared to the market introduction. Recently the line scanning camera Jena Optronik JAS-150 has been introduced. Mid-format cameras are growing with the pixel numbers and multi-head configuration of mid-format cameras are available, which in terms of terrain coverage now can compete or are even superior to the large format systems. For the evaluation of the geometric performance

not only the images itself, but also their combination with direct sensor orientation, leading to integrated sensor orientation (ISO), has to be considered. The selection of a camera type will not only be based on the geometric property and system size, depending upon the project definition, the selection has to be economic in relation to the varying project conditions. This paper only focuses on the geometric performance analysis; economical aspects have to be considered from later potential system users.

Up to now several tests for the geometric performance of digital cameras have been made, but only very few comparisons of different systems with images taken under similar conditions have been published. In (PASSINI & JACOBSEN 2008) the accuracy potential of block adjustments with DMC-, UltraCamD-, UltraCamX-, ADS40- and RC30-images with approximately 5 cm GSD have been analyzed, but the test of the DGPF includes two different ground resolutions, mid-format cameras and a second line scan camera. Up to now it is the most comprehensive test of digital aerial cameras.

Within the next section the participating institutions and data acquisition is presented, and then some general investigations on the use of self-calibration are made. This also includes some discussions on the stability and validity of additional parameter models. Finally the overall geometric accuracy is outlined, obtained from independent check point analyses after bundle adjustment.

## 2 Aerial Triangulation – Data Acquisition

The geometric performance of a camera system depends on the correct mathematical modelling, the multiple coverage of the project area, the block configuration, the quality of the input data, the automatic aerial triangulation (AAT) including number and distribution of tie points, manual measurement of control and check points as well as the direct sensor orientation (projection centres determined by relative cinematic GNSS and inertial measurement units (IMU)). Besides, the quality of the images itself is of importance, which also

might be influenced by the environmental conditions during image data acquisition.

In the frame of the DGPF-project for the camera evaluation different strategies have been used by the participants. Different programs for AAT, individual measurements of the control and tie points, different bundle block adjustment programs and block adjustments without direct sensor orientation and integrated sensor orientation (ISO) have been used. This does not allow direct comparison of the results achieved by the participants, but it opens the view to the wide range of possible solutions in photogrammetric projects. This also reflects the situation of later operational processing where each evaluation is based on the available process chain and maybe even more important the expertise of each user. In addition, not all image flights have been done in the planned configuration and the actual weather conditions for individual flights have been different, but this can be seen as more realistic conditions.

All camera manufacturers had access to 19 ground control points to check that their data sets are consistent and comparable to other flights. This was done before the data was sent to the pilot centre for further dissemination. The manufacturers had the possibility to optimize the post processing of sensor data, i.e. generation of the virtual images for the large format digital frame cameras or the optimum for the integrated sensor orientation. This may not be realistic for usual operational handling, so it has to be taken into account for the transfer of the achieved results to commercial projects.

### 2.1 Participating Institutions and Analyzed Data Sets

The results presented in this paper are mainly based on the investigations done by the photogrammetric institutes at Leibniz University Hannover (UH), University of Stuttgart (US), Graz University of Technology (TUG), Vienna University of Technology (TUV) and the RAG Deutsche Steinkohle (RAG) company in Herne (JAS-150 bundle adjustment) (cf. Tab. 1). This includes data sets (typically image coordinate measurements) generated by

**Tab. 1:** Analyzed sensor data sets from participating institutions.

Camera system	University of Hannover (UH)	University of Stuttgart (US)	TU Graz (TUG)	TU Vienna (TUV)	RAG Herne (RAG)
RMK	X	X	X	X	
DMC	X	X		X	
UltraCamX	X	X		X	
Quattro-DigiCAM	X	X	X		
ADS40	X	X			
JAS-150					X
AIC-x1	X	X			

University of Duesseldorf (Uni D), survey administration LVG Munich (LVG M) and the private company CuB Technik.

### 2.2 Manual Measurement of Image Coordinates

Image coordinates of control and check points usually are measured manually because of the strong variety of the shape of object points and varying background. The manual measurements partially dominate the determination of the object point coordinates. Centres of signalized points shown in the images are not in-

dependent upon the background in the object space. If the background is not homogenous, the imaged centres may be slightly shifted, leading to systematic pointing errors. Simple error propagation for such point locations cannot be used. In the case of this camera test especially for the data sets with 20 cm GSD the identification of corresponding image points was sometimes difficult. All signalized points were marked with  $60 \times 60 \text{ cm}^2$  white colour markings, in the central part of the Vaihingen/Enz site. Where the 8 cm GSD flights were done, these white targets were additionally provided with  $30 \times 30$  black squares in the centre of the white target. Fig. 1 shows with

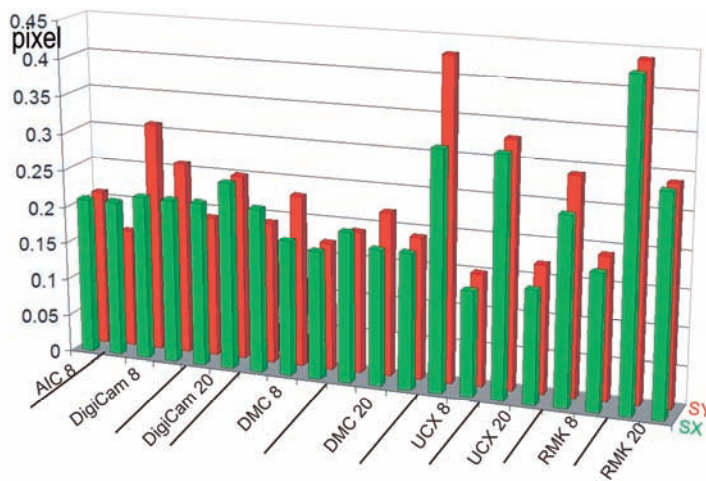


**Fig. 1:** Standard deviation of manual control and check point measurements [pixels] computed by differences of independent measurements (the number following the camera names indicates the GSD).

**Tab. 2:** Source of manual image point measurements of control and check points.

Camera	Image coordinates measured by
RMK	US, LVG M, TUV
DMC	US, LVG M, TUV, CuB Technik
UC-X	US, LVG M, TUV
DigiCAM	UH, US, TUV, CuB-Technik
AIC-x1	UH, US, Uni D

any pair of columns (SX and SY) typical root mean square differences (RMS) of the manual measurements of always two organizations (see also Tab. 2) divided by 1.414 to reduce it to the standard deviation of single manual pointing – what is correct if both of the compared measurements have the same accuracy. This may give a realistic view on the variations in manual image coordinate measurements and to some of the limitations of such a test with accurate reference.

The precision of the manual control and check point image coordinate measurements of course depends on the qualification and precision of the human operators, but also on the image quality. The point identification in the digitized analogue images of the RMK, especially with 20 cm GSD, is quite more difficult as with other images, which already reflects the lower radiometric quality of scanned analogue images compared to digital imaging. The slightly higher values for the Quattro-DigiCAM are concentrated to the same operator, while for the UltraCamX no clear explanation can be seen – the same operators got better pointing values with other cameras, so this may be caused by a learning process of the operators, measuring the same points in images taken with different cameras. Such a variation of the manual pointing is influencing the finally reached results of the block adjustments. The differences between the cameras may reflect also the impact of different environmental conditions during sensor flights, also influencing the radiometric performance of the image data.

### 3 Self-Calibration

#### 3.1 Systematic Image Errors

The geometry of photogrammetric cameras is approximated by the mathematical model of perspective geometry. The real image geometry does not correspond exactly to this model. Discrepancies can be caused by the optics, the planarity of the sensor plane and in case of the large format multi-head frame sensors the mosaicing of sub-images to homogenous virtual images. The discrepancies within the CCD usually can be neglected.

Geometric differences between the real image geometry and the perspective geometry, named systematic image errors, usually are determined and respected by self-calibration with additional parameters. This requires a systematic characteristic of the discrepancies, being constant within the used group of images. The number of used additional parameters should be limited to avoid weakening of the block geometry. On the other hand the parameters must be able to model the main part of the systematic image errors. Remaining systematic image errors after self-calibration with additional parameters can be analyzed through residuals at the image coordinates after bundle adjustment. By superimposing all image residuals in one image plane the residuals can be averaged in small image sub areas.

This grid can also be used as a correction grid for improving the image coordinates in a second block adjustment. The correction grids can be combined with self calibration, but also used without. Correction grids determined without self-calibration do not need any hypothesis about geometry of systematic image errors. The high number of sub areas of a correction grid may weaken the block adjustment and requires a high number and good distribution of image points. The following results are based on at least 100 residuals in average, minimizing random errors. The constant characteristic of the systematic image errors has been analyzed by subdividing the images of a block into two groups as function of the flight time to determine changes of the geometry between both sub-blocks, which can only be caused by a time depending change of the image geometry.

### 3.2 Additional Parameters

Different sets of additional parameters are in use. They may be based on a pure mathematical justification, as the 12 Ebner parameters (EBNER 1976), eliminating the systematic effects in a grid of  $3 \times 3$  points (Gruber points) or the 44 Grün parameters (GRÜN 1976) based on  $5 \times 5$  points. Such sets of additional parameters were justified at the time when tie points have been measured manually in just 9 Gruber-points, later also raised to a grid of  $5 \times 5$  points in the photos, but today equal distributed tie points are preferred. The Ebner set of 12 additional parameters has been shown as not satisfying for digital images (WU 2007), but also for analogue photos with distributed tie points distributed equally in the images. In Fig. 8, right hand side, it can be seen that the adjustment US(3), based on the Grün-parameters drastically improved the accuracy against the same data set adjusted with the Ebner-parameters (case US(2)). Despite the fact that these mathematical polynomials are implemented in many commercial software packages, they are not allowing a satisfying description of the actual image deformation, especially of modern multi-head digital frame cameras. The Vienna University of Technology by this reason has extended the Ebner parameters by two radial symmetric and two tangential parameters (using a balanced version of Brown's formulation), named as Ebner+4 in Tab. 4.

Another possibility is the use of parameter sets which can model physical justified effects like radial symmetric and tangential lens distortion, principal point offset or focal length refinement by a reduced number of additional parameters. The most common known parameter set of this type is the one introduced by

Brown (BROWN 1971). The bundle adjustment program BLUH (JACOBSEN 2007) uses a standard set of 12 parameters composed of mainly physical parameters. Physical parameter sets are also defined in the bundle adjustment software packages BINGO (KRUCK 1983), DGAP (University of Stuttgart), Orient (TU Vienna) and PhoBA (TU Graz). In addition to the standard parameter sets, specially designed parameters have to be used for the large format digital cameras DMC and UltraCam. They are able to handle small geometric deformations caused by the stitching process by operating on well defined image regions covered by the individual sensor units. Such parameter sets are implemented e.g. in the bundle adjustment programs BLUH and BINGO.

Still there is the need to know how well this modified parameter sets fit the true sensor geometry, which only may be analyzed through extensive empirical testing. Thus modifications to refine existing self-calibration models or to take care of new sensor designs have already been made or are under development. The BLUH bundle adjustment may serve as one example. There the physical parameters have to be added by some mathematical parameters for effects which are not properly covered. The 12 general additional parameters of the program system BLUH (typically used for the traditional block adjustment of analogue imagery) (JACOBSEN 2007) just recently have been complemented by the special parameters 81 up to 88 (cf. Tab. 3), modelling geometric effects of the image corners of digital mid-format cameras, which may be caused by non flatness and deformation of the sensor CCD array. For the large format digital cameras DMC and UltraCam special additional parameters are included to be able to cover

**Tab. 3:** Additional parameters of program system BLUH covering corner effects of digital mid-format cameras (AP81 – AP88 = numeric values of the additional parameters).

81. $x' = x + AP81 * ABS(x^3 * y^3) * 10^{-9}$	$y' = y - AP81 * ABS(x^3 * y^3) * 10^{-9}$	for lower right quarter
82. $x' = x + AP82 * ABS(x^3 * y^3) * 10^{-9}$	$y' = y + AP82 * ABS(x^3 * y^3) * 10^{-9}$	for lower left quarter
83. $x' = x + AP83 * ABS(x^3 * y^3) * 10^{-9}$	$y' = y - AP83 * ABS(x^3 * y^3) * 10^{-9}$	for upper left quarter
84. $x' = x + AP84 * ABS(x^3 * y^3) * 10^{-9}$	$y' = y + AP84 * ABS(x^3 * y^3) * 10^{-9}$	for upper right quarter
85. $x' = x + AP85 * x^2 * y^2 * 10^{-6}$	$y' = y + AP85 * x^2 * y^2 * 10^{-6}$	for lower right quarter
86. $x' = x + AP86 * x^2 * y^2 * 10^{-6}$	$y' = y + AP86 * x^2 * y^2 * 10^{-6}$	for lower left quarter
87. $x' = x + AP87 * x^2 * y^2 * 10^{-6}$	$y' = y + AP87 * x^2 * y^2 * 10^{-6}$	for upper left quarter
88. $x' = x + AP88 * x^2 * y^2 * 10^{-6}$	$y' = y + AP88 * x^2 * y^2 * 10^{-6}$	for upper right quarter

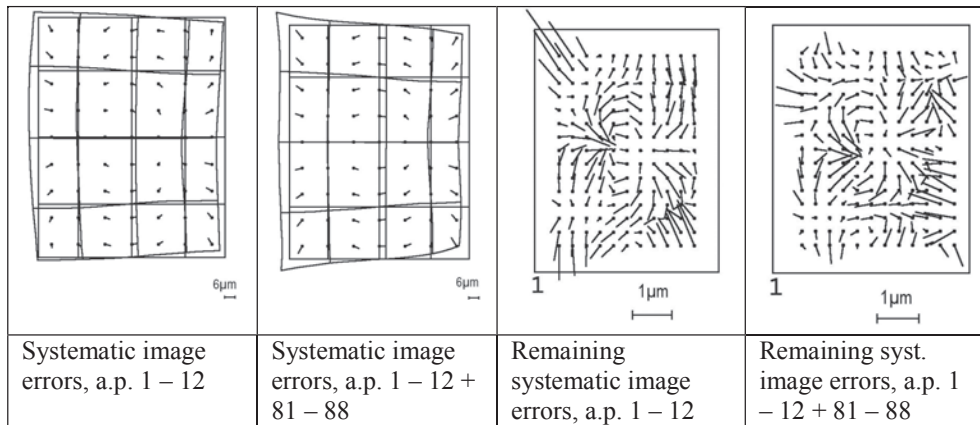


**Fig. 2:** Systematic image errors and remaining systematic image errors (Quattro-DigiCAM, camera 1, 20 cm GSD) based on adjustment with different sets of additional parameters (a.p.).

geometric effects of the image mosaicing (details in JACOBSEN 2007).

The positive impact of the recently introduced new BLUH parameters 81 up to 88 should exemplarily be illustrated by one of the 4 cameras of the Quattro-DigiCAM configuration (camera 1), shown in Fig. 2. The differences of the systematic image errors determined by the additional parameters 1-12 (standard 12 BLUH parameters) and 1-12 + 81-88 are limited to the image corners. Without use of additional parameters 81-88 the averaged and overlaid residuals, shown as remaining systematic image errors, show larger values at the image corners. The root mean square of the remaining systematic image errors for the Quattro-DigiCAM is reduced by the parameters 81-88 in the x- and y-component by 15 % to 25 % to  $\pm 0.4 \mu\text{m}$  and  $\pm 0.7 \mu\text{m}$ , respectively. Even though this improvement is well within in the sub- $\mu\text{m}$  level it is of influence for the later bundle adjustment, as long as no additional support from direct sensor orientation is available. A bundle block adjustment of the Quattro-DigiCAM configuration just based on 15 control points, not using direct observations for the positions of projection centres, leads to improved coordinates of independent check points of approximately 15 % in all 3 coordinate components. In general, non modelled systematic image errors are causing a block deformation especially in the height component if the block is not stabi-

lized by a higher number of well distributed control points or GPS-coordinates of the projection centres. The positive impact of these BLUH additional parameters 81-88 is similar for the Rolleimetric AIC-x1.

Instead of self-calibration with additional parameters also an iterative block adjustment with improvement of the image coordinates by correction grids, based on the overlaid and averaged residuals, is possible. This for example is implemented and used by BLUH, BINGO and PhoBA adjustment software and also used by the Intergraph/ZI software (DÖRSTEL 2007). But this method includes a high number of additional unknowns corresponding to the number of image sub-areas for averaging. In the example of Fig. 2,  $12 \times 15 = 180$  sub-areas are used. To avoid a too strong influence of random errors, the correction grids should be improved by weighted average filter. Block adjustments using correction grids are leading to approximately the same accuracy determined at independent check points in the case of the camera test, having a high number of image points. But only very limited possibilities of statistical tests of the justification of the correction grids within the bundle block adjustment are possible. The program system BLUH includes statistical tests of the additional parameters – not justified and too strong correlated additional parameters are removed automatically from the adjustment, so the final adjustment will be made with a reduced set of

additional parameters. Corresponding reduction of unknowns is not possible with correction grids. So correction grids should only be used for tests with data sets having a satisfying number and equal distributed image points. Even though such correction grids may have certain relevance for photogrammetric bundle adjustment their use for operational purposes may be dangerous, since they may handle random errors as systematic errors, leading to smaller  $\sigma_0$ , which not necessarily corresponds to better object coordinates.

### 4 Sensor Stability

The self-calibration requires constant systematic image errors for the group of images handled as one unit. If the image geometry is

changing within the data set caused by thermal or other influences, only the average systematic image errors can be determined and respected. In addition it is important to know, if systematic image errors are constant or if they are depending for example on the time and the flying height. Such dependencies are also limiting pre-corrections based on calibration sites. For the investigation of the geometric sensor stability, the images of the 8 cm GSD data sets have been separated into two groups corresponding to the flight time, i. e. the first half of the 8 cm GSD flight forms the first sub-block, the second half the second sub-block. The self-calibration has been computed with two sets of additional parameters, each limited to one group of images. The comparison of the so determined systematic image errors is answering the question if the image

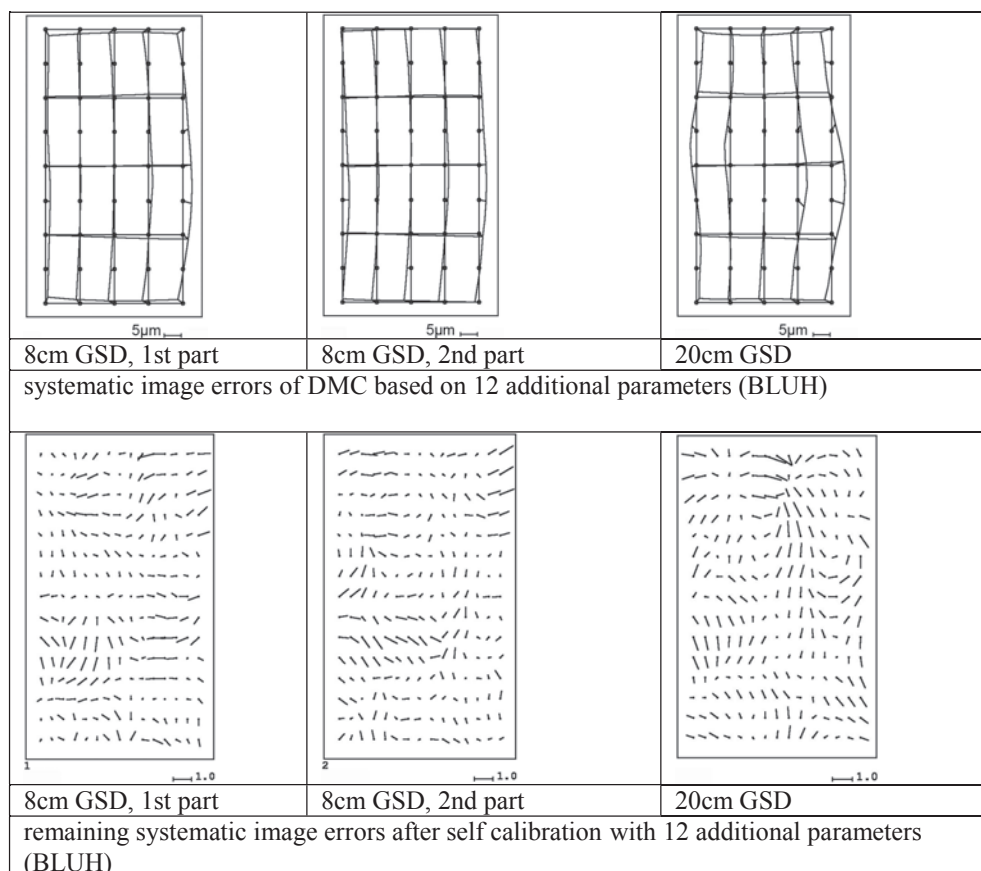


**Fig. 3:** Systematic image errors and remaining image errors of DMC based on 12 additional parameters (separately estimated for two 8 cm GSD sub-blocks and 20 cm GSD flight).

geometry is the same within the whole block. A comparison with the systematic image errors determined for the blocks with 20 cm GSD is showing the dependency on the flying height or the time.

The large format frame camera images DMC and UltraCamX are virtual images based on the merging of the smaller sub-images. So as additional source for systematic image errors the effect of mosaicing may exist. Program system BLUH includes special additional parameters for the DMC and also the UltraCam. The data of the DGPF-camera test show only limited improvements of the bundle block adjustments using in addition to the basic 12 additional parameters the camera specific parameters. Because of this fact, following only the results based on the basic 12 BLUH parameters is shown.

The systematic image errors of the DMC are limited (cf. Fig. 3 upper part). For the lower flying height (8 cm GSD) in the mean square just 0.8  $\mu\text{m}$  or 0.07 pixels are reached, while it is a little more with 1.3  $\mu\text{m}$  or 0.11 pixels for the upper flying height. A small change of the systematic image errors between the first and the second block part of the lower flying height can be seen, but with 0.5  $\mu\text{m}$  or 0.04 pixels in the mean square it can be neglected in the bundle block adjustment. Thus need for 2 different sets of parameters for the first and second block part of the lower flying height is not proven, which indicates the stability of the camera system.

The remaining systematic image errors (cf. Fig. 3 lower part) of the block adjustments with the 12 basic additional parameters are limited. For the lower flying height it is similar, for the upper flying height it is different, but some similarities can be seen. With sub-block specific additional parameters the results of the block adjustment with DMC images have been slightly improved, even if the effect to the systematic image errors is limited for the case of the DGPF test and can hardly be seen in later check point differences in object space. Thus, division of blocks and the use of different sets of self-calibration parameters for those smaller sub-blocks or groups of images are not applied in later adjustments presented in section 5.

Within the test similar investigations have been made with the other cameras, leading to similar results. The systematic image errors and the remaining systematic effects show only small differences between the first and the second block part. In no case it was justified to handle the block parts with different sets of additional parameters. In other words: a significant change of the systematic image errors within the blocks cannot be seen. Independent upon earth curvature and refraction correction the image geometry is changing more between the lower and the upper flight level. So a system calibration in one flight level cannot lead to the full accuracy potential if it will be used as a pre-correction for the other flight level if no self-calibration is used again.

## 5 Bundle Block Adjustments

Tab. 4 and 5 give an overview over the different strategies used by the participants for evaluation of the camera systems. Note that for several camera systems different parameter sets, GCP configurations and integration methods for GPS/IMU data have been tested by the participants. They are tagged by a version number which is also given in the graphical presentation of the various results (see Figs. 4–9).

As mentioned above, different strategies have been used by the participants for the evaluation of the camera data sets. In order to illustrate the performance of area based cameras, not overlaid by effects from direct sensor orientation, block adjustments without GPS/IMU data have been made by the Leibniz University Hannover (UH). This is also the case for systems which are used without GPS/IMU-sensors. Nevertheless, even though additional GPS/IMU sensors are only optional for large format frame based sensors DMC and UltraCamX in principle, almost all of the systems are equipped with such devices. These integrated systems are mandatory part of the line scanning sensors and also advantageous for multi-head medium format sensors, where the images are not merged to form a large format virtual image (see later discussion on the Quattro-DigiCAM data analysis).

**Tab. 4:** Configurations of bundle block adjustments of CCD-array cameras.

Cam. System	Institution	Tie Point	Bundle Adjustm.	#ADPA	GPS / ISO	#GCP 8 cm/20 cm	#ChP 8 cm/20 cm
DMC	UH	Match-AT (LVG M)	BLUH	12	no	9/9	45/95
	US	Match-AT	Match-AT	44 (Grün)	ISO	4/4	113/180
	TUV	Match-AT	Orient	Ebner+4	GPS	8/8	52/99
UCX	UH	Match-AT (LVG M)	BLUH	12	no	9/9	99/99
	US	Match-AT	PAT-B DGAP	44 (Grün)	ISO	4/4	111/180
	TUV	Match-AT	Orient	Ebner+4	GPS	8/8	52/99
RMK-Top15	UH	Match-AT (LVG M)	BLUH	1: 0 2: 12	no	14/14	40/82
	US	Match-AT	Match-AT	1: 0 2: 12 (Eb.) 3: 44 (Gr.)	no	14/14	107/172
	TUV	Match-AT	Orient	Ebner+4	GPS	8/8	49/93
	TUG	ISAT	PhoBA	5 (Brown subset)	1+2: GPS 3: no	59/82 5/5 5/5	56/67 110/77 110/77
Quattro-Digi-CAM	UH	ERDAS	BLUH	1: 4x12 2: 4x20	no	10/15	28/91
	US	Match-AT	Match-AT	4x12 (Ebner)	ISO	4/4	114/161
	TUG	Match-AT (IGI)	PhoBA	5 (Brown subset)	1+2: ISO 3: no	57/104 5/5 5/5	56/69 108/168 108/168
AICx1	UH	Uni Düsseldorf	BLUH	1: 0 2: 12 3: 20	not av.	47/-	10/-
	US	Match-AT	Match-AT	44 (Grün)		60/-	50/-

**Tab. 5:** Configurations of bundle block adjustments of CCD-line scan cameras.

Camera System	Institution	Tie Point Generation	Bundle Adjustm.	#ADPA	ISO	#GCP 8 cm/20 cm	#ChP 8 cm/20 cm
ADS40	UH	GPRo	ORIMA	0	ISO	9/-	52/-
	US	GPRo	ORIMA	6	ISO	4/4	121/182
JAS-150	RAG	Jena Optronik Software	BINGO	12	ISO	1: 0/0 2: 4/4 3: 19/19	75/105 71/101 56/85

**Tab. 6:** Abbreviations used in the graphical presentations.

p60 / p80	60% / 80% end lap	apE12	12 additional param. (Ebner)
q20	20% side lap	apE16	12 Ebner + 2 radial + 2 tang.
cr0 / cr2	0 / 2 crossing strips	apG44	44 additional parameters (Grün)
nDS	No direct sensor orientation	apB12	12 additional param. (BLUH)
GPS	Combined adjustment with GPS	apB20	apB12+parameters 81–88
ISO	Integrated sensor orientation	apBN12	12 additional param. (BINGO)
0ap	No self calibration	apBRs	Brown subset with 5 parameters

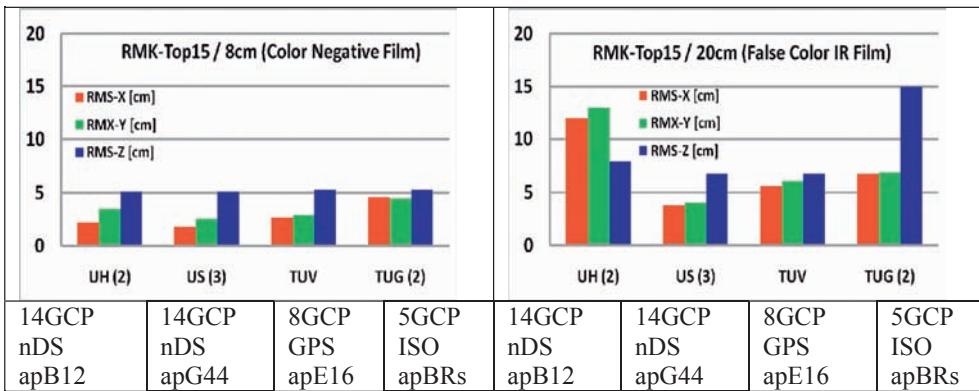


**Fig. 4:** RMS values from check point analyses RMK-TOP15 (overlap by camera system: p60, cr2).

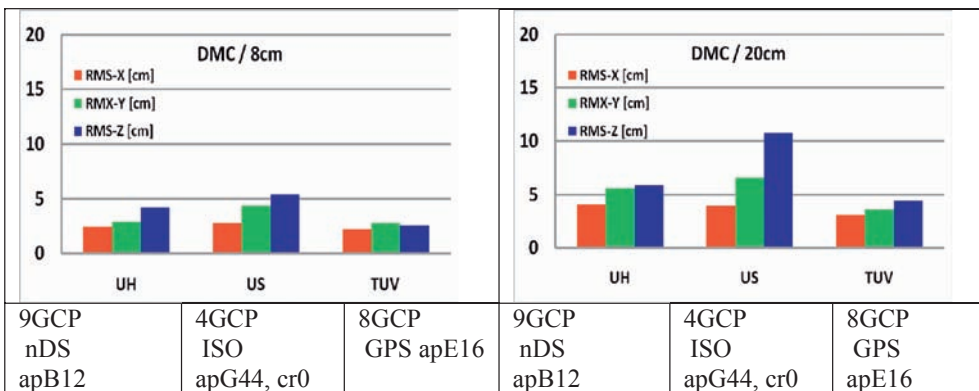


**Fig. 5:** RMS values from check point analyses DMC (overlap by camera system: p60, cr2).

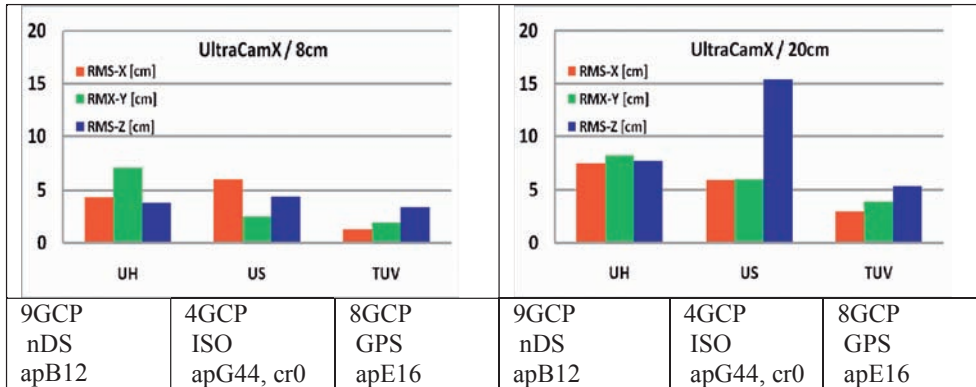


Fig. 6: RMS values from check point analyses UltraCamX (overlap by camera system: p80, cr2).

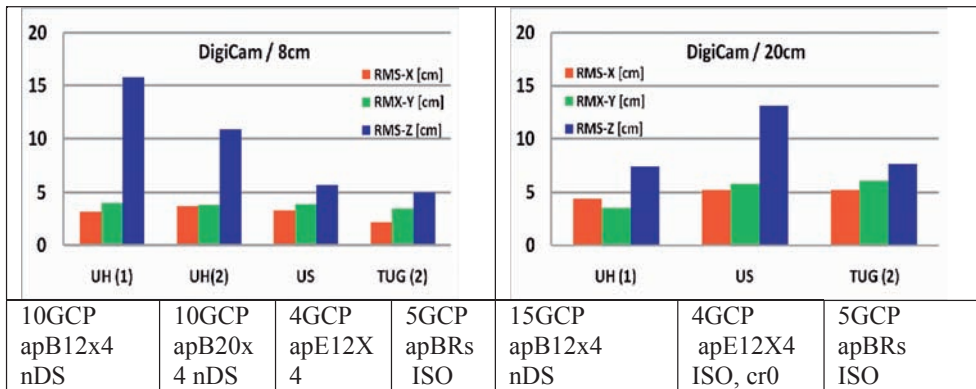


Fig. 7: RMS values from check point analyses Quattro-DigiCAM (overlap by camera system: p60, q60).

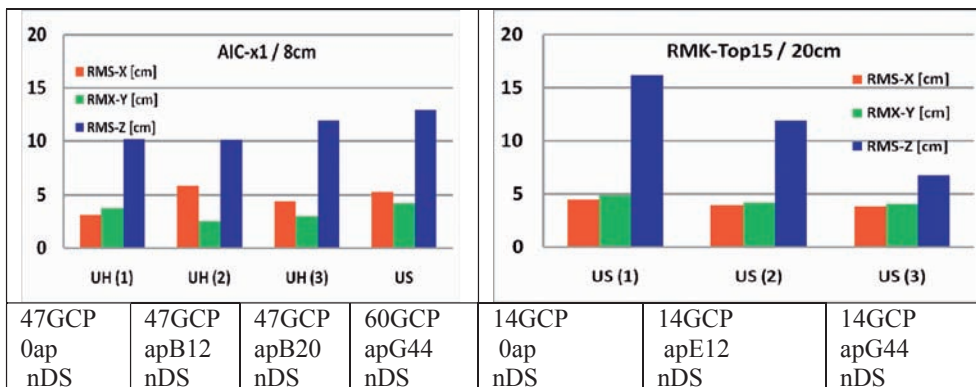


Fig. 8: RMS values from check point analyses AIC-x1 (left, cr0) and RMK-TOP15 (with the use of different additional parameter sets).

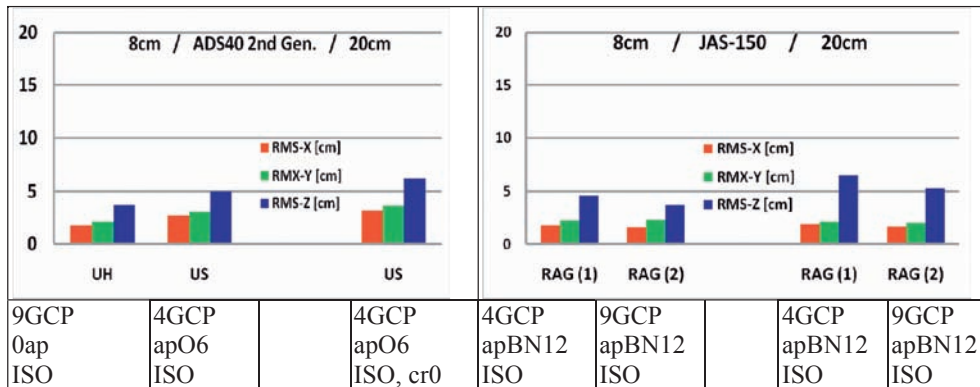


Fig. 9: RMS values from check point analyses ADS40 (left) and JAS-150 (right).

The Vienna University of Technology (TUV) preferred combined block adjustments with GPS-coordinates of the projection centres. From their investigation results from that were more accurate than using GPS/IMU data in integrated sensor orientation. The block adjustments of the University of Stuttgart (US) and Graz University of Technology (TUG) in most cases have been performed as integrated sensor orientation. Note that different direct sensor orientation equipment was used and this may dominate the results based on it more as the camera geometry itself.

For adjustments of University of Stuttgart no cross-strips (even though mostly available for all the flights) were introduced, in order to simulate a more operational like environment where often no cross-strips are flown, especially when integrated GPS/inertial systems are available.

Integrated sensor orientation causes an advantage for blocks with less strong image connections. In case of blocks having a limited size and good image connections, a non optimal modeling of systematic errors can cause a negative influence because proper weighting and separation of systematic errors from random errors are more difficult.

In the following figures, the RMS values at independent check points are presented with the dimension [cm]. The information 8 cm corresponds to the data sets based on 8 cm GSD, while 20 cm corresponds to 20 cm GSD. For better interpretation, some key information about the evaluation strategy used is given

below each graph. The exact meaning for each abbreviation is given in the following table. The results of the different block adjustments shown in Figs. 4 up to 9 show the large varieties of the solutions. It's not possible to directly compare the results of the different camera systems because the flight conditions have been different and also the end lap is varying between 60 % and 80 %. Even more, for one camera system results depend upon the different configurations used, as just based on GCPs, use of combined adjustment with relative cinematic GPS-positions of the projection centres or integrated sensor orientation, using the integrated GPS/inertial trajectory information for exterior orientation plus image and ground control points. In addition different sets of additional parameters have been used.

The influence of the sets of parameters to the block adjustment becomes very clear in Fig. 8 right hand side (exemplarily shown for the traditional RMK data set, but also similar for the other systems). Especially the height is strongly influenced by the radial component of systematic image errors as it is obvious at the Ebner parameters having problems to compensate radial symmetric and tangential image errors. With the 44 Grün parameters such effects can be compensated more efficiently, reducing the root mean square differences at independent check points drastically. The results from University of Stuttgart, shown above, are (mostly) based on the Grün parameter set (except for Quattro-DigiCAM). Vienna University of Technology extended

the Ebner parameters by two radial symmetric and two tangential additional parameters. Such parameters are included in the program system BLUH, so such problems did not appear. The Graz University of Technology even with just a subset of 5 Brown additional parameters was able to avoid such a problem of the Ebner parameters as shown in Fig. 8, right hand side.

The influence of exterior sensor orientation parameters is quite depending upon the block configuration and the number of GCPs, which can be seen from the Quattro-DigiCAM (see Fig. 7). The four images of the Quattro-Digi-Cam, taken at the same time, are not stitched together to a virtual image; they are handled as individual images during adjustment and later product generation. The 60% side lap of the system of 4 images corresponds only to a block with 20% side lap regarding to virtual images (see Fig. 10). This leads to a very strong influence of systematic image errors to the achieved results, which has to be compensated by additional parameters. If self-calibration is done properly, quite reasonable results can be obtained even without using directly measured exterior orientation elements. Still GPS/IMU components are an inherent part of the Quattro-DigiCAM product and use of directly measured exterior orientations is standard approach for processing such data sets. Thus, results shown in Fig. 7 not using direct sensor information are not corresponding to the recommended operational scenario, even if the accuracy has been strongly improved by self-calibration. For 20 cm GSD on the first view it seems to be different, but the different number

of GCPs has to be taken into account. It should be mentioned that IGI now also offers merged large format virtual images as an optional product from Quattro-DigiCAM. This type of image product was not considered in the DGPF test evaluations.

The standard deviation of the manual measurements of control and check points shown in Fig. 1 also demonstrate the strong influence of the point identification in the images. Especially in the RMK Top15 images with 20 cm GSD the exact identification of the points in the images is very difficult – here the operators of the University of Stuttgart benefited by quite better knowledge of the exact point location. In the other data sets some manually measured image positions had to be excluded from the block adjustment because of exceeding the tolerance limit. In general the results reached by the Vienna University of Technology does not correspond very well with the results coming from the other participants, while the range of the results by the other participants can be explained by the different handling parameters.

Because of weather conditions during photo flight for the Rolleimetric AIC-x1 only images with 8 cm GSD and 60% side lap and no crossing flight lines exist. It was the explicit wish of the system provider to do the flight test with a “low-cost data acquisition scenario”, i. e., using a very small aircraft without additional GPS/inertial components and effective camera stabilization. This finally leads to very strong variations of the orientation elements with up to  $\pm 4.0$  grads in phi,  $\pm 11$  grads in omega and  $\pm 5$  grads in kappa. As example

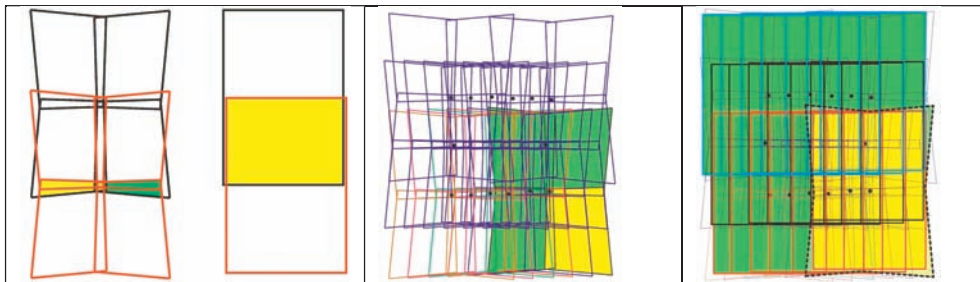


**Fig. 10:** Overlap and image tie – left: connection of images of a 4-image combination in relation to virtual images – both with 60% side lap, centre: connection of one image of a 4-image combination in a block with 60% side lap of the camera system, right: connection of images joined together to virtual images in a block with 60% side lap of the camera system.

the most north located flight line has partially only 40 % instead of 60 % side lap. No direct sensor orientation was available, requiring a high number of GCPs. The large size of systematic image errors is not influencing the block adjustment itself, it only has to be considered for the handling of the models. For the not optimal conditions of the block the achieved results are still satisfying (see Fig. 8), but they cannot be compared with the results based on the other cameras. Still, for operational projects more regular flights and use of directly measured exterior orientations (at least GPS perspective centre coordinates) should be recommended.

The point determination from the line scanning cameras ADS40 and JAS150 are on a very good accuracy level (cf. Fig. 9). The obtained accuracy of both systems is very similar and is fully comparable maybe also superior to the results obtained from frame based sensors. It is also interesting to see that results from GSD 20 cm and GSD 8 cm blocks from JAS-150 are almost of same accuracy, which should not be expected. Similar to all other data sets these results are based on these test flight evaluations only, and have to be verified from other data sets.

## 6 Conclusions

There is no more reason to use analogue photos instead of original digital images. Even with the wide angle RMK Top15 under approximately comparable conditions not the same vertical accuracy has been reached as with the large format digital aerial cameras. In addition the less optimal image quality from analogue scanned images became obvious at the manual identification of the control and check points in the images with 20 cm GSD. This also will be of importance for later DSM generation.

The line scanning cameras ADS40 and JAS-150 are providing quite good results. Of course the available test sites are limited in size, so an extrapolation to larger areas may be difficult. The handling for data acquisition following the orientation process still requires special software, which is not available in several locations.

The large format digital frame cameras DMC and UltraCamX confirmed their potential. The image geometry itself is somehow mixed with the influence of integrated sensor orientation or by combined block adjustment with GPS-coordinates of the projection centres, but this is realistic for operational application. Of course the limited test site does not allow a direct extrapolation to large blocks.

Using direct sensor orientation based on the results of the integrated GPS/IMU system, the Quattro-DigiCAM shows results that are comparable to results of the large format systems. This is different when larger blocks using individual images from camera heads are processed without GPS/IMU support and limited number of control points. Also the single mid-format camera Rolleimetric AIC-x1 can cover some important applications.

In general sub-GSD-accuracy can be reached especially for the horizontal component, but also in most cases for the vertical component of ground coordinates determined by block adjustment. This should not be mixed with the accuracy of photogrammetric data acquisition in stereo models which is just based on two images, while the block adjustment is using several images per object point. Depending upon the end and side lap the number of images per point for the block adjustment varies between 3.2 (Rolleimetric AIC-x1) over approximately 6 for blocks with 60 % end and side lap up to 10.6 for the block with 80 % end lap and 60 % side lap. In addition not all software packages for model handling are able to respect systematic image errors, leading to model deformation especially in the vertical component.

## References

- BROWN, D.C., 1971: Close-range camera calibration. – *Photogrammetric Engineering* 37 (8): 855–866.
- DÖRSTEL, C., 2007: DMC – (r)evolution on geometric accuracy. – *Photogrammetric Week '07*, Wichmann Verlag, 81–88.
- EBNER, H., 1976: Self Calibration Block Adjustment. – *Bildmessung und Luftbild*: 128–139.
- GRÜN, A., 1976: Die simultane Kompensation systematischer Fehler mit dem Münchener Bündelprogramm MBOP. – *ISP Congress Helsinki*.

- JACOBSEN, K., 2007: Geometric handling of large size digital airborne frame camera images. – Optical 3D Measurement Techniques **VIII**: 164–171.
- KRUCK, E., 1983: Lösung großer Gleichungssysteme für photogrammetrische Blockausgleichungen mit erweitertem funktionalen Modell. – Wiss. Arbeiten d. Univ. Hannover **128**.
- PASSINI, R. & JACOBSEN, K., 2008: Accuracy analysis of large size digital aerial cameras. – International Archives of Photogrammetry, Remote Sensing and Spatial Information Sciences **37** (B1): 507–51.
- WU, D., 2007: Geometric aspects of large size digital frame cameras and their use for photogrammetric data acquisition. – Diploma thesis, Leibniz University Hannover.

## Adressen der Autoren:

Dr.-Ing. KARSTEN JACOBSEN, Leibniz Universität Hannover, Institut für Photogrammetrie und Geoinformation, D-30167 Hannover, Nienburger Str. 1, e-mail: jacobsen@ipi.uni-hannover.de.

Dr.-Ing. MICHAEL CRAMER, Universität Stuttgart, Institut für Photogrammetrie (ifp), D-70174 Stuttgart, Geschwister-Scholl-Straße 24 D, e-mail: michael.cramer@ifp.uni-stuttgart.de.

Dr.-techn. RICHARD LADSTÄDTER, Laboratoriumstr. 29b, A-8053 Graz, Österreich, e-mail: richard.ladstaedter@alumni.tugraz.at.

Dr.-techn. CAMILLO RESSL, Technische Universität Wien, Institut für Photogrammetrie und Fernerkundung, A-1040 Wien, Österreich, Gußhausstraße 27–29, e-mail: car@ipf.tuwien.ac.at.

VOLKER SPRECKELS, RAG Deutsche Steinkohle, Geschäftsbereich Geoinformation / Vermessung BG G D-44623 Herne Shamrockring 1, e-mail: volker.spreckels@rag.de.

Manuskript eingereicht: Dezember 2009

Angenommen: Januar 2010





## Digital Photogrammetric Camera Evaluation – Generation of Digital Elevation Models

NORBERT HAALA, Stuttgart, HEIDI HASTEDT, Birmensdorf, Switzerland, KIRSTEN WOLF,  
Zurich, Switzerland, CAMILLO RESSL, Vienna, Austria & SVEN BALTRUSCH, Schwerin

**Keywords:** Three-dimensional, point cloud, LiDAR, image matching

**Summary:** During the implementation of the DGPF-project on Digital Photogrammetric Camera Evaluation a team “Digital Elevation Models” was established. The main goal was to use the test’s framework for documentation and evaluation of the current state-of-the-art on photogrammetric 3D data capture from automatic image matching. During these investigations the accuracy and reliability of DSM rasters and 3D point clouds as derived from imagery of digital photogrammetric camera systems were evaluated. For this purpose they were compared to reference measurements from ground truth and airborne LiDAR. In addition to the evaluation of standard products, the usability of elevation data from image matching was investigated while aiming at specific applications in the context of urban modeling and forestry.

**Zusammenfassung:** *Digitale photogrammetrische Kamera Evaluierung – Generierung von Digitalen Höhenmodellen.* Während des DGPF-Projektes zur Evaluierung digitaler photogrammetrischer Luftbildkamerasysteme wurde auch eine Auswertegruppe für die Bewertung der Genauigkeit der Höhenmodellgenerierung etabliert. Dabei sollte der DGPF-Test genutzt werden, um den derzeitigen Stand der Technik der photogrammetrischen 3D Erfassung mittels automatischer Bildzuordnung zu dokumentieren. Hierfür wurden DSM Raster und 3D Punktwolken aus Bildern der photogrammetrischen Kamerasysteme abgeleitet und die Qualität dieser Ergebnisse in Bezug auf Genauigkeit und Zuverlässigkeit bewertet. Dabei wurde ein Vergleich zu terrestrischen Referenzmessungen und flugzeuggestützten LiDAR Daten durchgeführt. Neben der qualitativen Bewertung von Standardprodukten wurde auch die Nutzbarkeit der Höhen- daten für spezielle Anwendungen beispielsweise im Kontext der 3D Stadmodellierung und Forstwirtschaft untersucht.

### 1 Introduction

High image dynamic and good signal-to-noise ratio are well known advantages of digital photogrammetric cameras. Compared to the use of scanned analogue images, these improvements of digital imagery are especially advantageous with respect to the accuracy, reliability and density of automatic point transfer. Thus, follow-up products like Digital Elevation Models, which are based on the use of automatic image matching, will potentially benefit, if digital photogrammetric camera systems are used. This progress can be demonstrated and documented very well using comprehensive test data sets as available with-

in the DGPF project on Digital Photogrammetric Camera Evaluation. In order to investigate the current state-of-the-art on image based generation of elevation data, which of course also influences the usability of such products, a special working group with members mainly from academia and administration was established. While the general goal of the DGPF project was to comprehensively analyze photogrammetric digital airborne camera systems, within this group the impact of the captured image data to the available quality of digital elevation models was investigated.

In order to evaluate the quality of such a photogrammetric product, the analysis can of

course not be restricted to image collection but has to pay attention to the respective software for the following data processing. Commercial software systems aiming at the generation of Digital Terrain Models from image matching were already introduced more than two decades ago (KRZYSZEK 1991, COGAN et al. 1991). Nevertheless, the improvements in the available quality of aerial imagery triggered a renaissance in software development to optimally benefit from these advancements. As an example, digital airborne camera systems can capture largely overlapping images at a relatively little additional effort. The availability of such high redundant multi-image information is especially beneficial in situations, where standard stereo matching is hindered due to occlusions. Algorithms which fully exploit this potential of digital aerial cameras by extending the traditional stereo matching to a multiple image matching have been implemented just recently. Such commercial software systems, which will also be used for our investigations are Next Generation Automatic Terrain Extraction (NGATE) from BAE Systems (DEVENEZIA et al. 2007), MATCH-T DSM from INPHO GmbH (LEMAIRE 2008) and SATellite image Precision Processing (SAT-PP) of the ETH Zürich (ZHANG & GRUEN 2004).

One general problem during the evaluation of height data from image matching is to separate the influence of the respective factors on the resulting quality. Major impact results from the quality of the available image data and the sophistication of the used matching algorithms. Additionally, the geometric complexity of the respective object surfaces is of considerable influence. An important factor for image quality is the accuracy and stability of its reconstructed geometry. This is again affected by the geometric configuration of the image block, the geometric stability of the camera and the accuracy and reliability of the camera model. Additionally, image quality depends on the signal-to-noise-ratio of the digitized image signal, which is again influenced by the quality of the sensor system but also by the respective illumination and texture of the depicted surface patches. Finally, the generation of elevation data is influenced by the respective algorithms applied for automatic

point transfer or surface interpolation and filtering. Thus, the wide range of interacting factors, which mutually influence the quality of the generated data complicates a comprehensive analysis of automatic image based elevation measurements.

In our opinion, in addition to a comparative analysis of the respective accuracies, application driven investigations are of even greater interest for potential users. For this reason, accuracy analyses using suitable reference data are complemented by investigations on the usability of elevation data from image matching. Within the paper, special interest is paid to tasks like city model generation or applications in forestry. Firstly, the available test and reference data will briefly be introduced in the following Section. In Section 3 signalized points and selected planar areas are used as reference for a comprehensive analysis of elevation data generated from different imagery and software systems. The quality and usability of DSM from image matching for different applications like data collection in urban areas, investigations in forestry and DTM generation will be discussed in Section 4, while Section 5 will conclude the paper.

## 2 Test Scenario and Reference Data

Within the investigations presented in this paper data sets from the cameras DMC, ADS 40 2<sup>nd</sup>, UltraCamX, Quattro DigiCAM and RMK-Top15 captured at two different flying heights and block configurations were used. In addition to the terrestrial reference points, LiDAR data was made available for comparison to the DSMs from image matching.

### 2.1 Block Configuration and Image Processing

For investigations on the elevation data generation from image matching, the availability of different ground sampling distances [GSD] and image overlaps is of special interest. This was the reason to plan the collection of image blocks with 20 cm GSD and 60% along- and across-track-overlap as well as flights with

GSD 8 cm and 80 % along- 60 % and across-track-overlap. Due to variations of the different cameras footprint and restrictions from the available ground control, slight deviations from this configuration had to be accepted. The parameters of the investigated camera systems as well as the test design including the respective block configurations are documented in more detail by (CRAMER 2010). During our investigations DSM grids with 0.2 m/0.25 m and 0.5 m raster width were computed for the 8 cm and 20 cm GSD flights in the central of  $5.0 \times 2.7 \text{ km}^2$  area of the test field.

### 2.2 Preprocessing and Accuracy Analysis of Collected LiDAR Data

For investigating the height accuracy of the derived height models, 63 reference ground points were made available to the test participants (see Section 3). This way, however, the height accuracy can only be checked at discrete locations. For a continuous accuracy check the entire area was therefore surveyed by LiDAR. In total 10 strips were captured with a Leica ALS50 system at  $45^\circ$  FOV with a mean flying height above ground of 500 m and

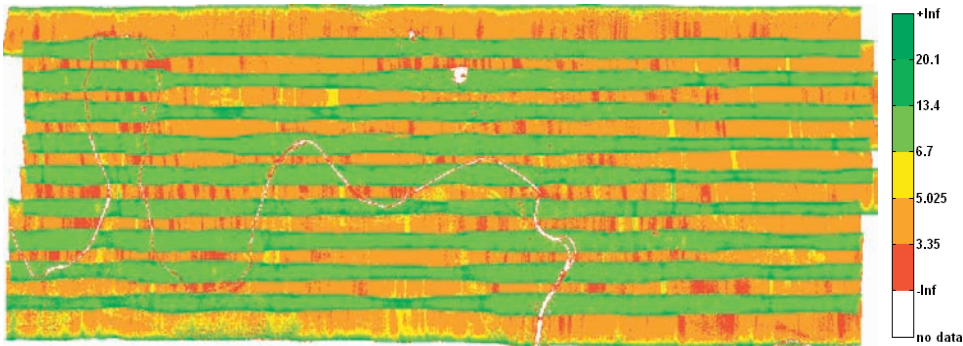


Fig. 1: Color-coding of the point density of all 10 LiDAR strips. The legend is in points/m<sup>2</sup>.



Fig. 2: Sample of a color-coded strip difference for the original georeferencing (top) and for the improved georeferencing after strip adjustment (bottom). Right: Legend of color coding. Black is used for the area outside the overlap of neighboring strips, but also for the parts covered by the roughness mask.

a mean strip overlap of 30 %. The median of the point density is 6.7 points/m<sup>2</sup>, however, the point density varies a lot over the whole block (see Fig. 1). Regions covered by only one strip have a mean density of 4 points/m<sup>2</sup>.

In order to use the LiDAR data as a reference for the height models derived from the aerial images, the georeferencing of the LiDAR data should be checked in advance. A simple and effective tool for checking the quality of the relative orientation of the LiDAR strips are strip differences (RESSL et al. 2008). For this a DSM is interpolated for each strip (with 1 m grid width) and then the difference of pairs of overlapping strip DSMs is computed. Because of the interpolation involved, the differences derived at rough surface areas, e. g., vegetation, are not suitable for judging the accuracy. For considering only smooth surfaces a roughness mask for each strip is used (RESSL et al. 2008).

Fig. 2 (top) shows a sample of a color-coded masked strip difference for the original georeferencing and Fig. 3 (left) shows the histogram of all 9 masked strip differences between the 10 strips. From this histogram a  $\sigma$ MAD value of 4.5 cm is derived for the masked strip differences.  $\sigma$ MAD is the standard deviation derived from the median of absolute differences (the so-called MAD) as  $\sigma$ MAD = 1.4826 · MAD. Although 4.5 cm may appear acceptable, the color-coding reveals large systematic errors visible at the buildings. There the large vertical differences exceeding 18 cm are caused by horizontal displacements between the neigh-

boring strips (i.e. errors of the relative orientation), which themselves result from residual errors in the individual system components: GNSS (Global Navigation Satellite System), INS (Inertial Navigation System), the laser scanner and the mounting calibration (which describes the rotation and translation between these individual components).

In order to minimize the systematic error patterns visible in the color-coded strip differences, a LiDAR strip adjustment was performed following the procedure described by (KAGER 2004). For this the GNSS/INS trajectory of the strips and 1110 corresponding tie planes were used in order to correct internal systematic errors (like a wrong mounting calibration) and to improve the relative orientation of the strips by minimizing the residuals at corresponding planes in the strips. For comparing the LiDAR data with the DSMs derived from the images, both should refer to the same datum. Therefore the absolute orientation of the LiDAR data should be adapted in case their GNSS/INS data refers to a wrong datum. However, no suitable ground control planes for the LiDAR data were available from terrestrial measurements. Therefore, 49 ground control planes were derived from the aerial triangulation (with available ground control points) of the DMC photos with 8 cm GSD. These control planes were used simultaneously in the strip adjustment together with the tie planes. This entire LiDAR strip adjustment therefore can very much be compared with block adjustment by integrated sensor orienta-

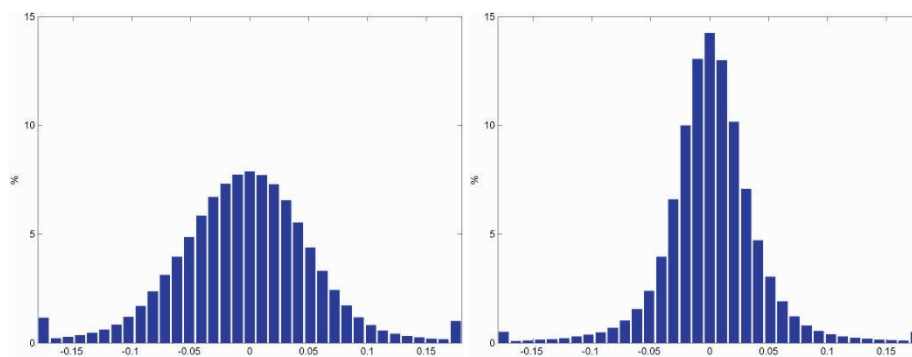


**Fig. 3:** Histogram of the strip differences (considering the roughness mask) based on all overlapping strips (ca. 6.5 million values). Left: original georeferencing ( $\sigma$ MAD = 4.5 cm). Right: improved georeferencing after strip adjustment ( $\sigma$ MAD = 2.9 cm).

tion in case of aerial images. The effect of the strip adjustment on the LiDAR data in flight direction is 1cm (mean), 13 cm (RMS) and 44 cm (max), across flight direction -6 cm (mean), 10 cm (RMS) and -23 cm (max), in height 0 cm (mean), 3 cm (RMS) and -15 cm (max). After the strip adjustment new strip differences were computed; see Fig. 2 (bottom). By comparing top and bottom of Fig. 2 one can clearly see that the systematic errors are largely removed. Fig. 3 (right) shows that the  $\sigma$ MAD of the strip differences improves from 4.5 cm to 2.9 cm.

Although the images are now used to adapt the reference LiDAR data, the effect on the later is only in the absolute orientation. The positive effect is that deviations between the DSM from the LiDAR data (with the improved georeferencing) and the DSM derived from the images cannot be attributed to residual orientation errors, but can primarily be attributed to the different quality of the local surface description of the LiDAR data and the DSM derived from the images. Although in this comparison it should be considered, that another LiDAR flight (with different flying height and/or point density) would give a different result.

### 3 Accuracy Investigations for DSM and Point Clouds

The Vaihingen/Enz photogrammetric test site where the flight campaigns of the DGPF test were realized consists of approximately 200 signalized and coordinated reference ground points, distributed in a  $7.5 \times 5.0$  km<sup>2</sup> area. The central area of the test field, where the investigations on elevation data generation from image matching were concentrated has a size of  $5.0 \times 2.7$  km<sup>2</sup> with approximately 63 reference ground points available for the test participants. The coordinates of all reference points were determined with static GPS base line observations, which provide an accuracy of 1 cm for horizontal and 2 cm for vertical coordinates. Using the vertical differences between the elevation data from image matching and the available reference points a quality estimate can be realized. For our investigations, DSM grids of 0.2 m raster width were generated from the 8 cm GSD imagery of the UltraCamX, Quattro DigiCAM and the scanned RMK images using the software MATCH-T DSM. Similarly, the 20 cm GSD blocks were used for computation of 0.5 m raster DSM grids. From these DSM, differences to the signalized points were computed and further analyzed. The results of these analyses are summarized in Tab. 1.

**Tab. 1:** Differences between DSM and reference points after gross errors elimination – MATCH-T DSM.

	Sensor	RMS [cm] no gross errors	Mean [cm]	$\Delta$ Max/Min [cm]		# points
LiDAR	ALS 50	3.3	0.4	9.4	- 6.7	59
GSD 8 cm	DMC	3.3	0.9	9.5	- 6.9	60
	UltraCamX	4.8	0.6	11.7	-10.0	60
Raster 0.2 m	DigiCAM	6.0	-1.7	15.5	-15.7	61
	RMK	4.6	2.4	8.2	-11.5	61
GSD 20 cm	DMC	16.2	-7.5	36.9	-30.5	61
	UltraCamX	7.5	-0.7	14.9	-16.8	60
Raster 0.5 m	DigiCAM	9.6	0.5	18.9	-23.1	61
	RMK	9.5	0.7	23.9	-25.9	61

As it is visible in the first column of Tab. 1, DSM grids with 0.2 m and 0.5 m raster width were computed for the 8 cm and 20 cm GSD flights, respectively. The second column gives the investigated camera systems DMC, UltraCamX, Quattro DigiCAM and RMK-Top15. As it is also visible, a DSM as generated from the available LiDAR flight was evaluated for comparison. The third column of Tab. 1 gives the RMS values calculated from the filtered differences between reference point and respective DSM surfaces. An analysis of all differences between the respective DSM and the available reference points shows, that in all cases the largest differences occur at areas potentially compromised to occlusions. In order to eliminate these potential gross errors, a simple threshold was used. First a RMS value was calculated from the height differences to all signalized points, which were available for the respective DSM area. In a second step all points with differences outside a range of  $\pm 3 \cdot \text{RMS}$  were eliminated as gross errors and the remaining differences were used to calculate the filtered RMS. Typically, one or two points were filtered out from the complete of signalized points. This was sufficient for our investigation. However more advanced methods for accuracy assessment of digital elevation models by means of robust statistical method are for example described in (HÖHLE & HÖHLE 2009). Tab. 1 also gives the mean as well as the maximum and minimum values  $\Delta \text{Max/Min}$  from all differences for each DSM. Again the point set with gross errors eliminated was used to calculate these values. The final column gives the number of points after filtering.

While the results in Tab. 1 are based on the use of the software MATCH-T, Tab. 2 shows the results for the DSM grids alternatively generated with BAE Systems NGATE. There the camera systems ADS 40, DMC and UltraCamX were investigated, while DSMs were computed with 0.25 m and 0.5 m raster width for the 8 cm and 20 cm flights, respectively.

As given in Tab. 1, the RMS value for the LiDAR DSM measured by the ALS 50 sensor is 3.3 cm. This is almost in the order of the vertical accuracy of the used reference points. Compared to this accuracy, the RMS values of the DSMs for the DMC, UltraCamX, Quattro DigiCAM and ADS 40 as given in Tab. 1 and 2 are only slightly larger. They correspond very well to the vertical component of the preceding block adjustment, which gave an accuracy of  $\frac{1}{2}$  GSD (JACOBSEN et al. 2007). Typically, the ground control points used to evaluate the DSM quality in Tab. 1 and 2 were installed at paved areas like small roads or parking lots. Such flat neighborhoods are of course beneficial for the filtering and interpolation process during DSM raster generation. For this reason, the results presented in Tab. 1 and 2 might give too optimistic accuracies for regions of higher geometric complexity. As an alternative 3D point clouds can be used to evaluate the matching quality during accuracy analyses without the influence of interpolation processes. Such point clouds can be optionally generated from modern photogrammetric software systems, and can for example be used as an alternative to the traditional 2.5D raster representations of Digital Surface Models during tasks like 3D object reconstruction.

**Tab. 2:** Differences between DSM and reference points after gross errors elimination – NGATE.

	Sensor	RMS [cm]	Mean [cm]	$\Delta \text{Max/Min}$ [cm]		# points
		No gross errors				
GSD 8 cm Raster 0.25 m	ADS 40	6.7	-1.1	13.9	-18.1	57
	DMC	4.4	-1.2	9.0	- 8.8	53
	UltraCamX	7.2	1.6	16.1	-11.8	59
GSD 20 cm Raster 0.5 m	ADS 40	4.8	1.9	12.9	- 8.8	60
	DMC	19.0	-2.7	51.3	-31.4	61
	UltraCamX	11.5	1.6	27.2	-21.6	61

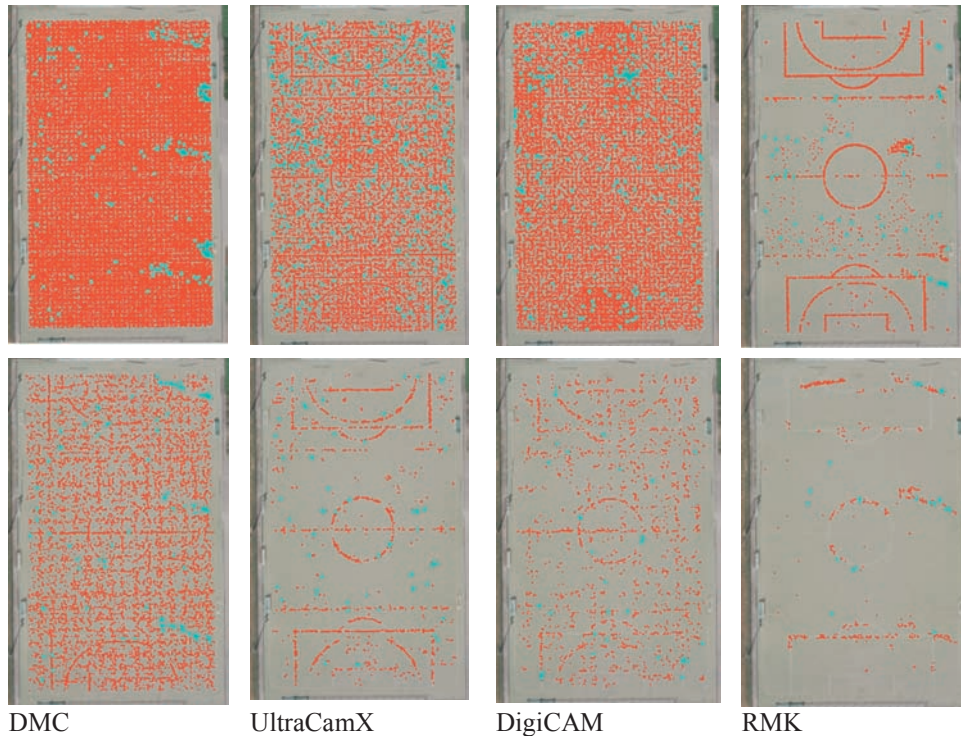


**Fig. 4:** Point clouds for investigated camera systems generated by MATCH-T DSM. The top row shows the results for the 8 cm GSD block, the bottom row for the 20 cm GSD block.

Within our investigations 3D point clouds were computed and evaluated for the data from the frame based camera systems DMC, UltraCamX, Quattro DigiCAM and RMK-Top15. In order to evaluate the accuracy of the generated 3D point clouds by a relatively simple process, a test area at a planar sports field was defined. The respective point clouds as generated from MATCH-T DSM are depicted

in Fig. 4. Results for the 8 cm GSD blocks are shown in the top row, while the matching results from the 20 cm GSD blocks are presented in the bottom row.

Since the matched 3D points are restricted to a planar area, their geometric accuracy can be determined based on the estimation of an approximating plane. After a best fitting plane is determined the perpendicular point distanc-

**Tab. 3:** Accuracy of 3D point clouds MATCH-T DSM and NGATE – GSD 8 cm.

Sensor	STD after filter [cm]		STD no filter [cm]		Elim.Pts [%]		Density Pts/m <sup>2</sup>	
	M-T	NGATE	M-T	NGATE	M-T	NGATE	M-T	NGATE
DMC	5.2	2.1	9.7	2.3	1.3	0.9	19.7	8.2
UltraCamX	6.8	13.1	8.0	15.6	0.4	1.5	19.0	8.2
DigiCAM	10.2		11.2		0.7		20.8	
ADS 40		2.3		2.6		0.7		8.2
RMK	17.2		27.3		3.2		0.8	
ALS 50	1.8		1.9		0.5		8.25	

**Tab. 4:** Accuracy of 3D point clouds MATCH-T DSM and NGATE – GSD 20 cm.

Sensor	Stdv. after filter [cm]		Stdv. no filter [cm]		Elim.Pts [%]		Density Pts/m <sup>2</sup>	
	M-T	NGATE	M-T	NGATE	M-T	NGATE	M-T	NGATE
DMC	17.2	7.5	25.4	9.1	1.1	1.7	2.7	4.0
UltraCamX	22.6	25.0	34.2	38.1	0.4	1.0	1.6	2.6
DigiCAM	34.1		48.2		2.5		2.6	
ADS 40		7.4		8.3		1.4		4.0
RMK	60.6		66.2		0.7		0.3	

es are used to determine the respective standard deviations, which represent the accuracy of 3D point measurement. Again, a threshold is used to eliminate points outside a range of  $\pm 3$ -RMS. These erroneous points usually correspond to shadow areas from the goals and the floodlight poles. Such time dependent shadow movement can result in considerable errors of automatic point transfer especially if high resolution images from different strips are matched. Within Fig. 4 points eliminated by the filter process are marked in light blue, while the remaining points are shown in red.

Tab. 3 and 4 summarize the results of point cloud analysis. There, the standard deviations from the matched points are given in addition to the percentage of points eliminated in this filtering process. The final column gives the point density as provided from image matching, which is an important indicator for the quality of this process. Using the software MATCH-T DSM, on average, a point density of about 20 pts/m<sup>2</sup> was reached using the GSD 8 cm images from the digital camera systems. In contrast, the matching of scanned RMK images gives less than 1 pt/m<sup>2</sup>. Obviously, the higher radiometric quality of digital images allows for much denser point matching while RMK-Top15 imagery is not suitable for the automatic derivation of high accurate surface models. This supremacy is verified for all digital camera systems. This result is especially relevant for the DMC and RMK images, which were recorded almost simultaneously at identical atmospheric and illumination conditions by using a double-hole aircraft.

Additionally, the results presented in Fig. 4 and Tabs. 3 and 4 show a considerable advan-

tage of point matching for the GSD 8 cm blocks compared to the GSD 20 cm blocks for all digital camera systems. For MATCH-T DSM, the point density using the GSD 8 cm images from the digital camera systems is even higher than the approximately 10 pts/m<sup>2</sup>, which were generated by the ALS 50 laser scanner at the sports fields. However, the standard deviation for the LiDAR data is better than 2 cm, almost without any gross errors, while an average of 5.5 cm for the filtered points is achieved from image matching. Thus, for the 8 cm block an accuracy of below 1 pixel GSD was achieved for the single point measurements. For the GSD 20 cm this value is slightly worse with an average standard deviation of 14.1 cm for the digital cameras. Compared to the 8 cm GSD block, the average point density of 1.8 pts/m<sup>2</sup> is much lower. For this reason, especially height data as it can be provided from largely overlapping high resolution imagery like the GSD 8cm blocks seems to be at least comparable to 3D data from LiDAR measurement.

While aiming at a joint evaluation of the different digital camera systems DMC, UltraCamX, Quattro DigiCAM and ADS 40 it has to be considered, that due to the test period of more than 2 months, there were significant changes in vegetation as well as atmospheric conditions and illumination. Some of the flights were done quite early in the morning, others were flown around noon. These differences in illumination of course influence the matching quality also for areas of little texture like the investigated sports field. Together with the variations of the block geometry these differences considerably influence the results

as available from the digital camera systems. Furthermore, the variations of the respective results with respect to the two applied software systems MATCH-T DSM and NGATE clearly indicate the influence of the respective matching and filtering algorithms on the generated elevation data. However, a comprehensive analysis of such influences is beyond the scope of this paper.

#### 4 Usability of Elevation Data from Image Matching

Dense and accurate elevation data are required for a large number of applications, like 3D-landscape visualization or the generation of products like true orthophotos, 3D-building models or DTMs. Especially if aerial images are already collected for other purposes, image matching is economically advantageous compared to the additional use of alternative sensors like RADAR or LiDAR. As an example, most national mapping agencies collect digital aerial images countrywide and resume the acquisition within short time periods mainly for generation of actual ortho imagery. This leads to the possibility of generating DSMs from image matching within the same time period.

Fig. 5 exemplarily depicts a DSM from DMC 8 cm GSD image matching and the ALS 50 LiDAR measurement for a part of the test area. As it is visible, the differences between

both surfaces are rather small and mainly correspond to vegetated areas. During the DGPF test, the DMC 8 cm GSD imagery was captured at July 24th 2008 while, airborne LiDAR (ALS) was collected at August 21th 2008. Due to the time gap of four week between the DMC and the LiDAR flight the differences between both DSM most probably result from plant growth. Additionally, as a result of the different measurement principles, the surface which is actually captured might be different in these areas. As an example, ALS measurement will partially penetrate a tree canopy, while matching will most probably relate to the visible surface. As discussed in the following sections such effects are especially important if the resulting elevation data is further analyzed for applications in forestry or for DTM generation.

##### 4.1 First Investigations in Urban Areas

For a first investigation of the potential of the camera systems for DSM generation in urban areas, interpolated, regular DSMs (25 cm grid) using the software package SAT-PP (Satellite Image Precision Processing, ETH Zurich) based on data from the frame based camera systems DMC and UltraCamX (8 cm GSD) were generated. Especially in urban areas time depending changes and the differences of the level of detail between the image matching

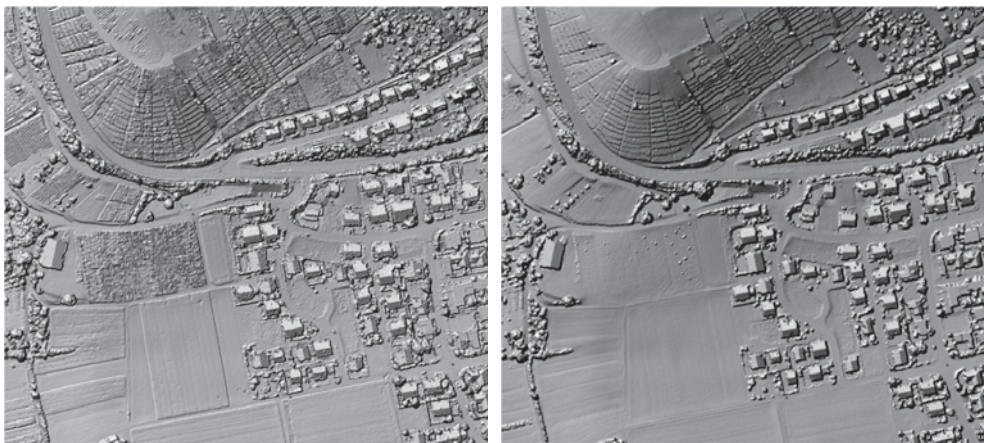
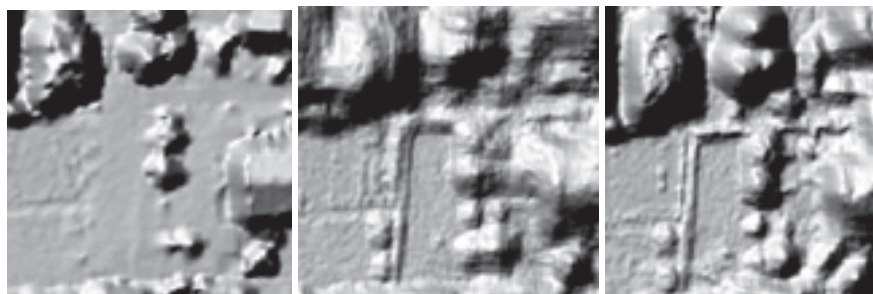


Fig. 5: DSM from image matching (left) and airborne LiDAR (right).

DSMs and the interpolated reference DSM (25 cm grid) from the LiDAR point cloud are problematically for the evaluation process. These differences make an area based comparison between the generated DSMs and the reference LiDAR DSM less representative and

less significant. Figs. 6 and 7 illustrate the different level of detail of the data sets. A small wall or hedge is visible in both image matching DSM, but not in the LiDAR DSM.

For simpler comparison DSM profiles are used instead of an area based evaluation meth-



**Fig. 6:** DSM from airborne LiDAR (left) and image matching for the data of the DMC, 8 cm GSD, 6 images overlapping (middle) and the UltraCamX, 8 cm GSD, 13 images overlapping (right).

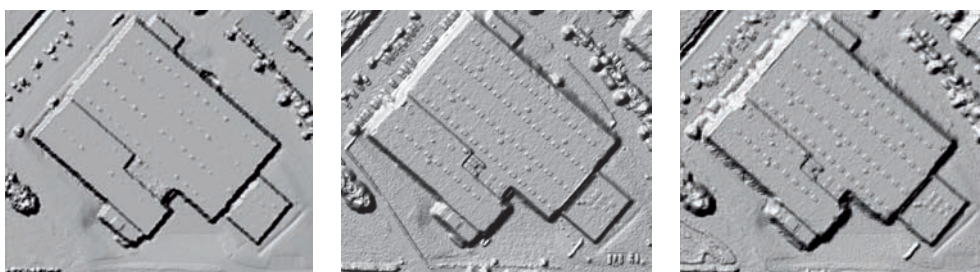


**Fig. 7:** DSM from airborne LiDAR (left) and image matching for the data of the DMC, 8 cm GSD, 6 images overlapping (middle) and the UltraCamX, 8 cm GSD, 10 images overlapping (right).

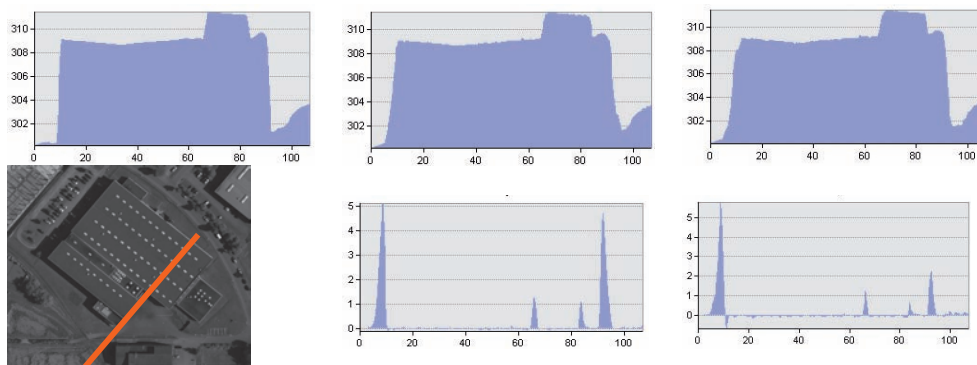


**Fig. 8:** Upper line: profile through the interpolated DSM from airborne LiDAR (left) and image matching for the data of the DMC, 8 cm GSD, 6 images overlapping (middle) and the UltraCamX, 8 cm GSD, 10 images overlapping (right). Lower line: original DMC, 8 cm GSD image (left), the position of the profile (red line) and the differences between the LiDAR DSM and the image matching DSM along the profile. All values are given in meters.

od; in general, the latter is more preferable. In the following results for an industrial building with a length of 113 m are discussed, exemplarily. Fig. 7 shows the different DSMs of the building and again the different level of detail.

Fig. 8 gives the original DMC 8 cm GSD image, the different profiles and the comparison between the LiDAR DSM and the image matching DSMs. The level of detail of the image matching DSMs is high, edges are reconstructed well, on top of the building the difference to the LiDAR DSM is very small, and blunders are detectable only in the area of buildings borders. The investigations discussed in this section were done before the georeferencing of the LiDAR data was improved by strip adjustment. Therefore, here the original georeferencing was used. Thus, the deviations at the building borders also indicate the need for improving the original georeferencing of the LiDAR data as discussed in Section 2.2.

#### 4.2 Forestry Applications

Information on height and 3D structure is a strongly needed input in many forestry applications. A dense, accurate and up-to-date digital surface model (DSM), assuming a digital terrain model (DTM) being available, is therefore required in order to get an appropriate canopy height model. Several investigations aim on the combination of LiDAR data and multispectral images to develop and evaluate methods for the determination of tree and forest attributes. Frequently, aerial image information is applied for classification purposes while LiDAR data is used for the estimation of DSM and DTM. Estimated as the difference from the DSM to its corresponding DTM, the canopy height model (CHM) is the base model within the aspired forestry applications.

$$\text{CHM} = \text{DSM} - \text{DTM} \quad (1)$$

DTMs are constant over a long time and supported by the national mapping agencies. DSMs not, in particular not with respect to environmental purposes, thinking of flooding, wind damages or shrub encroachment. In or-

der to be able to estimate a dense and accurate up-to-date CHM investigations on the generation and reliability of DSMs are required. In forestry applications CHMs are used to derive different forest attributes on single tree and stand level (e.g. height, crown closure, volume, structure). Using these attributes one can derive ecological data like above ground biomass, carbon pools, economical data like timber yield for forest management and input data for forest inventories (WASER et al. 2009). These parameters are also used to extract potential tree areas for semi-automatic estimations of main tree species and fractional tree covers. Other applications apply the CHM for the areal acquisition of forest gaps or use CHM in conjunction with Color and Intensity information of aerial images to derive forest areas (BÖSCH et al. 2007). The investigations on semi-automatic extractions of main tree species or forest areas are at present done within small test areas; at the Swiss Federal Institute for Forest, Snow and Landscape Research (WSL) they are currently in use for the evaluation of the canton Appenzell. Due to missing up to date LiDAR data but usage of most recent aerial images, semiautomatic methods for forestry applications are difficult to refine especially converting them to large areas like a whole country. High accurate and dense up to date DSMs from image matching are therefore the future for the derivation of the base model CHM for forestry applications. ST-ONGE et al. (2001) evaluated the potential of using DSMs from image matching with digitised analogue photographs. HEURICH et al. (2004) determined differences of forest surfaces comparing LiDAR and image matching methods using DMC data and clearly showed the potential of DSMs from image matching. In this context, investigations using data of the DGPF test are of considerable importance.

Besides the overall accuracy with respect to control points, which are mainly on ground and good textured surface, the differences of image matching with respect to LiDAR and 3D stereo measurements of single surface points in vegetation covered areas are interesting for environmental applications. First, the image matching results from matching with one stereo image pair are compared to LiDAR original and corrected data. In order to ex-

clude a benefit in areas of LiDAR overlapping data lines only one set of LiDAR data was used for each analysis. Secondly they are compared to stereo measurements in order to determine the differences from stereo matching to stereo interpretation, whereas the stereo interpretations could be considered as a most probable result of image matching at the specific stereo measurement positions. The differences of DSM to the different comparison values estimate the true values of canopy heights using image matching methods.

Therefore different areas in the test site Vaihingen/Enz are examined to estimate the potential and deviations with respect to LiDAR data and manual 3D measurements. The analyses give a good overview on the accessible data and its density and the limits in the usage of matching methods for environmental applications using BAE Systems NGATE. ADS 40 (CIR Images), DMC (RGB images) and UltraCamX (UCX; RGB Images) data with 20 cm resolution was used for analyses; all DSMs are calculated with a resulting Ground Sample Distance of 50 cm. The DSMs are generated using one stereo image pair on BAE Systems NGATE in conjunction with a specific parameter set defined at WSL.

### Example 1: Area with Compact Crown Closure

The first example area was chosen due to a compact crown closure with small height differences in the surface. Differences are calculated as an actual-target-comparison; actual = DSM and target = LiDAR – equation (2), its Root Mean Square Error is calculated with equation (3).

$$dZ = \text{actual} - \text{target} \quad (2)$$

$$RMS = \sqrt{\frac{\sum dZ^2}{n}} \quad (3)$$

For a first comparison with dense 3D data the generated DSMs and the LiDAR data (original and corrected) are taken for an actual-target comparison. In order to be able to evaluate the most probable deviation to the surface that can be calculated with image matching methods,

~110 manual 3D stereo measurements are done for each data set. This estimates the difference of LiDAR due to leafiness and variation in pulse responds with respect to stereo plotting. All 3D data sets are cross-calculated; the results are listed in Tab. 5. All results rely on a gross error filtering, only differences in the range of  $\pm 3 \cdot RMS$  are used for evaluations. Fig. 9 shows in the upper row the orthoimage section for each data set including the example area that leads to the results in Tab. 5. Beneath each image the corresponding difference model from raster calculation of DSM – LiDAR (original) is shown as a color-coded raster dataset (dark blue – high positive difference, bright blue – high negative difference). The LiDAR original point clouds are imported and merged to a raster data set using ESRI ArcGIS. All figures include the defined example area as blue polygon.

The trend for the deviations is similar in all data sets. For all datasets the DSMs are 25 cm (average) above the 3D stereo measurements surface. The deviation of LiDAR original with respect to the Stereo measurements only results for the ADS40 in a high value of about 70 cm, for DSM and UCX the value is about 35 cm. For all deviations the Stereo measurements are above the LiDAR data set. The mean

**Tab. 5:** Deviations of DSM, LiDAR and Stereo measurements cross-calculated by equation (2).

Sensor	actual	Target	Mean	RMS
			[m]	[m]
ADS 40	DSM	Stereo	0.3	0.5
	LiDAR	Stereo	-0.7	2.7
	DSM	LiDAR	2.0	4.2
	DSM	LiDARcorr	1.9	4.1
DMC	DSM	Stereo	0.2	0.8
	LiDAR	Stereo	-0.3	1.9
	DSM	LiDAR	1.8	4.2
	DSM	LiDARcorr	1.7	4.0
UltraCamX	DSM	Stereo	0.2	0.5
	LiDAR	Stereo	-0.4	1.9
	DSM	LiDAR	1.8	4.1
	DSM	LiDARcorr	1.7	4.0

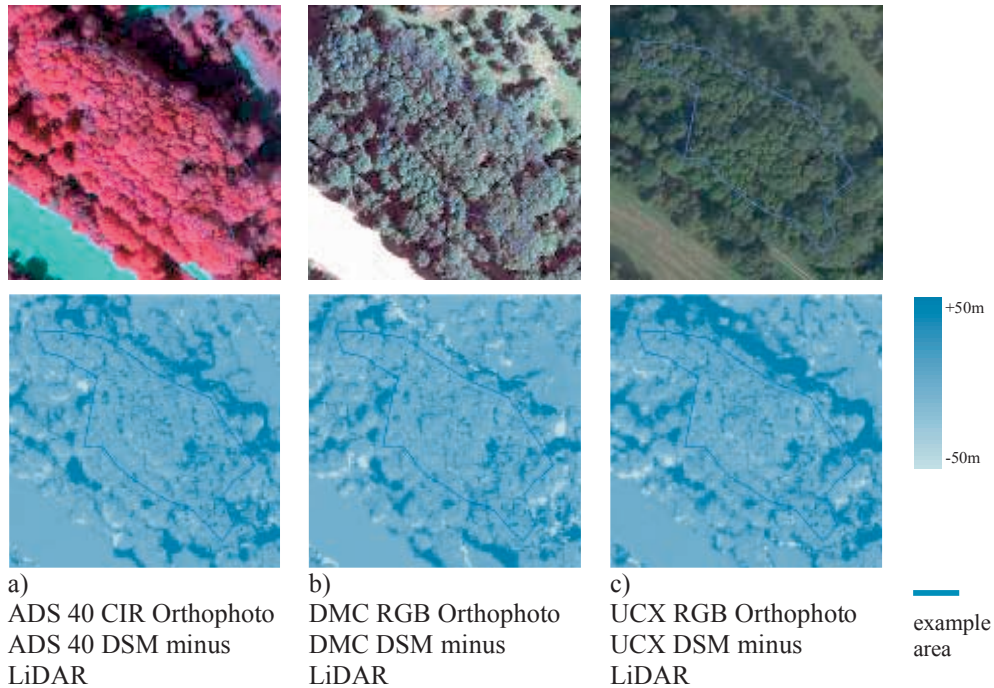


**Fig. 9:** Image sections and resulting differences from DSM to LiDAR data.

difference between DSM and LiDAR original and corrected is +1.9 m and +1.8 m respectively. Due to the higher density of LiDAR and DSM compared to the sample size of approximately 110 points for stereo measurements we assume the results for deviations of DSM to LiDAR to be more reliable and valid for overall and further analyses.

**Example 2: Area with Normal to Light Crown Closure**

The second example covers an area with normal to light crown closure. Gaps and local height differences characterize the example area. For a first comparison with dense 3D data the generated DSMs and the LiDAR data (original and corrected) are taken for an actual-target comparison. Due to the morphological structure and the strong shadows the deviations from DSM to LiDAR are higher compared to Example 1. Fig. 10 shows the corresponding stereo image pair sections of the UltraCamX data; the yellow polygon illus-

trates the example area. Here the strong differences of object space due to the different perspectives are obvious, which lead to higher deviations for image matching. Additionally the resulting color-coded difference model for DSM – LiDAR original is shown on the right side. The colors are chosen with respect to 1–3 sigma of the RMS values. Grey values are within 1 sigma, light blue within 2, dark blue within 3 and red areas are outside 3 sigma, they highlight the strong shadowed parts and areas with high perspective differences.

Tab. 6 concludes the results. All results rely on a gross error filtering, only differences <math><3 \cdot \text{RMS}</math> are used for evaluations. For all data sets the mean value of all differences from DSM to LiDAR original and corrected data is within 3–3.9 m and 2.9–3.8 m respectively; the DSMs therefore result in average 3.5 m above LiDAR.

The analyses for forestry applications show similar trends for the deviations in all data sets, even though the UltraCamX data relies on significant disadvantages in image quality due to weather conditions, which are mani-

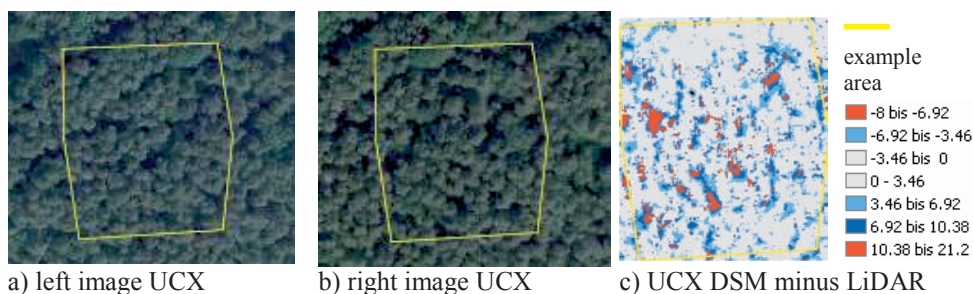


**Fig. 10:** Image sections of stereo image pair UltraCamX and resulting differences from DSM to LiDAR data.

**Tab. 6:** Deviations of DSM and LiDAR for example area 2.

Sensor	actual	target	Mean	RMS
			[m]	[m]
ADS40	DSM	LiDAR	3.0	5.9
	DSM	LiDARcorr	2.9	5.8
DMC	DSM	LiDAR	3.8	6.4
	DSM	LiDARcorr	3.7	6.3
UltraCamX	DSM	LiDAR	3.9	6.5
	DSM	LiDARcorr	3.8	6.3

fested in the results of plane analyses. Despite the correction of LiDAR data as described in Section 2.2, the benefit for forestry applications is not as significant as expected. The results show the high potential of new aerial images and the usage of new matching methods for vegetation areas, but further investigations are needed in order to evaluate overall accuracies and more reliable results for different areas and vegetation types.

### 4.3 Generation of ATKIS-DTM

As a component of the Authoritative Topographic-Cartographic Information System (ATKIS), the surveying and mapping agencies of the federal states in Germany provide area covering and actual Digital Terrain Models and digital ortho images. Originally, for high quality DTM generation airborne LiDAR data was used. Since most national mapping agencies take digital aerial images countrywide

and resume the acquisition within short time periods, the use of airborne imagery for automatic DTM update would be highly advantageous to improve the cost efficiency. In order to evaluate the potential of image based ATKIS®-DTM generation, 3D point clouds as provided from the software MATCH-T DSM were further analyzed. For this purpose, filter algorithms available within the software SCOP++ LIDAR from INPHO GmbH were used. This tool has so far been applied by the national mapping agency of Mecklenburg-Vorpommern in order to classify terrain points from airborne LiDAR measurements during the generation of DTM grids.

Fig. 11 shows six test areas used as reference for the following investigations. For these areas, filtered point clouds from different camera configurations Quattro DigiCAM, UltraCamX and DMC were compared to the LiDAR reference measurement. As expected, the existing setup for classification and filtering of LiDAR-points could not directly be used for the evaluation of point clouds from image matching. The available point density from image-matching especially from the 8 cm GSD flights is always higher than from LiDAR measurement. However, image matching provides point distributions, which are suitable for DSM generation, while in forest regions almost no points are available at the terrain surface. This is of course a prerequisite for DTM generation and already motivated the introduction of airborne LiDAR in the nineteen eighties.

In general, the generation of DTM in complex regions like urban areas depends very much on the quality of automatic filtering,



**Fig. 11:** Test areas for DTM generation.

sometimes still the use of additional map data or manual editing is required. At present, LiDAR data filtering still seems to be more advanced than post processing of photogrammetrically derived elevation data, however, it will be interesting to follow the future developments. Since filtering of the 3D points is the main problem during DTM generation, changes in overlap and GSD as well as the use of different camera systems (DigiCAM, UCX, DMC) did not result in significant differences of the result. Despite these problems, image matching can be useful at least for change detection as a prerequisite of DTM update. Usually, high vegetation, gives hint to constant terrain surface, where no update is required. However, low vegetation up to 50 cm like shrub can hide DTM changes. This is especially a problem for longer time periods like 3 years, which is the current flight interval for national mapping agencies.

Similar to LiDAR measurement, an image based generation of DTM requires flights outside the vegetation period – however for ATKIS ortho image generation usually data collection in summer or spring is preferred. Another point to be solved is the amount on computational power and time, which is still re-

quired especially if large areas like a complete federal state have to be covered by high resolution at large overlap. Estimates with actual hard- and software configuration range from 40 to 1470 days for a complete federal state like Mecklenburg-Vorpommern with an area of approximately 23.000 km<sup>2</sup>.

## 5 Outlook and Conclusions

The tests and investigations within the DGPF-project on Digital Photogrammetric Camera Evaluation clearly demonstrated the benefits of digital image recording for elevation data generation by image matching. Data from up-to-date digital airborne cameras facilitate the generation of 3D point clouds and 2.5D raster representations at a quality, which in the past was only feasible by LiDAR measurements. Elevation data from image matching can be used in deriving 3D-building models, roof shapes, canopy models, producing true orthophotos, 3D-landscape visualization and – at least partially – for generating and updating DTMs.

However, compared to LiDAR measurement results from image matching still are

compromised to errors. Potential problems, for example resulting from changing illumination or moving shadows still provide results of partly varying geometric quality. Despite the very promising results, current matching software does not yet fully exploit the complete potential of the new generation of aerial images. Further developments, investigations and tests are still required in the field of multi image matching to broaden potential applications. In order to allow for standard workflows while for example introducing this method into the working practice of National and State Mapping Agencies, also the question of the actually required magnitude of forward and sideward overlap has to be solved. Since any increase of sideward overlap results in longer flying time and therefore raises costs, the especially for large flight mission is very crucial from an economical point of view. Remaining challenges to ameliorate the further use of elevation data from image matching are a further improvement of filter approaches, the reduction of computational cost and an optimal adaption of algorithms for interpretation of surfaces or point clouds from image matching. Additionally, the full use of jointly collected high resolution radiometric and geometric information for the collection of detailed geodata is just at the beginning. It is the aim of efforts like the DGPF test to encourage such developments and further support the current comeback of digital image matching.

## References

- BÖSCH, R., GINZLER, C. & WANG, Z., 2007: Von Decken und Lücken. – Landesforstinventar (LFI) Info Nr. 8, Eidgenössische Forschungsanstalt für Wald, Schnee und Landschaft (WSL), Birmensdorf, Switzerland, 1–4, [www.lfi.ch](http://www.lfi.ch).
- COGAN, L., LUHMANN, T. & WALKER, A.S., 1991: Digital Photogrammetry at Leica, Aarau. – ISPRS Conference on Digital Photogrammetric Systems.
- CRAMER, M., 2010: The DGPF-Test on Digital Airborne Camera Evaluation – Overview and Test Design. – this issue.
- DEVENEZIA, K., WALKER, S. & ZHANG, B., 2007: New Approaches to Generating and Processing High Resolution Elevation Data with Imagery. – Photogrammetric Week 17 (5): 1442–1448.
- HEINZEL, J., WEINACKER, H. & KOCH, B., 2008: Full automatic detection of tree species based on delineated single tree crowns – a data fusion approach for airborne laser scanning data and aerial photographs. – *SilviLaser 2008*, 8<sup>th</sup> international conference on LiDAR applications in forest assessment and inventory, 76–85.
- HEURICH, M., SCHADECK, S., WEINACKER, H. & KRZYSTEK, P., 2004: Forest Parameter Derivation From DTM/DSM Generated From LiDAR And Digital Modular Camera (DMC). – *International Archives of Photogrammetry, Remote Sensing and Spatial Information Sciences* 37 (B): 84–89.
- HÖHLE, J. & HÖHLE, M., 2009: Accuracy assessment of digital elevation models by means of robust statistical methods. – *ISPRS Journal of Photogrammetry and Remote Sensing* 64: 398–406.
- JACOBSEN, K., CRAMER, M., LADSTÄDTER, R., RESSL, C. & SPRECKELS, V., 2010: DGPF-Project: Evaluation of Digital Photogrammetric Camera Systems – Geometric Performance. – this issue.
- KAGER, H., 2004: Discrepancies between overlapping laser scanning strips – simultaneous fitting of aerial laser scanner strips. *International Archives of Photogrammetry, Remote Sensing and Spatial Information Sciences* 35 (B1): 555–560.
- KRZYSTEK, P., 1991: Fully Automatic Measurement of Digital Elevation Models with MATCH-T. – *Photogrammetric Week 1991*.
- LEMAIRE, C., 2008: Aspects of the DSM Production with High Resolution Images. – *International Archives of Photogrammetry, Remote Sensing and Spatial Information Sciences* 37 (B4): 1143–1146.
- PERSSON, A., HOLMGREN, J., SÖDERMAN, U. & OLSSON, H., 2002: Detecting and Measuring Individual Trees using an Airborne Laser Scanner. – *Photogrammetric Engineering & Remote Sensing* 68 (9): 925–932.
- RESSL, C., KAGER, H. & MANDLBURGER, G., 2008: Quality checking of ALS projects using statistics of strip differences. – *International Archives of Photogrammetry, Remote Sensing and Spatial Information Sciences* 37: 253–260.
- ST-ONGE, B. & ACHAICHA, N., 2001: Measuring forest canopy height using a combination of LiDAR and aerial photography data. – *International Archives of Photogrammetry, Remote Sensing and Spatial Information Sciences* 34 (3/W4): 131–137.
- WASER, L.T., GINZLER, C., KÜCHLER, M., LANZ, A. & BALTSAVIAS, E., 2009: Semiautomatic prediction of main tree species using multi-temporal ADS 40 data. – *IUFRO Division 4 Symposium on Extending Forest Inventory and Monitoring over space and time*.

ZHANG, L. & GRUEN, A., 2004: Automatic DSM Generation from Linear Array Imagery Data. – International Archives of Photogrammetry, Remote Sensing and Spatial Information Sciences **35** (B3): 128–133.

Addresses of the Authors:

Apl. Prof. Dr. NORBERT HAALA, Institut für Photogrammetrie, Universität Stuttgart, Geschwister-Scholl-Str. 42D, D-70174 Stuttgart, Tel.: +49-711-685-83383, Norbert.Haala@ifp.uni-stuttgart.de.

Dipl.-Ing. HEIDI HASTEDT, Eidgenössische Forschungsanstalt für Wald, Schnee und Landschaft WSL, now: Fachhochschule Wilhelmshaven/Oldenburg/Elsfleth, Institut für Angewandte Photogrammetrie und Geoinformatik, Ofener Str. 16, D-26121 Oldenburg, Tel. +49-441-7708-3164, heidi.hastedt@hs-woe.de.

Dr. KIRSTEN WOLFF, Institut für Geodäsie und Photogrammetrie, ETH Zürich, now: swisstopo, Seftigenstrasse 264, CH-3084 Wabern, kirsten.wolff@swisstopo.ch

Dr. CAMILLO RESSL, Institut für Photogrammetrie und Fernerkundung, Technische Universität Wien, 1040 Wien, Austria, Gußhausstraße 27–29, Tel: +43-1-58801-12234, car@ipf.tuwien.ac.at.

Dipl.-Ing. SVEN BALTRUSCH, Landesamt für innere Verwaltung Mecklenburg-Vorpommern, Amt für Geoinformation, Vermessungs- und Katasterwesen, Lübecker Str. 289, 19059 Schwerin, Tel.: +49-385-48013202, sven.baltrusch@laiv-mv.de.

Manuskript eingereicht: Dezember 2009

Angenommen: Januar 2010





## DGPF-Project: Evaluation of Digital Photogrammetric Camera Systems – Stereoplotting

VOLKER SPRECKELS, LUZIE SYREK & ANDREAS SCHLIENKAMP, Herne

**Keywords:** Frame cameras (analogue/digital), photogrammetric stereo measurements, stereoplotting, quality control

**Summary:** This paper is a part of the DGPF project “Evaluation of Digital Photogrammetric Camera Systems” and encloses the analyses of the working group “Stereoplotting”. The digital imagery of the analogue camera Zeiss RMK Top 15, the digital large format frame cameras Vexcel Imaging UltraCamX and Intergraph/ZI DMC and the combination of four mid-format cameras Quattro DigiCAM from IGI have been used for stereoplotting. The individual point measurement accuracy has been determined for all cameras and ground sampling distances. The stereo-photogrammetric measurements for ground control points and for topographic point and line measurements have been compared between the cameras and to the terrestrial ground control point coordinates. The aerial flight campaigns are strongly influenced by the current weather conditions at the flying time. For this reason an – as far as possible – impartial evaluation could only be given by the comparison of the individual point measurement accuracy or identical point measurements in the mapping results of different aerial campaigns.

**Zusammenfassung:** *DGPF-Projekt: Evaluierung von Digitalen Photogrammetrischen Kamerasystemen – Stereoplotting.* Dieser Beitrag entstand im Rahmen des DGPF-Projektes „Evaluierung digitaler Luftbildkameras“ und behandelt die Auswertungen der Arbeitsgruppe „Stereoplotting“. Es wurden die stereophotogrammetrischen Auswertungen der Bilddaten der Reihenmesskammer Zeiss RMK Top 15 zu den großformatigen Flächensensorkameras Vexcel Imaging UltraCamX und Intergraph/ZI DMC sowie die Kombination von vier Mittelformatkameras Quattro DigiCAM der Fa. IGI untersucht. Dazu wurden die persönliche Einstellgenauigkeit in den jeweiligen Bilddatensätzen ermittelt, die stereophotogrammetrischen Messungen zu Passpunkten, topographischen Punkten und Linienmessungen in den Bilddatensätzen miteinander und zu den Soll-Koordinaten der terrestrischen Passpunktmessung verglichen. Die Bilddaten sind sehr stark durch die an den unterschiedlichen Bildflugzeitpunkten vorherrschenden Wetterbedingungen geprägt. Aus diesem Grunde kann eine möglichst objektive Beurteilung nur über die persönliche Einstellgenauigkeit und über die Ermittlung identischer Punkte in den Auswertungen der unterschiedlichen Bildflüge erfolgen.

### 1 Introduction

The tasks of the working group “Stereoplotting” is the analysis of the potential of digital aerial cameras for the generation of topographic maps, site plans, digital terrain models (DTM) and for 3D mapping of buildings (see Fig. 1). Up to now the results of the company RAG Deutsche Steinkohle (RAG) are available. RAG’s work in this project set up by the “German Society for Photogrammetry and Remote Sensing” (DGPF) currently averages

about 400 working hours. RAG has an experience in high-end photogrammetry of about 35 years (LÜTZENKIRCHEN 1974, BUSCH 1989). Since 2004 RAG performs stereoplotting in images of digital aerial cameras and made several analyses concerning the evaluation of the geometric accuracy (SPRECKELS et al. 2008). Further analyses for production purposes have been performed, e. g., by PERKO et al. (2004), NEUMANN (2004), ARIAS & GOMEZ (2007) or TALAYA et al. (2008).

Due to the expenditure of time RAG did not perform the Aerial Triangulation (AT) and used the AT results that were provided and distributed by the project management. At this it has to be taken into account that the individual point measurement accuracy of the different photogrammetric operators will have an influence on RAG's stereoplotting (see also the paper "Geometric performance", DGPF working group "Geometry"). All of RAG's stereo-photogrammetric measurements were performed by Mrs. Luzie Syrek, an operator with 23 years professional experience in stereoplotting for large area DTM and special detections for dynamic ground movements caused by underground hard coal mining. The measurements were carried out with ERDAS Imagine LPS/Pro600, NuVision stereoscopic viewing panel and polarized viewing glasses.

For the comparison of the stereoplotting results four test areas have been defined: Area 1 "Inner City", Area 2 "High Riser", Area 3 "Residential Area" and Area 4 "Quarry" (see Fig. 2).

The stereo-photogrammetric measurements for the areas 1 to 3 were performed with the aerial images in 8 cm and 20 cm ground sampling distance (GSD) of the cameras Zeiss RMK Top 15 (RMK), Intergraph/ZI DMC (DMC) and Vexcel Imaging UltraCamX (UCX). With the camera IGI Quattro Digi-

CAM (DigiCAM) up to now the areas 1 and 2 have been completed but the work will be continued. Area 4 "Quarry" has only been measured in the 20 cm GSD images because a comparison to the stereoplotting results from 8 cm GSD images did not show any improvement of the mapping result or considerable deviations for the DTM measurements.

For each camera RAG compared the stereoplotting results in 8 cm GSD to 20 cm GSD. Among the cameras the comparison was performed for the results from 8 cm GSD and for the results from 20 cm GSD images. As first conclusion it can be stated that the strongest influence on the photogrammetric measurements and image interpretation is due to the completely different weather conditions during the individual image flights (see Fig. 3).

For the achievements of more impartial statements of the stereoplotting results RAG decided to identify and select identical measurements for points and lines and even polygons. The individual point measurement accuracy of the operator was determined in 8 cm GSD images of the RMK, DMC, UCX and DigiCAM by the threefold measurement of all visible ground control points (GCP).

The stereoplotting results of the RMK, DMC and UCX for 8 cm GSD and 20 cm GSD that could be finished in spring 2009 have been sent to the members of the DGPF work-



Fig. 1: 3D-aspect with stereoplotting results, Area 1 "Inner City", UltraCamX, 8 cm GSD.

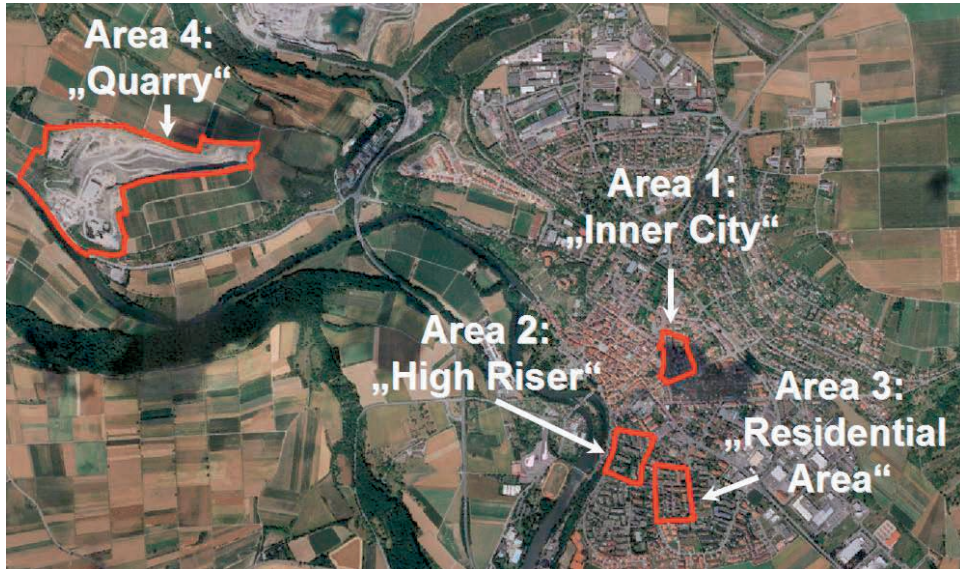


**Fig. 2:** Orthophoto mosaic Vaihingen-Enz, Germany, with an overview of the test areas.



**Fig. 3:** Aerial images of Area 1 “Inner City” at individual flying times: from left to right: ‘08-07-24 RMK, ‘08-07-24 DMC, ‘08-08-06 DMC, ‘08-08-06 DigiCAM and ‘08-09-11 UltraCamX.

ing group “Generation of Digital Elevation Models” as ESRI 3D-shapefiles and in MicroStation DGN format. A data set of 3D measurements of Area 1 “Inner City” with detailed building and roof structures (see Fig. 1) was sent to the project management and to the IS-PRS WGIII/4, “Complex Scene Analysis and Reconstruction” in 3D-shapefile and 3DS format.

## 2 Stereoplotting

As far as possible it was taken into account that first of all the images of the aerial flights with 20 cm GSD were used for stereoplotting

so that the measurement could not be influenced by the knowledge of the more detailed information from 8 cm GSD images. Furthermore the weather conditions to the individual flights were considered so that a flight campaign with sunny weather was followed by a flight campaign with overcast sky, what led to the following order: RMK 20 cm GSD, UCX 20 cm GSD, DMC 20 cm GSD, RMK 8 cm GSD, UCX 8 cm GSD and DMC 8 cm GSD. In autumn 2009 the stereoplotting for the two areas 1 and 2 followed for DigiCAM in 20 cm GSD and in 8 cm GSD.

The photogrammetric stereo measurements were performed using the German object-key catalogue “OSKA”. All group members using

ERDAS Imagine LPS/Pro 600 got this coding from RAG for a TIPRO KeyPad for the generation of consistent and comparable data sets. The data management of all used aerial images, project data and stereoplotting results was realized on an external Buffalo Tera-Station 4 TByte raid system, connected via Ethernet to the Digital Image Station.

Work with this constellation, LPS/Pro600 and external raid system as data storage, showed a slow and tardy screen display of the digital images for all digital camera data while zooming in and out. More worse was the performance for the adjustment of contrast and brightness in dazzled areas with harsh contrasts for the aerial flight campaigns with strong insolation.

This behaviour of the screen display is most likely caused by the inherent data structure of the different images and the pre-processing and therefore not camera specific. The images were distributed in different data formats, unsigned 8 bit for UCX (670 MB/image) and RMK (1.163 MB/image), unsigned 16 bit for DMC (1.020 MB/image) and DigiCAM (402 MB/image). The tile size was 256 pixel x 256 pixel for all images.

The image pyramids were calculated anew within ERDAS Imagine LPS for DMC, UCX and DigiCAM images. In following a noticeable better performance was reached for the handling of the digital images.

Due to the dull weather with shallow contrast it was easier and more pleasant to work with the RMK 8 cm GSD and with all UCX

images because nearly no adjustments for contrast and brightness had to be done implicating an efficient and uninterrupted workflow. An acceptably fast screen display resulted for RMK images with the original delivered image pyramids. The display speed was as fast as for DigiCAM with the anew calculated image pyramids and faster than for UCX images with the new LPS image pyramids – but the workstation definitely reached its limits with the display of the 16 bit DMC images even with the anew calculated image pyramids. Caused by the insolation the numerous adjustments for contrast and brightness made working with 16 bit DMC images most time-consuming (see Fig. 4).

All check measurements of GCP for the determination of the accuracy of the individual point measurement and the stereo-photogrammetric measurements were performed in Zoom Level 4 x (fourfold magnification). This ensures a consistent estimation of the digital image station's performance for stereo-photogrammetric analyses. Fig. 5 shows GCP no. 2203 in fourfold magnification for different aerial cameras.

The square GCP signals are coloured white in the size of 60 cm to 60 cm with a black coloured inner part of 30 cm to 30 cm size. In the beginning of the work RAG had reservations against this type of GCP signal but for 8 cm GSD this signalization is excellent for the measurement of GCP's when the cross-line mark reaches within the area of the white edge-strip. This allows the cross-lines to

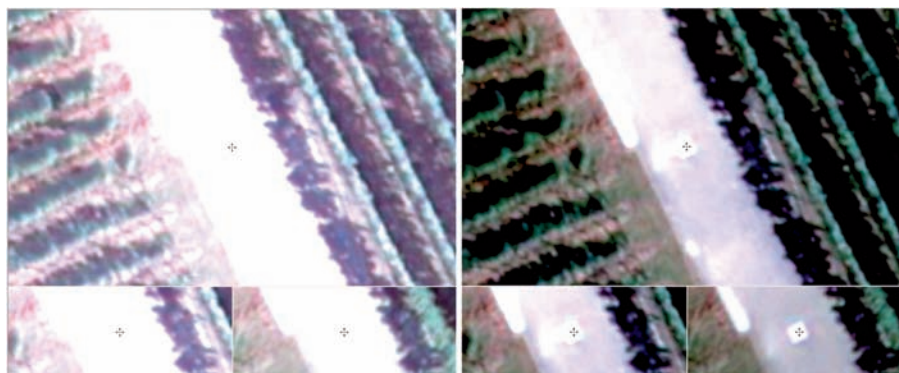


**Fig. 4:** GCP no.2409, Zoom Level 4 x, DMC: before (left) and after the adjustment of contrast and brightness (right). Each with the left and right image for stereo display (bottom).

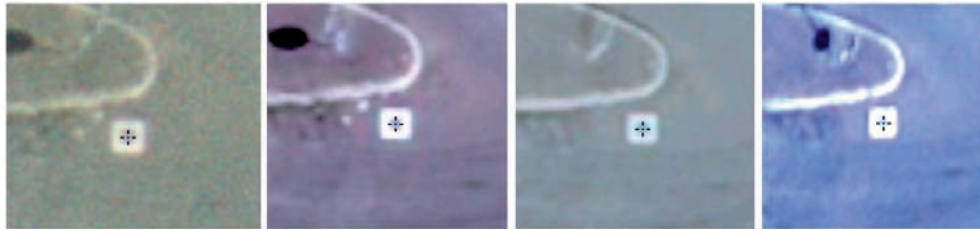


**Fig. 5:** GCP no. 2203, Zoom Level 4 x. From left to right: RMK, DMC, UltraCamX, DigiCAM.

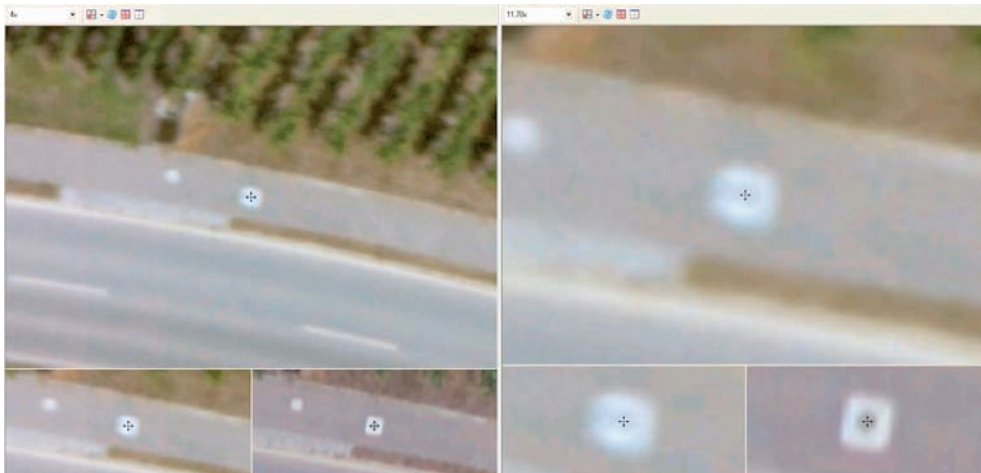


**Fig. 6:** Influence of the de-focused DigiCAM camera head no. 125 on GCP no. 3041029, 4 x zoom (left), 11.7 x zoom (right). Each with the left and right image for stereo display (bottom).

“lean” on the strip and prevents the mark from “sinking” into the dark area (see Fig. 5). In 20 cm GSD the inner dark part of the GCP signals is dazzled by the white strip and not visible.

Working with the four images of the DigiCAM was something getting used to. The images are taken from the same projection centers, but they are not joined together to a homogenous virtual image and for this reason they had to be handled as individual images. In LPS the four images of one flight path had to be separated into two parallel flight paths. Looking in flight direction, both right hand side images and both left hand side images were related to different flight strips. The image names were specified by the project management so that very long names evolved that often confused the assignment of the correct stereo partner. Due to the weather conditions numerous adjustments for contrast and bright-

ness had to be done while working with DigiCAM images, but related to the smaller image size a faster screen display resulted than for DMC images. For several DigiCAM images a slight blur could be detected, as for the left stereo image that is presented in Fig. 6.

The manufacturer IGI reported that this is implicated by the focus of the camera head no. 125 to 70 m. Nevertheless it seems possible that, regarding Fig. 6, an additional influence of the forward motion of the aircraft superimposes this effect. In contrary to DMC or UCX the DigiCAM has no Forward Motion Compensation (FMC). The local areas of slight haziness do have an influence on the recognition of the objects for stereoplottting. An effort was made to automatically detect GCP in the hazy areas of the de-focused camera to be excluded from the statistical evaluation for the determination of the point measurement accuracy. The results showed an influence of about

3/8 pixel against flight direction that could be proved by re-measurements of GCP even in the left and the right stereo image.

### 2.1 Comparison of Stereoplotting Results in 8 cm to 20 cm GSD

The stereoplotting results from each camera's 8 cm GSD and 20 cm GSD images have been compared. At this point it has to be mentioned that the 20 cm GSD images of the RMK are based on a colour-infrared film (CIR) but the 8 cm GSD images are true colour (RGB) what has to be taken into account for the detection of similar features leading to diversities in image interpretation. Furthermore the CIR images of the RMK are very dazzled and for this reason not really convenient for stereo-photogrammetric measurements.

As expected, the stereoplotting results from 8cm GSD images definitely do show more details (see Fig. 7, left). They are mainly influenced by the available number of stereo models for the test area, the location of the test area within the stereo models and within one or more flight strips, as well as by the individual weather conditions. For instance kerbstones can be accentuated by the sunlight or disappear in shallow areas. Manhole cover or GCP targets can be undetectable glared. With low contrast on the other hand kerbstones cannot definitely be measured or detailed features in some areas are not clearly to be separated – but partly better in other areas. Sometimes

these effects lead to misinterpretation, see Fig. 7, left hand side. Here the stereoplotting results are misinterpreted in 20 cm GSD due to the contrast and the vegetation cover. For this reason no camera specific conclusions can be made by only regarding the stereoplotting results.

### 2.2 Comparison of Stereoplotting Results in 8 cm to 8 cm and 20 cm to 20 cm GSD

For this comparison the stereoplotting results of different cameras have been combined. The substantial differences led from the influence of the weather conditions so that for instance some not hidden manhole covers could be detected in DMC images but not in UCX images – or the other way round (see Fig. 7, right hand side). Even these stereoplotting results show that no impartial validations can be made to detect camera specific characteristics. The detection and interpretation of objects depends on the already mentioned conditions like the position in a stereo model, number of stereo models and the according amount of hidden areas. At all events hard contrasts and different brightness involve additional adjustments and, for very bright areas, even the adaptation of the human eye until it was possible to continue the stereo measurements. For this reason no camera specific conclusions can be made by only looking on the stereoplotting results.



**Fig. 7:** Left: Area 2 "High Riser", comparison of stereoplotting results 8 cm GSD (red) to 20 cm GSD (blue), RMK. Right: Area 1 „Inner City“, comparison of stereoplotting results 8 cm GSD, UCX (red) to DMC (blue).

### 2.3 Comparison of Stereo-Photogrammetric Point Measurements

Like already mentioned in sections 2.1 and 2.2, the validation of stereo-photogrammetric measurements could be successful for the detailed analysis of one specified object but not for the whole area and not for all possible combinations in 8 cm and/or 20 cm GSD. Identical points should contain the same OSKA-coding and be located within a buffer of 50 cm. Within the 3D-shapefiles of the stereo-photogrammetric measurements recognisable points with the coding 3504 (manhole cover), 3505 (gully) and 5742 (lamp pole) were selected and statistically processed, see Tab. 1. Compared to all point measurements the better recognisability of manhole covers leads to smaller deviations in position but to the same level in height (see Fig. 8).

It has to be considered that the stereoploting in DigiCAM data is still in process and only results for Area 1 and Area 2 are present. Unfortunately the areas 1 and 2 are within the images of the de-focused DigiCAM camera head no. 125 (see Fig. 6). Re-measurements showed that this camera head has an influence

on the point measurements of about 3/8 pixel against flight direction. For each flight strip this influence leads to an offset of about 2 cm to 3 cm in x for 8 cm GSD and of about 6 cm to 7 cm in x for 20 cm GSD. It has to be mentioned that for the whole block these local influences will statistically be averaged and mostly be covered. The flight direction for 8 cm GSD is from west to east, for 20 cm GSD from east to west. So the combined influences in x reach an amount of about +7 cm to +9 cm, what has to be taken into account regarding Tabs. 1 to 6.

Compared to RMK and UCX a smaller number of identical points could be selected for DMC. This is not camera specific but due to the more disadvantageous weather conditions that led to different point measurements within the images of the two separate image flights for 8 cm GSD and 20 cm GSD. This has to be taken into account for the comparisons presented in Tabs. 1 to 9.

The height measurements of the digital aerial cameras are around 10 cm higher compared to the scanned aerial images of RMK. A reason could be the worse point recognition in CIR images compared to RGB images. Furthermore the scanned aerial images are noisier

**Tab. 1:** Comparison of identical point measurements for RMK, DMC, UCX and DigiCAM, **8 cm GSD to 20 cm GSD.**

Camera	No. of points	No. of Models		mean [cm]			median [cm]			stddev [cm]		
		8 cm	20 cm	dx	dy	dz	dx	dy	dz	dx	dy	dz
RMK	125	3	4	-1,9	0,7	17,7	-0,2	0,2	18,3	10,3	9,2	14,7
DMC	92	5	4	-0,7	2,2	6,2	-0,5	2,1	4,0	12,6	9,6	18,5
UCX	129	6	2	-2,0	6,1	7,3	-1,2	6,1	5,7	9,4	8,4	18,0
DigiCAM	63	11	6	10,9	5,5	11,6	10,6	7,6	13,1	13,6	15,3	17,6

**Tab. 2:** Comparison of identical manhole cover measurements for RMK, DMC, UCX and DigiCAM, **8 cm GSD to 20 cm GSD.**

Camera	No. of points	No. of Models		mean [cm]			median [cm]			stddev [cm]		
		8 cm	20 cm	dx	dy	dz	dx	dy	dz	dx	dy	dz
RMK	36	3	4	-1,0	1,6	20,0	0,0	0,2	21,6	6,0	8,3	12,8
DMC	21	5	4	7,6	1,0	6,5	5,8	1,0	3,4	10,3	7,0	13,9
UCX	29	6	2	-0,6	4,8	10,1	0,3	5,4	9,7	6,4	7,1	15,1
DigiCAM	13	11	6	10,1	12,9	11,7	10,6	21,8	7,8	5,9	14,4	18,3

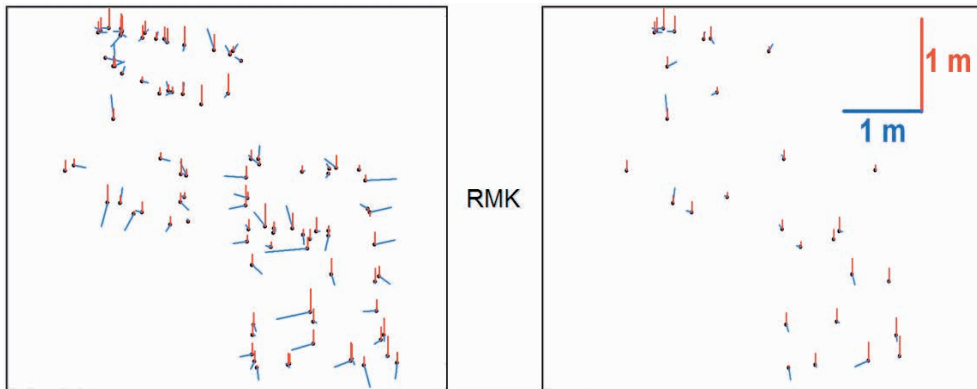


**Fig. 8:** Differences of all point measurements (left) and manhole cover measurements (right) for RMK, 8 cm GSD compared to 20 cm GSD for Area 2 and 3. Differences  $dx$  and  $dy$  (blue),  $dz$  (red).

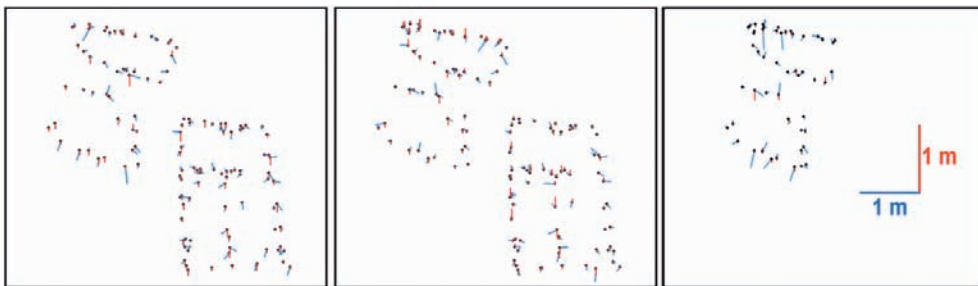


**Fig. 9:** Differences of all point measurements for Area 2 and 3 in 8 cm GSD. From left to right: RMK-DMC, RMK-UCX and RMK-DigiCAM (only northern Area 2). Differences  $dx$  and  $dy$  (blue),  $dz$  (red).

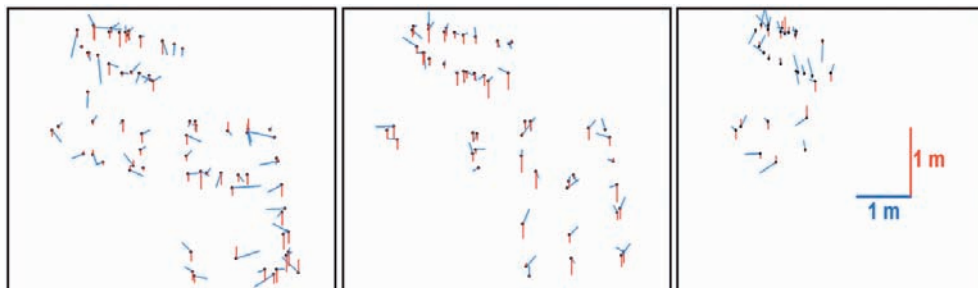


**Fig. 10:** Differences of all point measurements for Area 2 and 3 in 20 cm GSD. From left to right: RMK-DMC, RMK-UCX and RMK-DigiCAM (only northern Area 2). Differences  $dx$  and  $dy$  (blue),  $dz$  (red).

**Tab. 3:** Comparison of identical point measurements between RMK, DMC, UCX and DigiCAM, 8 cm GSD.

Cameras	No. of points	mean [cm]			median [cm]			stddev [cm]		
		dx	dy	dz	dx	dy	dz	dx	dy	dz
RMK - DMC	182	0,6	-2,6	1,7	1,2	-2,1	2,3	5,7	5,5	10,6
RMK - UCX	183	0,9	-0,9	2,6	1,2	-0,6	2,6	6,1	5,2	11,0
RMK - DigiCAM	104	0,9	-2,5	0,8	0,7	-1,9	0,8	7,3	7,9	8,4
DMC - UCX	184	0,3	1,7	4,5	0,2	1,8	4,0	4,7	5,6	11,1
DMC - DigiCAM	108	2,5	-0,3	-2	2,2	-0,3	-2	7,1	6,6	10,3
UCX - DigiCAM	130	3,3	-1,5	4,3	3,1	-0,7	3,8	6,8	6,8	9,4

**Tab. 4:** Comparison of identical manhole cover measurements between RMK, DMC, UCX and DigiCAM, 8 cm GSD.

Cameras	No. of points	mean [cm]			median [cm]			stddev [cm]		
		dx	dy	dz	dx	dy	dz	dx	dy	dz
RMK - DMC	53	-1,1	-1,9	-3,1	-1,3	-1,8	-3,4	2,9	5,2	7,7
RMK - UCX	54	-1,0	-0,5	2,9	-0,9	-0,6	2,6	3,6	4,9	8,3
RMK - DigiCAM	36	-0,1	0,2	1,2	-0,4	-0,8	-1,3	4,2	5,5	6,2
DMC - UCX	54	0,0	1,2	5,5	0,1	1,6	5,3	3,0	3,9	8,1
DMC - DigiCAM	35	0,9	0,3	-1,0	1,1	-0,1	-1,5	4,9	5,0	8,3
UCX - DigiCAM	45	1,7	-0,3	-6,3	2,5	-0,4	-5,0	4,8	4,8	7,2

**Tab. 5:** Comparison of identical point measurements between RMK, DMC, UCX and DigiCAM, 20 cm GSD.

Cameras	No. of points	mean [cm]			median [cm]			stddev [cm]		
		dx	dy	dz	dx	dy	dz	dx	dy	dz
RMK - DMC	97	-0,6	-2,1	- 9,7	- 0,6	-1,2	- 7,8	14,5	11,6	21,5
RMK - UCX	88	-0,9	2,3	-11,6	0,3	1,9	-18,5	9,4	10,6	23,3
RMK - DigiCAM	51	-6,6	2,3	0,9	- 6,9	1,5	- 1,5	14,3	17,0	18,3
DMC - UCX	72	-1,5	3,5	0,3	- 1,7	2,6	- 0,6	15,2	11,9	20,3
DMC - DigiCAM	37	-7,5	3,1	5,3	-11,6	3,6	2,7	18,0	14,3	23,4
UCX - DigiCAM	50	-7,1	1,1	2,1	- 9,0	2,1	5,3	14,1	13,3	25,4

**Tab. 6:** Comparison of identical manhole cover measurements between RMK, DMC, UCX and DigiCAM, 20 cm GSD.

Cameras	No. of points	mean [cm]			median [cm]			stddev [cm]		
		dx	dy	dz	dx	dy	dz	dx	dy	dz
RMK - DMC	20	7,5	-2,8	-14,1	6,8	-2,2	-17,0	11,7	8,8	20,7
RMK - UCX	22	-0,7	0,2	- 4,2	0,1	0,4	- 9,5	8,9	9,7	22,6
RMK - DigiCAM	11	-8,4	1,9	- 6,4	- 8,1	1,1	- 6,2	7,3	16,1	12,7
DMC - UCX	13	-6,7	3,6	1,7	- 6,5	0,9	5,0	10,5	11,3	14,0
DMC - DigiCAM	5	-19,3	8,9	- 4,1	-20,2	12,1	1,2	5,2	12,4	24,1
UCX - DigiCAM	11	-9,3	1,8	- 8,9	- 9,0	1,4	-26,5	7,8	14,3	29,1

than the digital aerial images leading to less precise height measurements. These height differences between scanned aerial images and digital aerial images correspond to RAG's experience on current projects for site plans and time series for earthworks on mine waste heaps, as up to 2008 only analogue cameras were used and from 2009 on selected digital aerial cameras. In the following a summary of these comparisons presented in Tabs. 3 to 6 will be given:

8 cm to 20 cm GSD, for each camera:

- For the RMK the stereo-photogrammetric height measurements in 8 cm GSD images are about 18 cm to 20 cm above the height measurements in 20 cm GSD.
- For the digital aerial cameras the stereo-photogrammetric height measurements in 8 cm GSD images are about 6 cm to 9 cm above the height measurements in 20 cm GSD.
- In 8 cm GSD images the dark inner part of the GCP is visible but not in 20 cm GSD. This leads to better point measurement conditions in height for 8 cm GSD images.

8 cm to 8 cm GSD, between different cameras:

- The accuracy for position measurements regarded between all cameras is 0.9 pixel and better.

- The accuracy for height measurements regarded between all cameras is 1.4 pixel and better.

20 cm to 20 cm, between different cameras:

- The accuracy for position measurements regarded between all cameras is 0.9 pixel and better.
- The accuracy for height measurements regarded between all cameras is 1.4 pixel and better.
- The RMK and DigiCAM height measurements are nearly on the same level. The height measurements of the RMK are about 10 cm below the height level of DMC and UCX, DMC and UCX are nearly on the same height level.

#### 2.4 Comparison of Stereo-photogrammetric Line Measurements

An attempt to analyse stereo-photogrammetric line measurements from different stereo-plotting results was made. Fig. 11 presents a comparison of stereo-photogrammetric line measurements in 8 cm GSD for RMK and DMC.

For this purpose identical points on lines within a buffer of 1 m for the OSKA-coding 5101 (road) and 5201 (path) have been selected. For these selected lines the attributes "no. of lines", "no. of line points", "difference in



**Fig. 11:** Line measurements in 8 cm GSD images for RMK (red) and DMC (blue). Background image: UCX orthophoto, 8 cm GSD.

**Tab. 7:** Comparison of identical line length measurements for RMK, DMC and UCX, 8 cm GSD to 20 cm GSD.

Camera	No. of lines	mean dl [cm]	median dl [cm]	stddev dl [cm]
RMK	83	5,3	2,1	7,4
DMC	57	8,7	3,7	10,1
UCX	87	5,7	2,1	7,6

**Tab. 8:** Comparison of identical line length measurements for RMK, DMC and UCX, 8 cm GSD.

Cameras	No. of lines	mean dl [cm]	median dl [cm]	stddev dl [cm]
RMK - DMC	85	2,9	1,4	4,8
RMK - UCX	102	4,2	2,3	5,3
DMC - UCX	111	3,2	1,2	5,0

**Tab. 9:** Comparison of identical line length measurements for RMK, DMC and UCX, 20 cm GSD.

Cameras	No. of lines	mean dl [cm]	median dl [cm]	stddev dl [cm]
RMK - DMC	65	7,4	3,0	10,6
RMK - UCX	83	4,7	2,0	7,7
DMC - UCX	57	7,3	2,8	9,0

length (dl)", "difference in position" and "shortest distance between lines" have been determined.

The comparisons in Tabs. 7 to 9 show that the identity of lines depends on the detectability of features due to weather conditions, the GSD and the better image quality of digital images. As it could be expected more identical lines were found for 8 cm GSD than for 20 cm GSD. The weather conditions for the DMC flight campaign seem to be worse for stereo-plotting purposes compared to RMK or UCX. Due to the contrast the visual perception of edges, like for kerbstones, is different between RMK and UCX or RMK and DMC in 8 cm GSD and in 20 cm GSD. But in 8 cm GSD UCX to RMK and UCX to DMC show a similar amount of identical lines. The influence of shadows leads to differences in position involving a smaller number of identical lines between RMK and UCX to DMC line measurements. But more interesting is the largest number of identical lines that was found for UCX and DMC in 8 cm GSD what leads to the

assumption that in this case the possibility to detect more detailed features in 8 cm GSD outmatches the influence of the insolation.

Even this comparison affirms the influence of the weather conditions in the way that no camera specific conclusions can be made by only regarding the stereoplotting results.

## 2.5 Determination of the Individual Point Measurement Accuracy and Differences to GPS Coordinates

Within the up to now presented comparisons and analyses the measurements of topographic points and lines were considered. For a more impartial analysis of the stereo-photogrammetric measurement accuracy, all GCP were triply re-measured in the 8 cm GSD images of RMK, DMC, UCX and DigiCAM. So the operator's individual point measurement accuracy could be determined (see Tab. 10).

Differing to the practical experience also the GCP outside the 60 % end lap stereo model

**Tab. 10:** Individual point measurement accuracy, 8 cm GSD.

Camera	Points in area	No. of GCP	No. of measurements	Individual point measurement accuracy [cm]								
				x			y			z		
				max	mean	std	max	mean	std	max	mean	Std
RMK	model	60	645	0,9	0,4	0,2	1,2	0,4	0,2	1,1	0,4	0,2
	border	45		0,9	0,3	0,2	1,3	0,4	0,2	1,0	0,4	0,3
DMC	model	58	735	1,2	0,4	0,2	1,6	0,4	0,2	1,6	0,6	0,3
	border	55		1,0	0,4	0,2	1,6	0,5	0,2	1,8	0,6	0,3
UCX	model	58	741	1,0	0,4	0,2	1,5	0,4	0,2	1,9	0,6	0,4
	border	50		1,2	0,4	0,2	1,1	0,5	0,2	1,7	0,6	0,3
DigiCAM	model	56	591	1,4	0,4	0,3	1,8	0,5	0,3	1,8	0,4	0,3

**Fig. 12:** Triply GCP re-measurements: Border lines of model area (yellow) and border area (red) for RMK, 8 cm GSD images.

area were measured to gain additional information about the measurement accuracy in the border areas (see Fig. 12). Depending on the four camera head technology it was not possible to allocate point measurements to the border areas for the DigiCAM. By this means the operator's individual point measurement accuracy could be determined to 0.5 cm in position and 0.6cm in height for all cameras in 8 cm GSD.

As already noted the stereo-photogrammetric point measurements still contain the influ-

ences of the AT. To describe and illustrate these deviations the manifold GCP measurements were compared to the coordinates of the terrestrial GPS measurements (see Tab. 11).

It can be noticed that the height measurements in the border areas of the RMK are noticeable worse than in the 60% end lap stereo model area. Over all the differences of the photogrammetric point measurements within the stereo model area compared to the GPS coordinates reaches an amount of better than 0.25 pixel in position and about 0.6 pixel in height.

**Tab. 11:** Differences of the threefold GCP re-measurements to the GPS coordinate.

Camera	Points in area	No. of GCP	No. of measurements	Difference to the GPS coordinate [cm]					
				x		y		z	
				mean	stdev	mean	stdev	mean	stdev
RMK	modell	60	125	-1,0	2,4	1,1	3,5	1,1	7,5
	border	45	90	-0,9	2,4	0,5	3,8	4,4	7,5
DMC	modell	58	122	-1,2	1,8	1,8	2,8	-1,3	3,4
	border	55	123	-1,3	1,9	2,3	2,6	-1,9	3,8
UCX	modell	58	134	-2,2	1,2	1,6	2,1	0,2	4,8
	border	50	113	-2,4	1,4	1,8	2,2	-2,1	5,4
DigiCAM	modell	56	197	-1,0	1,9	0,8	2,6	-2,9	3,4

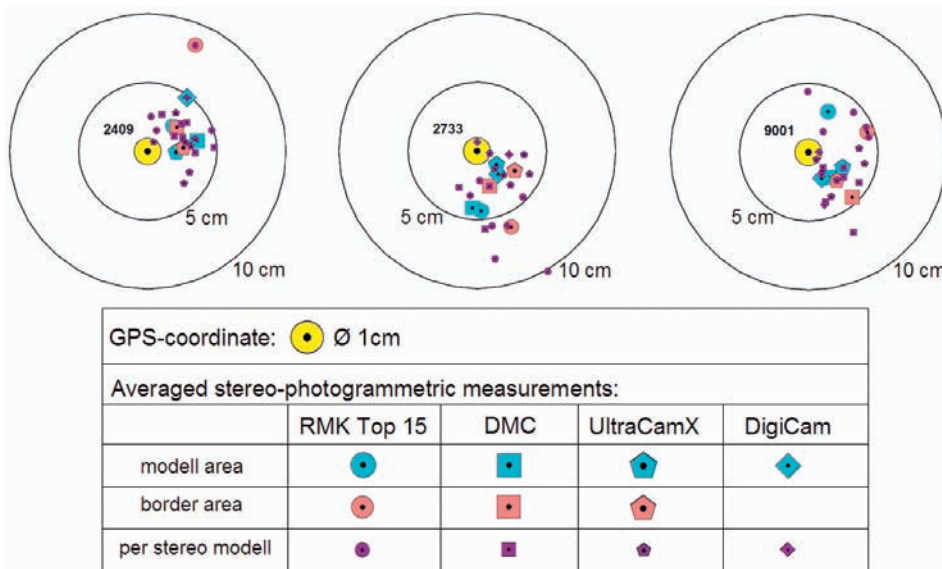


**Fig. 13:** Overview of the stereo-photogrammetric point measurements in 8 cm GSD for selected GCP related to the GPS coordinate. From left to right: GCP no. 2409, 2733 and 9001.

Fig. 13 shows the spreading of the point measurements related to the GPS coordinate for the three exemplarily chosen GCP 2409, 2733 and 9001. The circles show the 5 cm and 10 cm distance around the GPS coordinate. The blue symbols present all averaged GCP measurements in 8 cm GSD within the model area and the light red symbols the averaged GCP measurements for the border areas. Violet coloured symbols show the averaged location of each triply stereo-photogrammetric measurement. It can be seen that the measure-

ments in the images of all different cameras build clusters that lie relatively close to each other. The different location related to the GPS coordinate may give hints about the effects of the AT and bundle block adjustment.

### 3 Summary and Outlook

The comparison and analysis of the stereoploting results for the RMK Top 15, DMC, UltraCamX and Quattro DigiCAM revealed the

strong influence of the weather conditions, mostly the insolation. The different conditions for the flight campaigns in July, August, and September 2008 superimposed possible camera specific characteristics.

A non-camera specific point but important for the stereoplotting is the slow screen display by zooming in and out and, what is more, for the adjustment of brightness and contrast. This behaviour is caused by the inherent data structure (8 bit or 16 bit) of the digital aerial cameras images. Only with anew processed image pyramids for DMC, UltraCamX and DigiCAM the workings were feasible.

A difference in height with the amount of about 1 pixel could be depicted between scanned aerial images and digital images. The knowledge of this height difference is necessary if height measurements or DTM from diverse camera systems have to be compared. The analysis of the individual point measurement accuracy for RAG's operator was about 0.5 cm in position and 0.6 cm in height in all cameras' 8 cm GSD images. The difference of manifold re-measured GCP in 8 cm GSD images to the GPS-coordinate was in the amount of about 0.25 pixel in position and about 0.6 pixel height.

The accuracy between all cameras in 8 cm GSD and in 20 cm GSD was better than 0.9 pixel in position and 1.4 pixel in height. For the Quattro DigiCAM it has to be taken into account that one of the four camera heads was de-focused. It took getting used to work with the particular four image technique of the Quattro DigiCAM.

No recommendation for the one or the other camera can be given because this project showed that in daily practice the changing conditions like weather or insolation provide more uncertainties than the camera specific characteristics. The decision about which camera to use should thoroughly be considered by the application, the needed technical possibilities and the economic conditions.

In 2010 RAG will continue the working on Quattro DigiCAM and begin with Leica Geosystems ADS40 (2<sup>nd</sup> generation). Upon completion the stereoplotting results will be compared to the results of other group members that have to be expected in 2010.

## References

- ARIAS, B. & GOMEZ, J., 2007: Stereoscopic Accuracy. – International Archives of Photogrammetry, Remote Sensing and Spatial Information Sciences **36** (1/W51), on CD-ROM.
- BUSCH, W., 1989: Großräumige photogrammetrische Bodenbewegungsmessungen. – Das Markscheidewesen **96** (4): 323–327.
- LÜTZENKIRCHEN, K., 1974: Der erste Versuch einer großflächigen aerophotogrammetrischen Höhenaufnahme hoher Genauigkeitsforderung im Ruhrgebiet. – Schriftenreihe Lagerstättenerfassung und -darstellung, Bodenbewegungen und Bergschäden, Ingenieurvermessung **6**; Aachen, Institut für Markscheidewesen der RWTH Aachen.
- NEUMANN, K.J., 2004: Operational aspect of digital aerial mapping cameras. – International Archives of Photogrammetry, Remote Sensing and Spatial Information Sciences **35** (B1): 222–225.
- PERKO, R., KLAUS, A. & GRUBER, M., 2004: Quality comparison of digital and film-based images for photogrammetric purposes. – International Archives of Photogrammetry, Remote Sensing and Spatial Information Sciences **35** (B1): 136–1141.
- SPRECKELS, V., SCHLIENKAMP, A. & JACOBSEN, K., 2008: Geometric Characteristics of Digital Frame Cameras. – EARSeL Joint Workshop “Remote Sensing – New Challenges of High Resolution”, on CD-ROM.
- TALAYA, J., KORNUŠ, W., ALAMÚS, R., SOLER, E., PLA, M. & RUIZ, A., 2008: Analyzing DMC Performance in a Production Environment. – International Archives of Photogrammetry, Remote Sensing and Spatial Information Sciences **37** (B4): 1183–1188.

### Addresses of the Authors:

Dipl.-Ing. VOLKER SPRECKELS, LUZIE SYREK, Dipl.-Ing. ANDREAS SCHLIENKAMP, RAG Aktiengesellschaft, Geschäftsbereich Geoinformation/Vermessung (BG G), Photogrammetrie/Fernerkundung, Shamrockring 1, D-44623 Herne, Tel.: +49-2323-15-4640, Fax: -4611, e-mail: volker.spreckels@rag.de, luzie.syrek@rag.de, andreas.schlienkamp@rag.de.

Manuskript eingereicht: Dezember 2009

Angenommen: Januar 2010



# Status Report on the Evaluation of the Radiometric Properties of Digital Photogrammetric Airborne Cameras

MARIA VON SCHÖNERMARK, Oberpfaffenhofen

**Keywords:** Digital airborne cameras, radiometric properties, radiometric calibration

**Summary:** The new digital airborne sensors will open up new applications for photogrammetric sensors. This paper outlines the requests and the realisation of the radiometric analyses as part of the DGPF-project “Evaluation of digital photogrammetric aerial camera systems”. In order to learn the system properly sensor testing in operational conditions is essential. A short overview on the ground truth is provided. Investigations and results of the radiometric sensor evaluation – as far as available – will be presented and classified. At the end of the report some facts that should be improved in a subsequent mission are pointed out. The evaluation has not yet been finished.

**Zusammenfassung:** *Statusreport zur Evaluierung der radiometrischen Eigenschaften digitaler photogrammetrischer Luftbildkameras.* Digitale Luftbildkameras können neue photogrammetrische Anwendungsfelder erschließen. Dieser Aufsatz präsentiert Anforderungen und Realisierung der radiometrischen Qualitätsuntersuchungen als ein Teil des DGPF-Projekts zur „Evaluierung digitaler photogrammetrischer Kamerasysteme“. Um die Eigenschaften eines digitalen Sensors zu erfassen, sind Testflüge unter operationellen Bedingungen unerlässlich. Die durchgeführten Untersuchungen und Ergebnisse zum radiometrischen Test – sofern sie vorliegen – werden dargestellt und eingeordnet, wenn auch die Evaluierung zum gegenwärtigen Zeitpunkt noch nicht vollständig abgeschlossen ist. Am Ende des Berichts werden Verbesserungsvorschläge für eine nachfolgende Kampagne gegeben.

## 1 Introduction

The German Society of Photogrammetry, Remote Sensing and Geoinformation has initiated a project to test digital airborne cameras. An overview on the whole concept of the project and the airborne cameras and spectrometers participated in the test is given by CRAMER (2010) in the issue. This report covers only the activities of the radiometric team for the radiometric evaluation of the airborne digital cameras.

Digital airborne cameras are increasingly coming into operation to meet demands for remote sensing. Analogous cameras have been used for remote sensing applications to a much lesser extent due to the complexity of their radiometry. The expectation is that the new features of the digital cameras like linearity,

lower noise level and better radiometric resolution improve the image quality and the accuracy of the derived products and hence permit more remote sensing applications. However these aspired applications require a growing awareness of all involved persons for the problems of radiometry and radiometric calibration. The possibility to convert the digital numbers into radiation units opens up new and more sophisticated applications and allows us to realise the well-defined standards of digital image processing. For example, a challenging remote sensing task could be the estimation of the chlorophyll content of leaves or the determination of the leaf area index (MALENOVSKY et al. 2007, ZHANG et al. 2008, HUNT et al. 2008, ARS PROJECT 2009). Standard algorithms, applied previous to digital imaging processes, are for instance an at-

mospheric correction or a correction caused by the dependence of the reflection factor on the angles of illumination and observation which is known as BRDF (Bi-Directional Reflectance Distribution Function) correction (BEISL 2001, YENN et al. 2004, SCHÖNERMARK 2005, GARCIA-HARO et al. 2006, BEISL et al. 2008, ATCOR 2009). Calculations by YENN et al. 2004 for low flight altitude remote sensing data, have demonstrated that "Scattering and absorption due to aerosols can account for ~20% loss in the detected signal." Calibrated digital data of the cameras opens the possibility to correct this loss. Due to the BRDF a ground target may have a different look if the Sun or observer position changes. A normalisation of all data to a fixed illumination and viewing angle improves the possibility of correct comparison of different datasets and avoids the appearance of edges in the process of image mosaicking.

The consideration of increasing importance of the radiometric properties of digital airborne cameras has resulted into the decision to expand the evaluation of digital airborne cameras also within the DGPF-project into the region of radiometric review.

The idea to involve the radiometric properties into the evaluation process of digital cameras is not new. Since the availability of digital cameras on the market in-flight radiometric quality comparisons have been carried out (MARKELIN et al. 2008, EMMOLO et al. 2008, HONKAVAARA et al. 2007, MARKELIN 2006). In the initiative on camera certification of the European Spatial Data Research Network the radiometric performance and calibration of digital airborne cameras is one of the main topics and is fulfilled by HONKAVAARA, REULKE & DESSEILLIGNY. A report about these activities can be found by CRAMER (2009).

## 2 Concept of Radiometric Evaluation

### 2.1 *Classification in the Frame of the DGPF Project*

One of the main goals of many users of digital airborne cameras is the classification according to classes or states of objects, provided by

a statement of requirements. As an example one could consider the classification of land use or a vitality-classification of crown trees. The selection of a digital camera for such remote sensing tasks will be determined by its radiometric properties, such as the layout and the width of the spectral channels, the radiometric dynamics, the signal to noise ratio and the linearity of the response function. In addition, the importance of planning, scope of image processing and costs are decisive factors, however these points are not under discussion here.

Depending on demands some decent land cover or land use classifications can be processed using digital numbers (KLONUS 2009, LIM et al. 2009) if they are supported by significant operator intervention. For other tasks, such as the estimation of a crown tree's vitality, a pre-processing is necessary, for instance a BRDF correction (GERAD & NORTH 1997, SCHOMAKER 2007, GOUGEON 2009). A BRDF correction means a correction of the reflectance factor, which depends on the illumination and observation angle. Such a pre-processing requires a radiometric calibration of the sensor first, because the radiation units are needed for the calculations.

In order to minimise the different working teams the project leader set up a group of specialists for classification within the team of radiometric evaluation. Hence the report begins with some main activities of this group. The members of the classification group did a lot of ground truth work in order to allocate training data sets which can be used for a supervised classification. Furthermore data sets for the validation of classification accuracy are required. Due to bad weather conditions and subsequently a long period of evaluation flights, the ground truth work had to be repeated in dependence on occurrence of maturity or harvest. Afterwards the ground truth data sets of the different groups were harmonised and electronically stored (JORDAN et al. 2009). Figs. 1 and 2 depict for land use classification the selected classification area and the distribution of trainings/validation sets.

First results of land use classifications using the data of different digital airborne cameras (DMC, RMK-TOP, Quattro DigiCAM, JAS-150 and Ultracam-X) over the test site Vaihini-



**Fig. 1:** Vaihingen /Enz und selected classification area in red (KLONUS 2009).

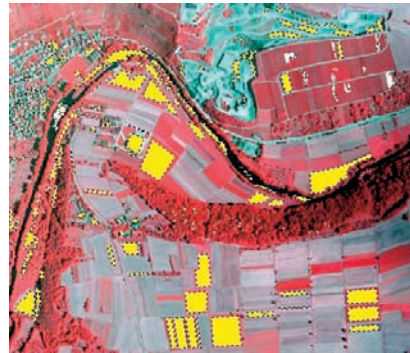


**Fig. 2:** Orthophoto of the distribution of the data sets in yellow which can be used for training or validation (with best thanks to Mr. KLONUS).

gen/Enz can be found in KLONUS et al. (2009) and KLONUS (2009) and in the issue on hand (WASER et al. 2010).

In Fig. 3 an example is given for the class “Shadow” taken from the work of KLONUS (2009). The different digital cameras took the flights over the test sites under different at-

mospheric conditions and at different time (Sun position). Problematic regions as shadows could be better separated by using an atmospheric and BRDF-correction. But unfortunately, up to now an atmospheric or BRDF-correction of the data of the different cameras has not yet been performed.

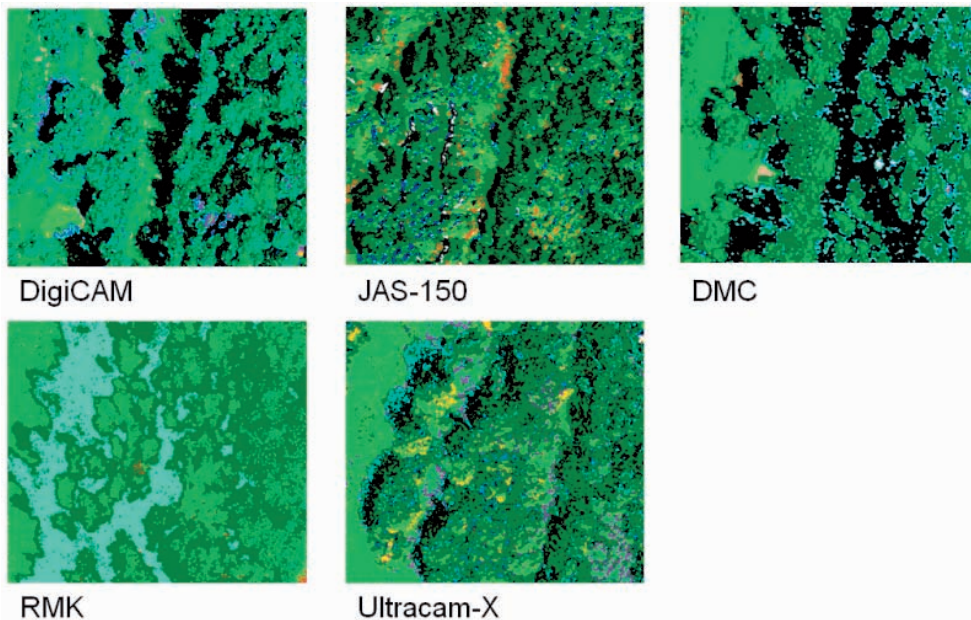


**Fig. 3:** Class “shadow” (for more explanations see KLONUS 2009), obtained from the data sets of the DGPf-evaluation project. The differences result on the one hand from the various properties of the cameras and on the other hand from the different weather conditions.

## 2.2 Ground Truth

In order to achieve the aim of the radiometric evaluation, a programme of ground truth measurements was installed on the so called radiometric field (CRAMER 2010). Coloured artificial planes and a large Siemens star were spread over the test site (cf. Fig. 2 in CRAMER 2010, this issue). Using the spectrometer AvaSpec-128-USB2 the spectral surface-leaving radiance of the coloured planes, of the white and black parts of the Siemens star and of some natural surfaces as grass, bare field and asphalt were measured (cf. Fig. 4).

In addition to these spectrometric measurements conducted by the University Stuttgart during every overflight, spectrometric reflectance measurements of different surfaces were performed sporadically by two other experts (Leica/Geosystems, University Halle, ASD Field Spec FR). Some measured ground truth spectra you can find in SCHOENERMARK 2008 und SCHWARZBACH 2008. The whole data set is stored at the University Stuttgart, Institute of Space Systems. The performed spectrometric ground truth measurements of the artificial coloured planes were compared with the laboratory spectral measurements of the German Aerospace Center, DLR (JUNG 2008). The differences were within the limits of the accuracy of the instruments and the laboratory calibration equipment (Ulbricht sphere).

In addition the so called bi-directional reflectance factor (BRF) was determined above grass. The BRF describes the reflected radiance in dependence on the illumination and observation conditions. The BRDF measure-



**Fig. 5:** BRDF-instrument GRADIS in operation.

ments were carried out with the instrument GRADIS (Ground Reflectance Angular Distribution Investigation System) which was built at the University Stuttgart, Institute of Space Systems. It is a lightweight transportable instrument with a central sensor design (cf. Fig. 5). It collects data in the blue, green, red and NIR region (SCHWARZBACH & SCHOENERMARK 2009A, 2009B).

Furthermore a Sun photometer of the Schulz & Partner GmbH (cf. Fig. 6) was used to measure the aerosol optical depth. These measurements allow us to evaluate the presence of clouds in front of the Sun. The knowledge of the aerosol optical depth is required to calculate the radiative transfer through the atmosphere with sufficient accuracy. The results of these calculations are needed for the calculation of the surface reflectance using the measured surface-leaving spectral radiance (GEIGER 2001, SCHÖNERMARK 2004).

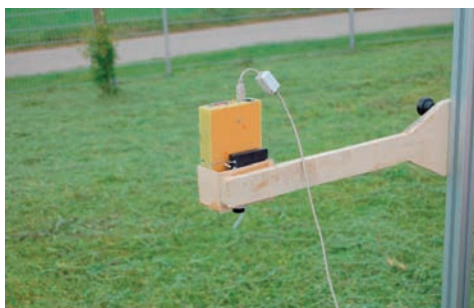


**Fig. 4:** Spectrometer AvaSPEC in operation at Vaihingen/Enz.



**Fig. 6:** Sun photometer on the test site at Vaihingen/Enz.

### 2.3 Radiometric Tests

The radiometric evaluation provides a basis for the further image processing. Topics as the histogram analysis, detection of artefacts, noise analysis and the linearity of the response function of sensors are investigated. The data analysed showed that the compression of the data have to be done very carefully. Often it is a source of error. Detailed information is given by HANUSCH & BALTSAVIAS (2009) and ZHOU (2009). Furthermore the analysis demonstrated that better and more comprehensive information from the manufacturers of the cameras and a closer cooperation is necessary to clarify some peculiarities of the different cameras. Details of the analysis can be found in HANUSCH & BALTSAVIAS (2009), who investigated DMC, ADS 40 and UltraCamX, SCHOENERMARK et al. (2009) looked at the linearity of DMC and JAS-150. ZHOU (2009) discussed some radiometric properties of DMC and JAS-150. The investigations of the last two authors mentioned are not comprehensive, they are a by-product of the efforts, to organise an in-flight-calibration.

The DGPF- project of evaluation digital cameras is a project without financial support. Unfortunately some institutions did not have the possibility to participate in the project or they were only able to operate on a small scale or they had to reduce the scale of operations in the course of time. This holds particularly for the radiometric evaluation of the digital airborne cameras. In addition some scientific institutions having volunteered for the evaluation had to concentrate on specific tasks linked up with their basic research. Therefore no complete radiometric evaluation can be expected in this project; desirable investigations are missing up to now. However without an optional participation of some institutions, radiometric investigations of digital airborne cameras would not exist at all!

In support of the radiometric evaluation two hyperspectral measurement flights were performed over the area of Vaihingen/Enz. On the 2nd of July the AISA+ sensor, provided and maintained by Hochschule Anhalt, took a spectral data set. The flight with the ROSIS sensor of the German Aerospace Center (DLR) was on the 15th of July. Currently the data sets

of these two flights are being analysed. First results are expected in July 2010.

### 2.4 In-flight Calibration

Another goal of the radiometric team was the in-flight-calibration of the digital airborne cameras. With exception of the ADS40 a relationship between grey levels (Digital numbers DN) in each channel and radiation units is not applicable for the users up to now. As it has been already mentioned, such a relationship presents a basis for challenging image processing inclusive pre-processing. In the frame of our project the information about the absolute values in radiation units of each camera channel would have been the ideal initial point for comparing the cameras and interpreting the different classification results.

To realise an in-flight-calibration, the properties of the surfaces (spectral surface-leaving radiance respectively the spectral reflectance) as well as the properties of the atmosphere (aerosol optical depth) have to be measured reliably. Based on these input data the radiance coming into the sensor of the airborne camera must be calculated using a precise radiative transfer code (no analytical solution is possible). The calculated radiance at the sensor has to be compared with the digital numbers registered by the sensor. Doing this procedure over different surfaces one will obtain a relationship between the radiance and the DN. This is the general concept of the so-called reflectance-based in-flight-calibration (BIGGAR et al. 1994, SLATER et al. 1987). For an airborne sensor flying in low altitudes one has to use this method. Special methods and algorithms for this procedure (for instance ATCOR 2009) exist for special conditions. The equations used for in-flight-calibration in the special programme ATCOR presume isotropic reflectance of the surface. Natural surfaces exhibit more or less anisotropy; however the artificial coloured planes displayed a very strong anisotropy (cf. Fig. 7). Unfortunately the team carrying out the spectrometer measurements at the ground quantified mainly the spectral reflectance of the artificial planes and only a few of natural surfaces. Therefore our in-flight-calibration using the programme



**Fig. 7:** Strong anisotropy of the artificial planes.

ATCOR failed. Generally the author and Dr. Richter have learned that an in-flight calibration using the ATCOR-programme requires the spectral reflectances of natural surfaces.

Another possibility to solve the problem would be the use of another appropriate algorithm for the correction of the influence of the atmosphere and the calculation of the reflectivity. Taking the equations of FRASER & KAUFMAN (1985) an appropriate algorithm has to be derived and calculated for the actual case. This is a very time consuming work and up to now no scientific institution could invest the necessary time into this task, hence an atmospheric or BRDF-correction has not been carried out up to now.

### 3 Constraints of the Radiometric Evaluation

The bad weather conditions in summer 2008 were the most serious obstacle. In Fig. 8 the measured aerosol optical depth at the wavelength of 533 nm is plotted. It can be seen, that a stable and low aerosol optical depth exists only on four or five days (2.7., 24.7., 9.9., 19.9. and constricted on 15.7.). A stronger variability and high values suggest evidence for clouds in front of the Sun. In this case the illumination conditions changed drastically and along with that also the reflectance of the surface depending on the illumination condition.

In order to minimize Sun glint the flight lines over the radiometric test site were flown North-South.

The team for the radiometric evaluation advised the flight over the radiometric test site at the true local midday time. This should guarantee that the changes of the Sun position can be kept at a low level so that all evaluation flights meet approximately the same illumination conditions. Fig. 9 depicts the reflection of a pinewood. It can be seen, that the time of least change in the reflectivity is noon. Furthermore the figure depicts the differences between cloudy and cloud free conditions. Hence the importance of the weather conditions for the in-flight calibration may be understood. In

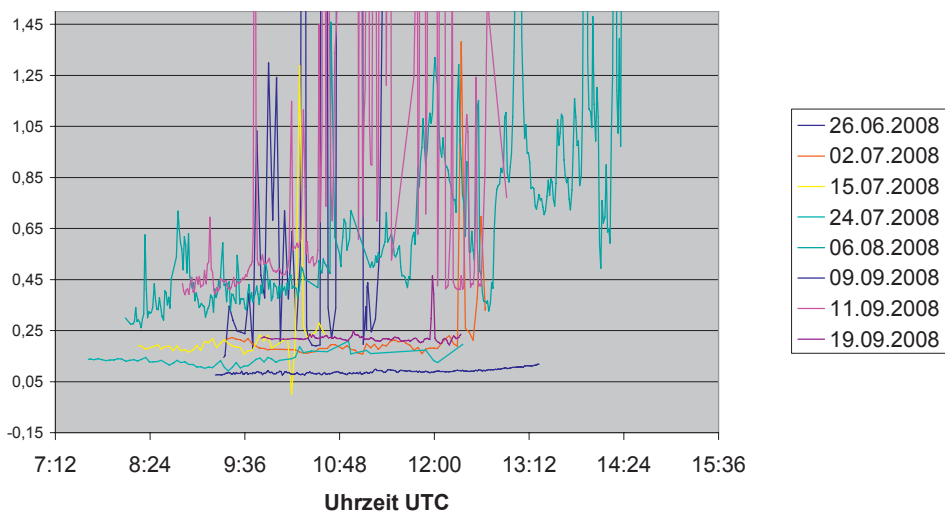


**Fig. 8:** Aerosol optical depth at 533 nm on the different days of evaluation flights, measurement at Vaihingen/Enz radiometric test site.

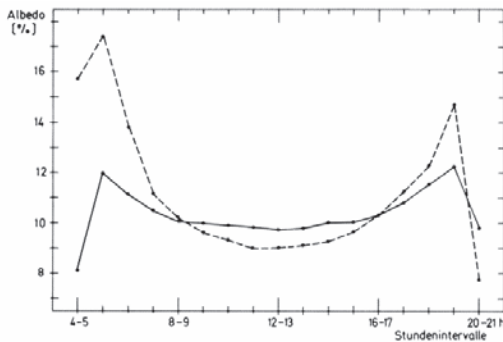


**Fig. 9:** Averaged diurnal variation of the reflectance (albedo) of a pinewood (KESSELER 1985). The continuous line holds for the situation of strong cloudiness (7/8 to 8/8), the dashed line for cloudless conditions (0/8 to 1/8).

addition the different reflections under different conditions of cloudiness and Sun position also influence the results of the classifications (see Fig. 3).

Due to the appearance of clouds in the morning, the flights over the radiometric test site were often earlier than advised or they were skipped completely.

#### 4 Conclusions – Lessons Learned by the Team

The radiometric evaluation has not yet been brought to an end. First results about sensor evaluation are published; partly these documents carry a preliminary character, because in the discussions with the manufacturers some misunderstandings could be resolved. Hence it would be advantageous, if information about the preprocessing of the data sets was provided by the manufacturers at the beginning of the next campaign.

By analysing the data sets it has become apparent that for a next campaign of experimental radiometric evaluation of airborne cameras it would be favourably to have available larger homogeneous radiometric test sites.

The usefulness of the artificial coloured planes is an issue under discussion. The advantage of these planes is that their spectral behaviour can be determined in the laboratory and does not change within the vegetation pe-

riod. Here we have to assume, that the planes are well cleaned before each overflight. The planes used in our evaluation period had a strong BRDF. One could be on the lookout for other planes with a less BRDF effect (BEISL 2009) or try to get information by the defence industry. The size of our planes were too small ( $2 \times 2$  m) for the spectrometers mounted on the airplanes.

Natural targets have the disadvantage that they rapidly change with the vegetation period and the measuring persons have to be careful to keep off the target. For a serious camera evaluation (for instance for a histogram analysis or the detection of artefacts) one needs large widely homogeneous targets, but for this purpose it is not necessary to control the spectral characteristics of these large targets. In contrast for an in-flight calibration the reflectivity of the natural targets must be known very exactly. They should exhibit widely isotropic behaviour, if one wants to apply atmospheric correction programmes which are available within the community. Otherwise one has to invest time into basic research or come into contact with military research.

The pros and cons of the use of asphalt, rock plateaus or concrete have to be taken into considerations also.

If one decides to use natural targets the operators shall reconsider how to take such measurements. Due to the inhomogeneity of natural targets, several measurements should be taken which have to be averaged afterwards.

#### Acknowledgements

Different groups of specialists participated in the field survey in order to get ground truth data for the classification: University Düsseldorf, chair in physical geography, EFTAS remote sensing, University Osnabrueck, Institute of Remote Sensing and Geoinformatics, C+B Techniques mbH, Martin-Luther-Universität Halle, Institute of Geosciences. Many thanks to them for their time consuming work! A team from the University Stuttgart, Institute of Space Systems (IRS) performed mainly the ground truth measurements in the test field. It was a time consuming and very hard work. In

addition to the ground-truth team of the IRS Dr. A. Jung from the University of Halle-Wittenberg and Dr. U. Beisl from Leica-Geosystems did spectrometric measurements of different surfaces. A lot of thanks to all!

And last but not least many thanks to Dr. R. Richter, DLR, Cluster of Applied Remote Sensing, who used his programme ATCOR to perform an in-flight-calibration of DMC and JAS-150 together with D. Zhou, student of the University of Stuttgart.

## References

- ARS Project: Evaluation of airborne color-infrared digital Camera to assess crop status and environmental conditions (2009–2011). – [www.ars.usda.gov/research/projects/projects.htm](http://www.ars.usda.gov/research/projects/projects.htm) (21.12.09).
- ATCOR 4, 2009: Atmospheric and Topographic Correction for wide FOV airborne optical scanner data. – [www.rese.ch/atcor/atcor4/index.html](http://www.rese.ch/atcor/atcor4/index.html) (2.12.09).
- BEISL, U., 2001: Correction of Bidirectional Effects in Imaging Spectrometer Data. – PhD Sensing Series Thesis, Remote 37, RSL, University of Zürich.
- BEISL, U., TELAAR, J. & SCHOENERMARK, M.V., 2008: Atmospheric correction, reflectance calibration and BRDF correction for ADS40 image data. – [www.isprs.org/congresses/beijing2008/proceedings/7\\_pdf/1.../02.pdf](http://www.isprs.org/congresses/beijing2008/proceedings/7_pdf/1.../02.pdf) (2.12.09).
- BEISL, U., 2009: personal information.
- BIGGAR, S.F., SLATER, P.N. & GELLMAN, D.I., 1994: Uncertainties in the In-Flight Calibration of Sensors with Reference to Measured Ground Sites in the 0.4–1.1  $\mu\text{m}$  Range. – *Remote Sensing of Environment* 48: 245–252.
- CRAMER, M., 2009: [www.ifp.uni-stuttgart.de/euroedr/index.html](http://www.ifp.uni-stuttgart.de/euroedr/index.html) (17.12.09).
- CRAMER, M., 2010: The DGPF-Test on Digital Airborne Camera Evaluation – Overview and Test Design. – this issue.
- EMMOLO, D., ORLANDO, P. & VILLA, B., 2008: Radiometric and Geometric Evaluation of the Capabilities of the new airborne digital Photogrammetric sensors. – *International Archives of the Photogrammetry, Remote Sensing and Spatial Information Sciences* 37 (B).
- FRASER, R.S. & KAUFMAN, Y.J., 1985: The relative importance of scattering and absorption in remote sensing. – *IEEE Transactions on Geosciences and Remote Sensing* 23: 625–633.
- GARCIA-HARO, F.J., COCA, F.C. & MELIA, J., 2006: Retrieving leaf area index from multi-angular airborne data. – *Annals of Geophysics* 49 (1): 209–218.
- GEIGER, B., DEMIRCAN, A. & SCHÖNERMARK, M. V., 2001: Exploiting multi-angular observations for vegetation monitoring. – *SPIE* 4171: 58–68.
- GERARD, F.F. & NORTH, P.R., 1997: Analyzing the effect of structural variability and canopy gaps on forest BRDF using a geometric-optical model. – *Remote Sensing of Environment* 62 (1): 46–62.
- GOUGEON, F.A., 2009: The Individual Tree Crown (ITC) Approach for Forest Inventories: Satellite and Aerial Sensor Considerations. – [blue.for.msu.edu/meeting/proc2/Gougeon.pdf](http://blue.for.msu.edu/meeting/proc2/Gougeon.pdf).
- HANUSCH, TH. & BALTSAVIAS, E., 2009: Evaluation of digital photogrammetric aerial camera systems, Radiometric Evaluation of DMC, ADS 40 and Ultracam X. – *DGPF Tagungsband* 18.
- HONKAVAARA, E. & MARKELIN, L., 2008: Radiometric Performance of Digital Image Data Collection – A Comparison of ADS40/DMC/ULTRACAM and EmergeDSS. – [www.ifp.uni-stuttgart.de/phowo07](http://www.ifp.uni-stuttgart.de/phowo07) (16.12.09).
- HONKAVAARA, E., MARKELIN, L.E., PELTONIEMI, J., AHOKAS, E., KUITTINEN, R., HYYPPÄ, J., SUOMALAINEN, J. & KUKKO, A., 2008: Radiometric calibration and characterization of large-format digital photogrammetric sensors in a test field. – *Photogrammetric Engineering & Remote Sensing* 74 (12): 1487–1500.
- HUNT, E.R., HIVELEY, W.D., DAUGHTRY, C.S.T., MCCARTY, G.W., FUJIKAWA, S.J., NG, T.L., TRANCHITELLA, M., LINDEN, D.S. & YOEL, D.W., 2008: Remote Sensing of Crop Leaf Area Index Using Unmanned Airborne Vehicles. – [www.asprs.org/publications/proceedings/pecora17.../0018.pdf](http://www.asprs.org/publications/proceedings/pecora17.../0018.pdf) (21.12.09).
- JORDAN, E., LÜCKE, C. & KLONUS, S., 2009: Status Landnutzungserhebungen Vaihingen. – [www.ifp.uni-stuttgart.de/dgpf/update300109/DGPF-StatusUpdate-Landnutzung-270109.pdf](http://www.ifp.uni-stuttgart.de/dgpf/update300109/DGPF-StatusUpdate-Landnutzung-270109.pdf) (1.10.2009).
- KESSLER, A., 1985: Über die kurzweilige Albedo eines Kiefernwaldes. – *Meteorologische Rundschau* 38: 82–91.
- JUNG, A., 2008: [www.dgpf.de/neu/project/Hannover08/HannoverTreffen.pdf](http://www.dgpf.de/neu/project/Hannover08/HannoverTreffen.pdf).
- KLONUS, S., HAGEDORN, C., JORDAN, E., CASTILLO, K., GONZALO, J. & VELEZ, F., 2009: Digitalisierung der Landnutzungserhebungen und erste Klassifikationsergebnisse. – Nachträgliche Publikation zum Vortrag auf der Jahrestagung Jena 2009, [www.ifp.uni-stuttgart.de/dgpf/PDF/JT09-Klonus\\_etal\\_statusreport.pdf](http://www.ifp.uni-stuttgart.de/dgpf/PDF/JT09-Klonus_etal_statusreport.pdf) (1.10.2009).

- KLONUS, S., 2009: Thematische Klassifikation von DMC, RMK, DigiCAM, JAS-150 und UCX-Bildern. – [www.ifp.uni-stuttgart.de/dgpf/Stuttgart09/2\\_4-KLONUS.pdf](http://www.ifp.uni-stuttgart.de/dgpf/Stuttgart09/2_4-KLONUS.pdf) (1.10.2009).
- LIM, H.S., MATJAFRI, M.Z. & ABDULLA, K., 2009: High Spatial Resolution Land Cover Mapping Using Remotely Sensed Image. – *Modern Applied Science* **3** (5): 82–91.
- MALENOWSKY, Z., ZURITA-MILLA, R., HOMOLOVA, L., MARTIN, E., SCHAEPMAN, M.E., GASTELLU-ECHTEGORRY, J.P., POKORNY, R. & CLECCERS, J.G.P., 2007: Retrieval of Coniferous Canopy Chlorophyll Content from high spatial Resolution Spectra Data. – [www.commission7.isprs.org/ispmsrs07/T17\\_Malenovsky\\_Ch1.pdf](http://www.commission7.isprs.org/ispmsrs07/T17_Malenovsky_Ch1.pdf).
- MARKELIN, L., HONKAVARA, E., PELTONIEMI, J., SUOMALAINEN, J. & AHOKAS, E., 2006: Radiometric Evaluation of Digital Aerial Cameras. – [www.isprs.free.fr/documents/Papers/T01-02.pdf](http://www.isprs.free.fr/documents/Papers/T01-02.pdf) (16.12.2009).
- SCHÖNERMARK, M.V., GEIGER, B. & RÖSER, H.P. (eds.), 2004: Reflection Properties of Vegetation and Soil with a BRDF data base. – Berlin, ISBN 3-89685-565-4.
- SCHÖNERMARK, M.V., 2005: Aufnahmeobjekt und Atmosphäre. – Kap. 3 in *Digitale Luftbildkamera*, Wichmann.
- SCHÖNERMARK, M.V., 2008: [www.ifp.uni-stuttgart.de/dgpf/Hannover08/11.pdf](http://www.ifp.uni-stuttgart.de/dgpf/Hannover08/11.pdf) (7.1. 2010).
- SCHÖNERMARK, M.V., KIRCHGÄSSNER, U., SCHWARZBACH, M., PUTZE, U. & ZHOU, D., 2009: Überblick über die Arbeiten der Radiometriegruppe zur DGPF-Jahrestagung. – [www.ifp.uni-stuttgart.de/dgpf/PDF/Jena09-Paper-Schoenermark-Radiometrieueberblick.pdf](http://www.ifp.uni-stuttgart.de/dgpf/PDF/Jena09-Paper-Schoenermark-Radiometrieueberblick.pdf) (1.10.2009).
- SCHOMAKER, M.E., ZARNOCH, S.J., BECHTHOLD, W.A., LATELLE, D.J., BURKMANN, W.G. & COX, S.M., 2007: Crown-condition classification: a guide to data collection and analysis. – Gen. Tech. Rep. SRS **102**, Asheville, NC: U.S. Department of Agriculture, Forest Service, Southern Research Station.
- SCHWARZBACH, M., 2008: [www.ifp.uni-stuttgart.de/dgpf/Hannover08/11.pdf](http://www.ifp.uni-stuttgart.de/dgpf/Hannover08/11.pdf) (7.1. 2010).
- SCHWARZBACH, M. & SCHÖNERMARK, M. v., 2009a: Advances in BRDF field measurement: new principle and instrument. – IEEE International Geoscience and Remote Sensing Symposium (IGARSS).
- SCHWARZBACH, M. & SCHÖNERMARK, M. v., 2009b: High resolution BRDF measurement of natural surfaces. – *ISRSE 2009*, PS-C4–1.
- SLATER, P.N., BIGGAR, S.F., HOLM, R.G., JACKSON, R.D., MAO, Y., MORAN, M.S., PALMER, J.M. & YUAN, B., 1987: Reflectance- and Radiance-Based Methods for the In-Flight Absolute Calibration of Multispectral Sensors. – *Remote Sensing of Environment* **22**: 11–37.
- WASER, L.T., KLONUS, S., EHLERS, M., KÜCHLER, M. & JUNG, A., 2010: Potential of Digital Sensors for Land Cover and Tree Species Classifications – A Case Study in the Framework of the DGPF-Project. – this issue.
- YUEN, P.W.T., KILLY, A., HOBSON, S. & BISHOP, S.H., 2004: Atmospheric Correction Preprocessing Techniques in Hyperspectral Remote Sensing. – 1st EMRS DTC Technical Conference.
- ZHANG, Y., CHEN, J. M., MILLER, J.R. & NOLAND, TH.L., 2008: Leaf chlorophyll content retrieval from airborne hyperspectral remote sensing imagery. – *Remote Sensing of Environment* **112**: 3234–3247.
- ZHOU, D., 2009: Radiometric assessment for digital airborne cameras. – Student thesis, Universität Stuttgart, not published.

## Address of the Author:

Dr. MARIA VON SCHÖNERMARK, Deutsches Zentrum für Luft-und Raumfahrt, Institut für Raumflugbetrieb und Astronautentraining, Münchner Str. 20, 82234 Weßling, Tel.: 08153-28-2527, FAX: -2468, e-mail: maria.schoenermark@dlr.de.

Manuskript eingereicht: Dezember 2009

Angenommen: Januar 2010





## Potential of Digital Sensors for Land Cover and Tree Species Classifications – A Case Study in the Framework of the DGPF-Project

LARS T. WASER, Birmensdorf, Switzerland, SASCHA KLONUS, MANFRED EHLERS, Osnabrück, MEINRAD KÜCHLER, Birmensdorf, Switzerland & ANDRÁS JUNG, Halle

**Keywords:** Digital airborne Systems, Land Cover Classification, Logistic Regression, Maximum Likelihood, Tree Species

**Summary:** The study is intended as a contribution to assessing the value of digital image data for semi-automatic analysis of classified land cover and tree species and was carried out in the framework of the DGPF-project. Sensor specific strengths of ADS40-2<sup>nd</sup>, Quattro DigiCAM, DMC, JAS-150, Ultracam-X, and RMK-Top15 cameras and weakness for classification purposes are presented and shortly discussed. The first approach is based on a maximum likelihood method in combination with a decision tree and produces 13 land cover classes. The second approach is based on logistic regression models and produces eight tree species classes.

The classified images were visually assessed and quantitatively analyzed. The accuracy assessment reveals that in both approaches similar classification results are obtained by all sensors with overall Kappa coefficients between 0.6 and 0.9. However, a real sensor comparison was not possible since the image data was acquired at different dates. Thus, some variations in the classification results are due to phenological differences and different illumination and atmospheric conditions. It is planned for the future that the classifications of the first approach will be adjusted to the characteristics of each sensor. In the second approach, further work is needed to improve distinguishing non-dominant, small and partly covered deciduous tree species.

**Zusammenfassung:** *Potenzial digitaler Sensoren zur Klassifizierung der Landbedeckung und Baumarten – eine Fallstudie im Rahmen des DGPF-Projektes.* Anhand der Bilddaten aus den Kamerasystemen ADS40-2<sup>nd</sup>, Quattro DigiCAM, DMC, JAS-150, Ultracam-X, und RMK-Top15 wurden zwei Klassifikationsverfahren (Maximum Likelihood und logistische Regression) getestet. Dabei wurden sensor-spezifische Eigenschaften erläutert, sowie die Stärken und Schwächen der einzelnen Systeme aufgezeigt.

Die Resultate wurden visuell und quantitativ bewertet. Direkte Sensorvergleiche erwiesen sich dabei als schwierig, da zum Aufnahmezeitpunkt der einzelnen Bilddaten sowohl eine unterschiedliche Vegetationsentwicklung wie auch Unterschiede in den Beleuchtungs- und atmosphärischen Verhältnissen vorherrschten. Quantitative Analysen zeigen, dass sich mit jedem Kamerasysteme sehr ähnlich gute Resultate erzielen liessen. Das erste Verfahren zeigt für 13 Landnutzungsklassen Kappa Koeffizienten von gut 0,6 bei allen verwendeten Systemen. Allerdings unterscheidet sich die Genauigkeit der einzelnen spezifischen Klassen wie Mais oder Kartoffeln für die unterschiedlichen Kameras. Hierzu soll in weiteren Analysen das Klassifikationsverfahren an die jeweiligen Kameras angepasst werden. Für das zweite Verfahren liegt der Kappa Koeffizient für 8 Baumarten zwischen 0,7 und 0,9. Bei diesem Verfahren soll in zukünftigen Analysen die Genauigkeit der Erkennung von nicht dominanten, kleinen und teilweise verdeckten Baumarten erhöht werden.

## 1 Introduction

This paper compares different aerial cameras for land cover classification purposes. It was carried out in the framework of the project of the German Society for Photogrammetry, Remote Sensing and Geoinformation (DGPF). An overview and test design of this project is given in this issue (CRAMER 2010). In the DGPF-project "Evaluation of digital aerial cameras" a special interest group "Thematic Analysis" was initiated within the radiometry working group. The objective of this group is the comparison of the different aerial cameras in terms of information extraction.

While there are many articles related to the radiometric comparison between different aerial cameras (MARKELIN et al. 2006; HOONKVAARA et al. 2009), there are only a few articles related to a comparison of the classification accuracy between different aerial cameras. E. g. EHLERS et al. (2007) used different supervised classification methods to compare DMC, UCD and ADS40 data. ROSSO et al. (2008) compare different spectral curves of specific plant species from DMC, UCD and ADS40 data. Further articles are related to this project (KLONUS 2009; KLONUS et al. 2009).

The focus of the Institute for Geoinformatics and Remote Sensing (IGF) at the University of Osnabrück in this article is on an entire land cover classification whereas the group Pattern Recognition and Photogrammetry at the Swiss Federal Research Institute (WSL) focusses on the classification of forest area and different tree species.

The general objective of an image classification is the automatic allocation of all pixels to land cover classes or specific themes. The grey value of each pixel is the numeric base for this allocation (LILLESAND & KIEFER 1994). According to JENSEN (2005) the multispectral classification can be processed using one or more of the following approaches:

- algorithms based on parametric and non-parametric statistics
- supervised and unsupervised classification algorithms
- the use of hard or soft classifications (Fuzzy)
- pixel and object based classification algorithms

- or hybrid approaches.

None of these classification methods is superior to another. The most appropriate classification strategy depends on different parameters such as the biophysical characteristics of the research area, the homogeneity of the remote sensing data and the "a priori" knowledge (JENSEN 2005). Even a standard algorithm, such as the maximum likelihood, could produce better results than modern algorithms such as ANN (artificial neural networks) (ERBEK et al. 2004) or boosting (BAILLY et al. 2007). An overview of classification algorithms is given in (LU & WENG 2007).

According to SCOTT et al. (2002), modern regression approaches are particularly useful for modelling the spatial distribution of tree species and communities. When analyzing the relationship between categorical dependent variables and remotely sensed data logistic regression models are very powerful. Thus, regression analyses with explanatory variables derived from high-resolution remote sensing data seem very promising for the second part of this article – modelling tree area and tree species. Some recent forest research has focused on integrating multisensor data to estimate forest area (WANG et al. 2007; WASER et al. 2008a), forest composition and tree species (HEINZEL et al. 2008). But only few studies have already shown that optical digital airborne data have also been opened up new opportunities for tree species classification: The data are recorded by frame-based sensors, e. g. DMC (HOLMGREN et al. 2008), Ultracam-X (HIRSCHMUGL et al. 2007) or line-scanning sensors, e. g. ADS40 (WASER et al. 2008b), which provide stereo-overlap of up to 90 % or entire image strips with higher radiometric resolution.

The main objective of this article was to show the potential of frame-based camera systems (DMC, Quattro DigiCAM, Ultracam-X), two line scanning systems (ADS40-2<sup>nd</sup>, JAS-150) and a classical analogue camera (RMK-Top15) for two different classification approaches. Sensor specific strengths and weakness for classification purposes will be briefly investigated and emphasis was placed on objectivity and not only on accuracy of classification.

## 2 Material

### 2.1 Study Area

The DGPF-project study area is located about 20 km north-west of Stuttgart/Germany in a hilly area providing several types of vegetation and land use, mostly rural area with smaller forests and villages, quite steep vineyards and some quarries.

To save processing time, two smaller areas of the DGPF-project study area were chosen as test sites for the classification algorithms (cf. Fig. 1). To collect ground truth data for interpretation and classification of the recorded scenes different field trips were carried out. Both particular locations were chosen, because they present the highest heterogeneity of our study area and include artificial and natural areas. In test site 1 nearly all crops were represented, whereas test site 2 is characterized by different forest types.

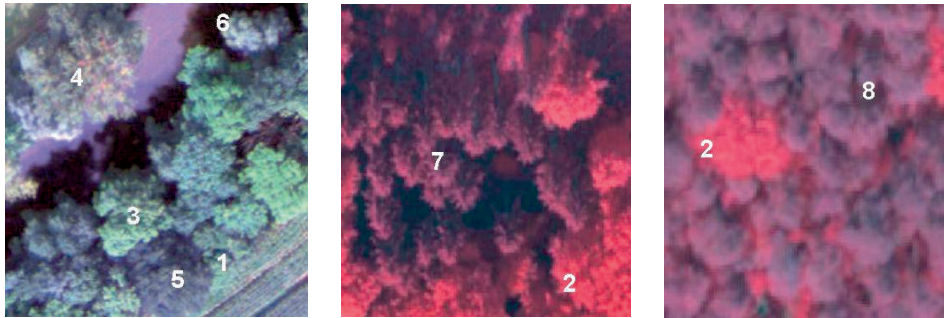
#### Test Site 1

Test site 1 is located between the villages Vaihingen and Rosswag. And is approx. 2 km<sup>2</sup> in area. The terrain is mostly characterized by agricultural fields in the South and vineyards in the northern part. The area is crossed by a forest, a stone quarrel and the river Enz.

The first field survey was carried out on 12<sup>th</sup> and 13<sup>th</sup> of April 2008 and arranged by the company EFTAS of Münster. Summer and winter crops as well as different objects in the settlements were recorded. The entire spectrum of field crops (nearly 85% of the area) and tree species in selected forest areas were recorded between 20<sup>th</sup> and 22<sup>nd</sup> of June 2008 by experts from the University of Düsseldorf (HHUD). The field survey of the University of Osnabrück was carried out during the first flights of the digital aerial cameras between 27<sup>th</sup> and 31<sup>st</sup> of July 2008. The data was collected for selected areas and updated from the HHUD. During the recording of the Ultracam-X and AIC images another field survey from 10<sup>th</sup> of September to 3<sup>rd</sup> of October 2008 was carried out by the company C+B Technik GmbH. The mapping also included the field crops in autumn. The last field survey was carried out by experts of the University of Düsseldorf from 18<sup>th</sup> to 19<sup>th</sup> of October 2008. The field crops from the first field trip were updated and the current field crops were recorded. Prior to digitizing and storing the field information in vector files all field surveys were documented with photographs in the directions North, South, East and West for the different field crops.



Fig. 1: DMC RGB Orthoimage of test sites 1 and 2.



1. Maple, 2. Beech, 3. Ash, 4. Poplar, 5. Oak, 6. Willow, 7. Norway spruce, 8. Scots pine

**Fig. 2:** Examples of the 8 sampled tree species in test site 2 as they appear in the ADS40-2<sup>nd</sup> imagery (RGB and CIR).

## Test Site 2

Test site 2 is located in the southern part of the village Rosswag and is approx. 1.75 km<sup>2</sup> in area. The terrain varies (forest slopes and flat areas along the river Enz) with mixed land cover and forest. The altitude ranges from 240 m to 410 m a.s.l. The forest area covers approx. 0.7 km<sup>2</sup>, and is mostly characterized by mixed forest (approx. 80%) and riverside woodland (approx. 20%). The dominating deciduous tree species are ash (*Fraxinus sp.*), beech (*Fagus sp.*), poplar (*Populus sp.*) and willow (*Salix sp.*) and less frequently maple (*Acer sp.*) and oak (*Quercus sp.*). Norway spruce (*Picea Abies*) and Scots pine (*Pinus sylvestris*) are the main coniferous trees. The ground truth data to validate the different outputs was collected in the natural environment to be representative for test site 2. For the validation of the tree cover (forest area), two types of samples were distinguished (tree area / non tree area) and a total number of 2 × 60 samples were digitized from the four input orthoimages. To determine the eight main tree species, a ground survey visiting 240 trees was carried out on 10<sup>th</sup> of June 2009. Typical examples of each tree species as seen in the ADS40-2<sup>nd</sup> RGB and CIR images are shown in Fig. 2. This information was used to calibrate and validate the logistic regression models.

## 2.2 Optical Sensors

In the framework of the DGPF-project, data was recorded by nine different aerial cameras: DMC, ADS40-2<sup>nd</sup>, JAS-150, Ultracam-X, RMK-Top15, Quattro DigiCAM, AIC-x1, AIC-x4 and DLR 3K-Kamera. Most of the cameras (DMC, RMK-Top15, ADS40-2<sup>nd</sup>, Quattro DigiCAM) recorded the data on 06<sup>th</sup> of August 2008, whereas the data from JAS-150, Ultracam-X, AIC-x1, was recorded at the beginning of September. The data of the Canon 3K camera from DLR, which was recorded on 15<sup>th</sup> of July 2008 was not used in this study due to large seasonal differences. Tab. 1 gives an overview of the characteristics of the six camera systems for which the data was available on time and therefore have been tested for classification of land cover and tree species. Although the image data was recorded with a ground sampling distance (GSD) of 8 and 20 cm by all cameras, a GSD of 20 cm was considered to have sufficient terrain detail for our study.

In terms of spectral characteristics DMC and JAS-150 recorded the data in the visible red, green and blue and in the near-infrared (NIR) range. Ultracam-X recorded the data in the same wavelengths, but provided only the visible bands for the test sites. The Quattro DigiCAM recorded the data only in the three visible bands: red, green and blue. For the RMK-Top15 camera the NIR, red and green data was available at 20 cm resolution. To use

**Tab. 1:** Summary of characteristics of the image data used in this study.

Sensor	ADS40-2nd	DMC	RMK-Top15	Quattro DigiCAM	JAS-150	Ultracam-X
Used in test site	2	1,2	1	1	1,2	1,2
Acquisition date	06/08/2008	06/08/2008	06/08/2008	06/08/2008	09/09/2008	11/09/2008
Spectral resolution (nm)	RGB+NIR B: 428-492 G: 533-587 R: 608-662 NIR: 833-887	RGB+NIR B: 429-514 G: 514-600 R: 600-676 NIR: 695-831	RG+NIR B: -- G: -- R:-- NIR:--	RGB B: 400-540 G: 480-600 R: 580-660 NIR: --	RGB+NIR B: 440-510 G: 520-590 R: 620-680 NIR: 780-850	RGB+NIR B: 400-580 G: 500-650 R: 590-675 NIR:--
Spatial resolution	20 cm	20 cm	20 cm (RGB: 8 cm)	20 cm	20 cm	20 cm
Radiometric resolution	12 bit	12 bit	--	14 bit	12 bit	>12 bit

at least three different bands of each sensor DMC, JAS-150, DigiCAM and Ultracam were studied together using the RGB bands. RMK-Top15 was also included but using the band combination RGN (red, green, near infrared). The objectivity of our comparisons is slightly reduced by this compromise. The usage of the NIR band of the RMK-Top15 has the advantage that the entropy is substantial higher than it is when only using optical bands, because the RGB bands have a higher correlation between each other and therefore lower entropy. Additionally, the main advantage of the NIR information is the better detection of plants (ALBERTZ 2001). Concerning the four band classifications only ADS40-2<sup>nd</sup>, DMC and JAS-150 data could be compared since only for these three cameras all four channels were available.

### 2.3 LiDAR DTM and DSM

In addition to the image data, a LiDAR flight was realized on 21 August 2008 by a Leica ALS 50 scanner with an average point density of 5 points / m<sup>2</sup>. For our investigations DSM and a DTM grid of 0.25 m raster width was produced from the raw data. A colour coded hillshade of the LiDAR DSM is given in Fig. 9. 20 cm orthoimages have been calculated from each data set using the LiDAR DTM.

## 3 Methods

### 3.1 Land Cover Classification

To ensure the objectivity of the comparison, the same training areas for all different cameras were chosen. The training areas were chosen after the criteria by DENNERT-MÖLLER (1983). They had to be

- connected and large enough
- all the pixels in an area need to be contiguous
- homogeneous with an unmixed spectral signature
- be representative for each class
- and spectrally well separable.

The classification method consisted of two steps: a pixel-based maximum likelihood classification (JENSEN 2005) and a decision tree based classification. The maximum likelihood method was used because it showed the best results among other six classification methods for different agricultural scenes in a previous study (KLONUS & EHLERS 2009). Additionally, a higher objectivity is ensured since it is relatively simple and only a few parameters need to be defined. To avoid an inaccurate classification, weights to each of the classes were added. These weights were the same in all the scenes of all the cameras and were determined using experienced data from other classifications.

The normalized difference vegetation index (NDVI) was added as an additional input parameter for the comparison between DMC and JAS-150 data. The results of the maximum likelihood classification (in the form of a layer) together with the grey value information of the input bands (and the NDVI – if available) were used to build the decision tree.

A decision tree is a hierarchy of rules and consists of different nodes. The first or root node is displayed at the top, connected by successive branches to other nodes. These are similarly connected until a leaf node is reached, which has no further branches. Each leaf node is similar to a class in Tab. 3. The classification of a particular pattern (vector in feature space) begins at the root node. Each node contains a rule, e. g.  $NDVI > 500$ . The different branches from the root node correspond to the different possible answers, in this case yes or no. Based descendent on the answer it follows the appropriate branch to a subsequent or descendent node. Therefore the branches must be mutually distinct and exhaustive. The next step is to make the decision at the sub-tree appropriate subsequent node, which can be considered the root of a sub-tree. This way is continued until a leaf node is reached, which has no further rule (DUDA et al. 2001).

To guarantee a high objectivity of the classification the settings for the decision tree were extracted automatically from the training areas using the mean and standard deviations of the pixel values in these areas. Overall, fourteen different classes were distinguished for this classification (see Tab. 3). The images were visually assessed and quantitatively analysed using 255 randomly chosen points in the classified images. Then the points were compared to field data, and producers' and users' accuracy and the kappa coefficient were calculated. Classes that had less than five points were not included in the analysis (see also Tab. 2).

### 3.2 Tree Species Classification

#### Variables Derived from Remotely Sensed Information

The extraction of tree area and classification of tree species is based on logistic regression models (for details see, e. g., HOSMER & LEMESHOW 1989). As explanatory variables several geometric and spectral signatures were derived from the remote sensing data using standard digital image processing methods as described in (GONZALES & WOODS 2002).

A detailed extraction of geometric and spectral explanatory variables derived from airborne remote sensing data is described in WASER et al. (2007 and 2008a). The explanatory variables used in this study consist of four commonly used geometric parameters derived from the LiDAR DSMs (slope, curvature, and two local neighbourhood functions: rate of change in slope for each cell and assessment of topographic position). For further details, see BURROUGH (1986).

Based on experiences made in WASER et al. (2008b) as spectral input variables we produced for each data set: four original bands (RGB and NIR) of ADS40-2<sup>nd</sup>, DMC and JAS-150, Ultracam-X (only 3 bands RGB were available); the 3 ratios of each RGB band divided by the sum of the corresponding three bands; and the three colour transformations from RGB to IHS into the 3 channels intensity (I), hue (H), and saturation (S). In total we have derived ten spectral input variables from each of the ADS40-2<sup>nd</sup>, DMC and JAS-150 data sets and 9 from the Ultracam-X where no NIR channel was available for this study.

#### Image Segmentation

Homogenous image segments of individual tree crowns or tree-clusters are needed to extract the tree area and to classify tree species (see below). The four orthoimages were therefore subdivided into patches by a multi-resolution segmentation using the Definiens 7.0 software (BAATZ & SCHÄPE 2000). The RGB bands are used as input data with the LiDAR DSMs providing additional geometric information (height and slope). Segmentation was iteratively optimized using several levels of detail

and an adapted to shape and compactness parameters.

Finally, the means and standard deviations of the remotely sensed explanatory variables, the variables derived from them were calculated for each segment.

### Tree Cover

The extraction of the tree area is a required input in classification of the tree species approach. Tree canopy and non-tree area masks were generated in five steps. First, a digital canopy height model (CHM) was produced subtracting the LiDAR DTM from the DSM. In a second step, pixels with CHM values  $> 2$  m were used to extract potential tree areas. Then four shadow masks were empirically generated using the spectral information (ratio of channels) from the four input orthoimages. In a fourth step, non-tree objects, e. g. buildings, roofs, artefacts in the CHMs were removed using NDVI values (ADS40-2<sup>nd</sup>, DMC, JAS-150) or ratio of red / green bands (Ultracam-X) information (curvature) about the image segments (e. g. segments on buildings have lower curvature values and ranges). These four steps resulted in a canopy cover per data set (four in total) providing discrete tree / non-tree data.

Then in a fifth step, based on these canopy covers, four fractional tree covers were produced using logistic regression and the four topographic variables from the CHM as described above, with a probability for each image segment that it belongs to the class “tree”. The probability (P) for each pixel that belongs

to the class “tree” ranges between 0 and 1. Segments with a tree probability of 0.5 or more were assigned to the class “tree”, the others to the class “non-tree”. To validate the method, a similar regression was applied to segments with our ground truth data with a tree or non-tree sample unit by at least 50%. The validation consisted of a 5-fold cross-validation of the logistic model.

### Tree Species Classification

The tree species were classified within the tree covers (for each data set) using logistic regression models. Prior to modelling the tree species for the whole area, the variables were selected empirically using the image segments of each data set with species assignments. The best model runs were obtained using the variables derived from the IHS transformations of the original image bands (means and standard deviations) and the NIR bands (if available). As output, probabilities for each tree species within an image segment were obtained for each data set. The following eight tree species were modeled: ash, beech, maple, Norway spruce, oak, poplar, Scots pine, and willow.

## 4 Results and Discussion

### 4.1 Visual Analysis

Prior to image classification of test site 1 a visual analysis was performed to detect similar training areas. For interpretation purposes the images of the different sensors are displayed



**Fig. 3:** Red band of DMC (left) and RMK-Top15 (right).



**Fig. 4:** Red band of Quattro DigiCAM (left) and JAS-150 (right).

in the red band (Figs. 3–5). The red band was chosen since only the red and green bands were available for all sensors. At first glance, visual analysis revealed that most of the images of the different cameras have a similar quality and the different field crops and land cover classes could be easily extracted.

However, the missing atmospheric correction is clearly visible in the RMK-Top15 and the JAS-150 images. The position of the sun during image acquisition was east of the scenes and the effects can be clearly seen on the roof of the big farmyard at the bottom.

Some differences in the appearance of the vegetation are also visible in the field in the north of the big farmyard. While the contrast between the different fields in images from DMC and RMK-Top15 is high, images from Ultracam-X are characterized by a lower contrast. Additionally to the atmospheric differ-



**Fig. 5:** Red band of Ultracam-X.

ences, differences in contrast might be caused by the different phenological state due to the different dates of image acquisition.

#### 4.2 Thematic Classification

The overall classification accuracies for each sensor are summarized in Tab. 2. Figs. 6–8 show the examples of the land cover classifications based on the different sensors. With variations of the kappa coefficient of only 0.15 (Tab. 2) the quantitative results confirmed what the visual assessments suggested (cf. Figs. 3–5), that all cameras performed similarly.

The relatively low kappa coefficients are caused by different factors: (a) The application of the same method to all different images, (b) different weather conditions during the recording of the images, (c) phenological differences between the images and (d) bi-directional reflectance distribution function (BRDF)-related problems such as the natural in-field variations or the missing atmospheric corrections. Atmospheric corrections were not applied since they are hardly used in praxis. A consideration of the BRDF may lead to better results since the final greyvalues in the image strongly depend on the position of the sun and the position of the observer relative to the sun (DEMIRCAN et al. 2009). To reduce these effects, an attempt was made to use only one image per classification. Image mosaics were solely used if the single images were smaller than the study area.

**Tab. 2:** Fourteen thematic classes (all data except of Cohen's kappa coefficient ( $K$ ) is given in %, for cells with --- less than 5 reference points were available).

Class	RMK-Top15 (RGN)	DMC (RGB)	DMC (RGBN)	JAS-150 (RGB)	JAS-150 (RGBN)	Quattro Digi-CAM (RGB)	Ultracam-X (RGB)
Fallow ground	97.05	60.36	79.69	69.23	81.86	74.03	85.08
Water with Algae	---	---	60.00	80.00	75.00	62.50	---
Grassland	83.32	69.46	74.30	64.65	74.74	77.10	75.72
Potato	---	---	---	---	---	---	---
Corn	---	53.70	25.75	---	60.72	54.17	---
Shadow	66.67	80.77	78.25	84.45	80.98	77.27	62.22
Quarry	65.39	42.43	53.34	12.70	80.81	62.22	57.15
Stubble field	91.67	53.62	82.02	90.45	85.06	94.15	63.05
Streets	34.09	71.47	75.56	29.83	41.67	32.15	66.97
Buildings	49.09	58.93	59.09	59.53	51.76	75.00	75.00
Forest	69.09	81.38	74.80	78.90	79.76	70.38	69.61
Water	96.42	67.33	92.04	92.13	94.77	76.51	88.99
Vineyard	---	58.34	---	---	---	62.50	66.67
Sugar beets	78.57	63.64	62.50	62.92	38.57	71.43	67.50
$K$	0.66	0.53	0.63	0.62	0.68	0.68	0.58

Figs. 6–8 clearly show that most of the grassland are correctly classified. However, in some parts of the RMK-Top15 and JAS-150 images this class is mixed with pixels of sugar beets. The characteristics of the river Enz are clearly visible in all classified scenes and only the size of the area of algae varies. Especially in the JAS-150 images most of the algae are classified as forest. Further problems occurred in separating sugar beets from grassland and corn from forest.

The detection of corn shows a relatively low accuracy. In one corn field no single pixel has been classified as corn and distinction between fallow and stubble fields was not always possible using the JAS-150, RMK-Top15 and Ultracam-X images. The real distribution of stubble or fallow lands could not accurately be determined due to the time differences between the flights and the lack of information on the field crops of each day. Generally, the accuracy for these two classes is about 80%. The misclassified pixels mostly belong to other crops, and only the JAS-150 images show

misclassified pixels which corresponded to artificial structures such as stones or buildings.

Another problem occurred when classifying the vineyards. The usage of 20 cm resolution images did not absolutely guarantee pure pixels of vineyards for the trainings areas. Therefore the overall accuracy of the classification is reduced by the vineyard class. Nearly 5% better results are obtained when performing a classification without vineyards.

The analysis of the shadow class has been separated into three types: shadows over water, shadow in vegetation and shadows in settlements. The RMK-Top15 detected most of the shadows in vegetation as water with high amount of algae; the usage of this sensor also generates problems with shadows over water because the majority was not detected. The extraction of shadows in vegetation and water was good using the images from DMC and Quattro DigiCAM. In the Ultracam-X images most of the shadows in settlements are classified as water. The best results are again obtained for DMC and Quattro DigiCAM. Since

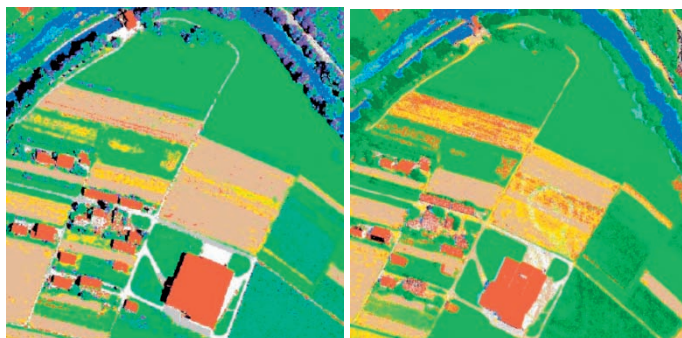


**Fig. 6:** Classification results for Quattro DigiCAM (left) and RMK-Top15 (right).

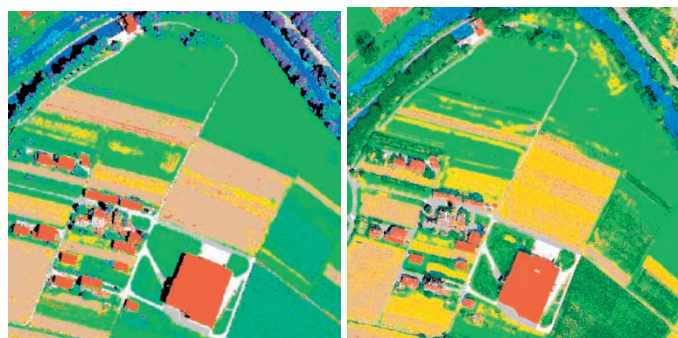


**Fig. 7:** Classification results for DMC (left) and Ultracam-X (right).

**Tab. 3:** The 14 thematic classes of the land cover classification approach.

Class	Color	Class	Color
Fallow ground	Yellow	Stubble field	Brown
Water with algae	Teal	Streets	Grey
Grassland	Green	Buildings	Orange
Potato	Red	Forest	Dark Green
Corn	Light Green	Water	Blue
Shadow	Black	Vineyard	Purple
Quarry	White	Sugar beets	Light Green



**Fig. 8:** Classification results for JAS-150.

the quarry stone class is mixed with the street class in all images low accuracies are obtained for both with the exception of the DMC classification where an accuracy of over 70% is obtained. In the Quattro DigiCAM images the marks on the streets and the borders of the streets are mostly classified as quarry stone.

In the JAS-150 images especially the larger streets are extracted as buildings whereas the

small streets are predominantly correctly classified. In the RMK-Top15 images many of the street pixels are classified as quarry stone and fallow field. Generally, buildings can be visually separated from the remaining classes. Misclassified buildings in the JAS-150 images are mostly due to strong light reflections on one side of the roofs which in turn are caused by the low altitude of the sun. The best results

are obtained using the images from Quattro DigiCAM and Ultracam-X.

Since only one potatoe field exists in test site 1 only few reference points were allocated to this class. The visual inspection shows, that this class has a low accuracy and more than 40% of the pixels are classified as other crop types. High accuracies are obtained for the forest class by all sensors. The Quattro DigiCAM scene shows a lot of corn pixels in the final result. Best results for this class are obtained when using the DMC and the JAS-150 images. On the other hand, in all images most of the corn pixels have been classified as forest. The relatively high accuracy obtained by the RMK-Top15 images is due the additional usage of the near infrared band.

### 4.3 Tree Species Classification

The modelled tree covers were cross-validated using a patch-to-patch comparison to the ground truth data (120 tree and non-tree samples), i. e. segments overlapping at least 50% with a tree or non-tree sample unit. Tab. 4 summarizes the correspondence between the randomly sampled tree / non-tree samples and the modelled tree covers for each of the four datasets of this study. The accuracy of the classified trees was generally high in all four data sets. The fact that the geometric parameters alone almost suffice for the generation of the tree covers underlines the importance of the LiDAR DSM quality. An example of the CHM and the tree cover classification is given in Fig. 9.

**Tab. 4:** Correctly classified tree / non-tree segments (%) and Cohen's kappa coefficient ( $K$ ).

	ADS40-2 <sup>nd</sup>	DMC	JAS-150	Ultracam-X
Tree segments	524	521	533	512
Non-tree segments	454	465	432	448
Correct (%)	99	99	99	99
$K$	0.95	0.96	0.95	0.95

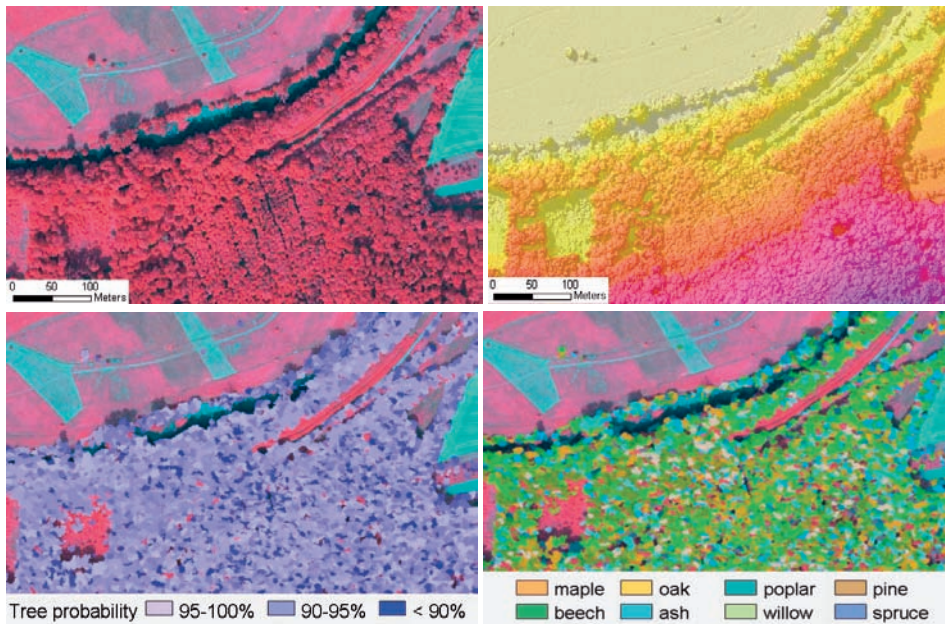


**Fig. 9:** Top left: ADS40-2<sup>nd</sup> CIR orthoimage of a part of test site 2; top right: colour-coded hillshade of LiDAR DSM, classification of tree probabilities (bottom left) and tree species (bottom right).

In order to validate the classification of the main tree species, the reference tree data was assigned to the corresponding image segments using ArcGis 9.3.1. Each of the 240 delineated

reference tree species was assigned to an image segment if the overlapping area of the specific species was at least 10 %. If this was the case, for each segment the tree species with

**Tab. 5:** Confusion matrices for tree species classification using different data sources, proportion of correctly classified trees (prop. corr. %) of different tree species, overall accuracy (ov. acc. %), and Cohen's kappa coefficient ( $K$ ). The number of tree segments used varies in each model; in the segmented DMC image 456 tree segments were assigned, 500 in the ADS40-2<sup>nd</sup>, 452 in the JAS-150, and 462 in the Ultracam-X image.

Field	Classified as								Ov. acc. %	$K$
	Maple	Beech	Ash	Poplar	Oak	Willow	Spruce	Pine		
<b>DMC</b>										
Maple	6	0	7	3	0	0	0	0		
Beech	0	<b>89</b>	19	2	0	0	0	0		
Ash	0	15	<b>79</b>	3	0	0	0	0		
Poplar	0	1	3	<b>72</b>	0	0	0	0		
Oak	0	0	0	0	<b>4</b>	0	0	0		
Willow	0	0	0	0	0	<b>69</b>	0	0		
Spruce	0	0	0	0	0	0	<b>58</b>	0		
Pine	0	0	0	0	0	0	0	<b>26</b>		
Prop. corr.(%)	38	71	63	86	100	100	100	100	<b>88.4</b>	<b>0.86</b>
<b>ADS40-2<sup>nd</sup></b>										
Maple	<b>8</b>	5	3	0	0	0	0	0		
Beech	6	<b>109</b>	10	1	0	0	0	0		
Ash	6	22	<b>71</b>	2	1	1	0	0		
Poplar	5	2	2	<b>52</b>	0	4	0	0		
Oak	0	0	2	1	<b>3</b>	0	0	0		
Willow	2	3	1	2	0	<b>67</b>	0	0		
Spruce	0	0	0	0	0	0	<b>74</b>	0		
Pine	0	0	0	0	0	0	0	<b>35</b>		
Prop. corr. (%)	23	69	59	73	43	84	100	100	<b>83.8</b>	<b>0.81</b>
<b>JAS-150</b>										
Maple	<b>3</b>	9	1	0	0	0	0	0		
Beech	1	<b>97</b>	11	1	0	1	2	0		
Ash	0	31	<b>49</b>	4	0	1	1	0		
Poplar	0	3	3	<b>59</b>	0	2	0	0		
Oak	0	0	0	0	<b>5</b>	0	0	0		
Willow	0	0	0	0	0	<b>67</b>	1	0		
Spruce	0	2	0	0	0	0	<b>65</b>	0		
Pine	0	0	0	0	0	0	0	<b>33</b>		
Prop. corr.(%)	21	61	41	82	100	94	93	100	<b>80.3</b>	<b>0.76</b>
<b>Ultracam-X</b>										
Maple	<b>1</b>	7	4	0	0	3	1	2		
Beech	1	<b>77</b>	18	4	0	0	9	1		
Ash	1	20	<b>73</b>	2	0	4	2	1		
Poplar	0	1	3	<b>66</b>	0	3	0	0		
Oak	0	5	0	0	<b>2</b>	0	0	0		
Willow	0	3	1	9	0	<b>53</b>	1	1		
Spruce	0	5	0	1	0	1	<b>47</b>	1		
Pine	0	2	0	1	0	0	0	<b>25</b>		
Prop corr.(%)	5	53	50	73	29	67	70	74	<b>74.1</b>	<b>0.69</b>

the most overlapping area was assigned. The classified tree species were then cross-validated (5 times) using a segment-to-segment comparison on the delineated reference tree data per sensor. To test the ‘robustness’ of the methods and to see whether consistent results could be achieved, the training and testing samples were exchanged. Tab. 5 shows the four confusion matrices for tree species classification. An example of the classified tree species based on the ADS40-2<sup>nd</sup> input data are depicted in Fig. 9.

Tab. 5 shows that overall classification accuracies are generally high for each input data set and variations of the kappa coefficient lay within 17%. The model based on DMC data produced highest accuracies for all tree species. At first glance, visual assessments of the classifications suggest that all cameras performed quite similarly and that the agreements in most parts of the site are good. Some differences are visible between deciduous and coniferous trees and within deciduous tree species. Coniferous tree species are generally better classified than deciduous trees when using the DMC, ADS40-2<sup>nd</sup> and JAS-150 data sets. The lower accuracies of coniferous trees in the Ultracam-X data set are obvious and most probably due to the missing NIR channel. The analysis showed that the results for deciduous trees are generally less accurate. Oaks as a non-dominant tree species vary from 29% (Ultracam-X) to 100% (DMC, JAS-150) correctly classified, however this classification is based on very few samples. Second best results are obtained for poplar and willow (67% to 100%). Again highest accuracies are obtained from DMC and JAS-150 data. The analysis showed that the classification of maple was the least accurate. Most errors involved maple being misclassified as beech (ADS40-2<sup>nd</sup>, JAS-150, Ultracam-X) or ash (DMC). Beech is often misclassified as ash (all data sets) or as Norway spruce (Ultracam-X). Visual image inspection showed that old and tall beeches and ashes are often difficult to distinguish since they have a similar structure (opened crowns with tall branches and few leaves) and very often also spectral similarities. Even within species, spectral variability can be large because of illumination and view-angle conditions, openness of trees,

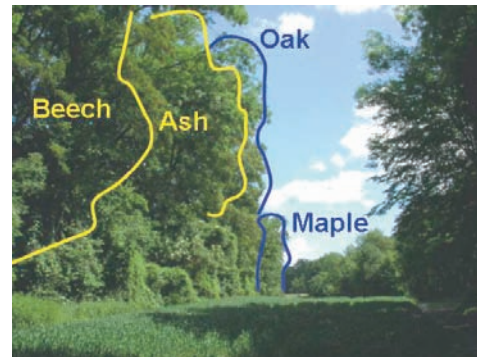


**Fig. 10:** Illustration to show the problems involved in identifying deciduous trees. Both beech and ash have a similar structure with large partly leaf-less branches, at the background a dominant oak is partly covering a smaller maple which is characterized by having a smaller crown diameter.

natural variability, shadowing effects and differences in crown health.

Spectral separability between species and the variability of trees within species have also been analysed and described in LECKIE et al. (2005). Maples as non-dominant deciduous tree species in this region can be more difficult to identify because they may be short and shaded or obscured by nearby large tree species, or by the merging of close crowns. The field visit and visual stereo-image interpretation revealed that maples are often not grouped, have smaller crowns and are therefore partly covered by each other or by larger trees. Fig. 10 illustrates this situation.

## 5 Conclusions and Recommendations

The present study shows the potential and the limits of classifying thirteen land cover and eight tree species classes using newest digital airborne sensors tested in the the DGPF-project. Small variations in classification results are most probably due to phenological differences, different illumination and atmospheric conditions. However, an absolute and clinical one to one comparison between the classification results obtained by the different camera systems was not possible due to the following reasons: 1) the usage of different

bands or band combinations, 2) different dates of image acquisition which causes phenological differences in vegetation growth (especially for cropland), and 3) varying atmospheric conditions (illumination and visibility).

The first approach which uses imagery from the five aerial cameras DMC, RMK-Top15, Quattro DigiCAM, JAS-150 and Ultracam-X produces a similar overall Kappa coefficient, but very different classification accuracies are obtained for the single classes. The classification accuracy is relatively low, but in order to keep the objectivity of the comparison, the first classification approach was not adjusted to the characteristics of each camera. This is planned to be done in the near future. Other reasons for the low accuracy are the weather conditions and BRDF related problems.

The most significant achievement of the second approach is the demonstration that combining the four data sets of ADS40-2<sup>nd</sup>, DMC, JAS-150, Ultracam-X with logistic regression models to classify tree species has a very high potential to produce meaningful results, especially when supported by the NIR bands. Promising classification results for the main tree species were confirmed with ground information and what can be seen visually on the imagery. Further work is needed to improve distinguishing non-dominant, small and partly covered tree species.

To overcome these problems we suggest atmospheric corrections, and radiometric corrections for future work as the requests and the realisation of the radiometric analyses as a part of the DGPF-project is outlined in SCHÖNERMARK (2010). This also implies BRDF-related problems or investigation of influences of the BRDF in terms of classification accuracy. During the vegetation period only few days (e. g. after precipitation) may change the spectral properties and thus separability of some crops significantly. This problem could be solved and the ground truth could be further improved by collecting more samples and field visits during the image acquisition.

Nevertheless, the experiences of the newest digital airborne sensors made in this study may be of practical interest or serve as a basis for decisions for tasks of environmental agencies, forest inventories or land surveying offices.

## References

- ALBERTZ, J., 2001: Einführung in die Fernerkundung, Grundlagen der Interpretation von Luft- und Satellitenbildern. – Wissenschaftliche Buchgesellschaft, Darmstadt.
- BAATZ, M. & SCHÄPE, A., 2000: Multiresolution Segmentation – an optimization approach for high quality multi-scale image segmentation. – *Angewandte Geographische Informationsverarbeitung XII*: 12–23; Wichmann, Heidelberg.
- BAILLY, J.S., ARNAUD, M. & PUECH, C., 2007: Boosting: a classification method for remote sensing. – *International Journal of Remote Sensing* **28** (7–8): 1687–1710.
- BURROUGH, P.A., 1986: Principles of Geographical Information Systems for Land Resources Assessment. – Oxford University Press, New York, USA.
- CRAMER, M., 2010: The DGPF-Test on Digital Airborne Camera Evaluation – Overview and Test Design. – This issue.
- DEMIRCAN, A., SCHUSTER, R., RADKE, M., SCHÖNERMARK, M. v. & RÖSER, H.P., 2000: Use of a wide angle CCD line camera for BRDF measurements. – *Infrared Physics & Technology* **41** (1): 11–19.
- DENNERT-MÖLLER, E., 1983: Untersuchung zu digitalen multispektralen Klassifizierung von Fernerkundungsaufnahmen mit Beispielen aus den Wattgebieten der deutschen Nordseeküste. – *Wissenschaftliche Arbeiten der Fachrichtung Geodäsie und Geoinformatik*, Hannover.
- DUDA, R.O., HART, P.E. & STORK, D.G., 2001: Pattern classification. – John Wiley & Sons, New York, USA.
- EHLERS, M., SCHIEWE, J., ROSSO, P. & KLONUS, S., 2007: Prüfung von Luftbilddaten zweier unterschiedlicher Aufnahmesensoren hinsichtlich eines optimalen Aufnahmesystems zur Erfüllung von Aufgaben von Vermessungs- und Umweltverwaltung für das Landesamt für Natur und Umwelt (LANU). – *gi-reports@igf*, **9**, Universität Osnabrück.
- ERBEK, F.S., ÖZKAN, C. & TABERNER, M., 2004: Comparison of maximum likelihood classification method with supervised artificial neural network algorithms for land use activities. – *International Journal of Remote Sensing* **25** (9): 1733–1748.
- GONZALES, R.C. & WOODS, R.E., 2002: Digital image processing – Second edition; Prentice Hall, Upper Saddle River, NY, USA.
- HEINZEL, J.N., WEINACKER, H. & KOCH, B., 2008: Full automatic detection of tree species based on delineated single tree crowns – a data fusion approach for airborne laser scanning data and aer-

- ial photographs. – *SilviLaser – 8th international conference on LiDAR applications in forest assessment and inventory*, 76–85.
- HIRSCHMUGL, M., OFNER, M., RAGGAM, J. & SCHARDT, M., 2007: Single tree detection in very high-resolution remote sensing data. – *Remote Sensing of Environment* **110**: 533–544.
- HOLMGREN, J., PERSSON, A. & SODERMAN, U., 2008: Species identification of individual trees by combining high resolution LiDAR data with multi-spectral images. – *International Journal of Remote Sensing* **29**: 1537–1552.
- HONKAVAARA, E., ARBIOL, R., MARKELIN, L., MARTINEZ, L., CRAMER, M., BOVET, S., CHANDELIER, L., ILVES, R., KLONUS, S., MARSHAL, P., SCHLÄPFER, D., TABOR, M., THOM, C. & VEJE, N., 2009: Digital Airborne Photogrammetry – A New Tool for Quantitative Remote Sensing? – A State-of-the-Art Review On Radiometric Aspects of Digital Photogrammetric Images. – *Remote Sensing* **1**: 577–605.
- HOSMER, D.W. & LEMESHOW, S., 1989: Applied logistic regression. – Wiley, New York, USA.
- JENSEN, J.R., 2005: Introductory digital image processing: A remote sensing perspective. – Prentice Hall, Upper Saddle River, NY, USA.
- KLONUS, S., 2009: Thematische Klassifikation von DMC, RMK, DigiCAM, JAS-150 und UCX-Bildern. – [www.ifp.uni-stuttgart.de/dgpf/Stuttgart09/2\\_4-KLONUS.pdf](http://www.ifp.uni-stuttgart.de/dgpf/Stuttgart09/2_4-KLONUS.pdf) (17.12.2009).
- KLONUS, S. & EHLERS, M., 2009: Additional benefit of image fusion method from combined high resolution TerraSAR-X and multispectral SPOT data for classification. – 29th Earsel Symposium, in press.
- KLONUS, S., HAGEDORN, C., EKKEHARD, J., CASTILLO, K., GONZALO, J. & VELEZ, F., 2009: Digitalisierung der Landnutzungserhebungen und erste Klassifikationsergebnisse. – Wissenschaftlich-Technische Jahrestagung der DGPF.
- LECKIE, D.G., TINIS, S., NELSON, T., BURNETT, CH., GOUGEON, F.A., CLONEY, E. & KPARADINE, D., 2005: Issues in species classification of trees in old growth conifer stands. – *Canadian Journal of Remote Sensing* **31** (2): 175–190.
- LILLESAND, T.M. & KIEFER, R.W., 1994: Remote Sensing and Image Interpretation – Third Edition; Wiley, New York, USA.
- LU, D. & WENG, Q., 2007: A survey of image classification methods and techniques for improving classification performance. – *International Journal of Remote Sensing* **28** (5): 823–870.
- MARKELIN, L., HONKAVAARA, E., PELTONIEMI, J., SUOMALAINEN, J. & AHOKAS, E., 2006: Radiometric Evaluation of Digital Aerial Cameras. – *International Archives of Photogrammetry, Remote Sensing and Spatial Information Sciences* **36** (1): 75–80.
- ROSSO, P.H., KLONUS, S., EHLERS, M. & TSCHACH, E., 2008: Comparative Properties of Four Airborne Sensors and their Applicability to Land Surface Interpretation. – *International Archives of the Photogrammetry, Remote Sensing and Spatial Information Sciences* **37** (B1): 545–550.
- SCHÖNERMARK VON, M., 2010: Status Report on the Evaluation of the Radiometric Properties of Digital Photogrammetric Airborne Cameras. – This issue.
- SCOTT, J.M., HEGLUND, P.J., SAMSON, F., HAUFLE, J., MORRISON, M. & WALL, B., 2002: Predicted species occurrences: issues of accuracy and scale. – Island Press, Covelo, California, USA.
- WANG, Z., BOESCH, R. & GINZLER, C., 2007: Color and LiDAR data fusion: Application to automatic forest boundary delineation in aerial images. – *International Archives of the Photogrammetry, Remote Sensing and Spatial Information Sciences* **36** (1/W51).
- WASER, L.T., KÜCHLER, M., ECKER, K., SCHWARZ, M., IVITS, E., STOFER, S. & SCHEIDEGGER, CH., 2007: Prediction of Lichen Diversity in an Unesco Biosphere Reserve – Correlation of high Resolution Remote Sensing Data with Field Samples. – *Environmental Modeling & Assessment* **12** (4): 315–328.
- WASER, L.T., BALSAVIAS, E., ECKER, K., EISENBEISS, H., GINZLER, C., KÜCHLER, M., THEE, P. & ZANG, L., 2008a: High-resolution digital surface models (DSM) for modelling fractional shrub/tree cover in a mire environment. – *International Journal of Remote Sensing* **29** (5): 1261–1276.
- WASER, L.T., GINZLER, C., KÜCHLER, M. & BALSAVIAS, E., 2008b: Potential and limits of extraction of forest attributes by fusion of medium point density LiDAR data with ADS40 and RC30 images. – *SilviLaser – 8th international conference on LiDAR applications in forest assessment and inventory*, 625–634.

#### Addresses of the Authors:

Dipl. Geograph LARS TORSTEN WASER, Swiss Federal Research Institute WSL Birmensdorf, Airborne Remote Sensing for forest applications, Zuercherstrasse 111, CH-8903 Birmensdorf, Tel.: +41-44-739-22-92, e-mail: lars.waser@wsl.ch.

Dipl. Umweltwiss. SASCHA KLONUS, Prof. Dr.-Ing. MANFRED EHLERS, Universität Osnabrück, Institut für Geoinformatik und Fernerkundung, Barbarastrasse 22b, D-49076 Osnabrück, Tel.: +49-541-969-

3921, -3910, Fax: -3939, e-mail: sklonus@igf.uni-osnabrueck.de, mehlers@igf.uni-osnabrueck.de.

Dr. MEINRAD KÜCHLER, Swiss Federal Research Institute WSL Birmensdorf, Biotopbeurteilung, Zuercherstrasse 111, CH-8903 Birmensdorf, Tel.: +41-44-739-24-67, e-mail: meinrad.kuechler@wsl.ch.

Dr. ANDRAS JUNG, Martin-Luther-Universität Halle-Wittenberg, Institut für Geowissenschaften, Von-Seckendorff-Platz 3-4, D-06120 Halle, Tel.: +49-345-552-6021, Fax: -8228, e-mail: andras.jung@geo.uni-halle.de.

Manuskript eingereicht: Dezember 2009

Angenommen: Januar 2010

## Berichte von Veranstaltungen

### **ISPRS/COST-Workshop “Quality, Scale and Analysis Aspects of City Models” vom 3.–4. Dezember 2009 in Lund, Schweden**

The ISPRS/COST-workshop on “*Quality, Scale and Analysis Aspects of City Models*” was held at the Geocenter of Lund University, Sweden, from December 3–4, 2009. The workshop was organized by the working groups II/2 (Multi-Scale Representation of Spatial Data), II/3 (Spatial Analysis and Data Mining), and II/4 (Uncertainty Modeling and Quality Control for Spatial Data) of Commission II (Theory and Concepts of Spatial Information Science) of the International Society for Photogrammetry and Remote Sensing (ISPRS), together with the Swedish Development Council for Geographic Information (ULI) and the EU COST Action TU0801 on “Semantic enrichment of 3D city models for sustainable urban development”.

The scientific committee was represented by LARS HARRIE (Lund University, Sweden), MONIKA SESTER (University of Hanover, Germany), Liu Yaolin (Wuhan University, China), ALFRED STEIN (ITC, The Netherlands), CLAUDE MÉTRAL (University of Geneva, Switzerland), GERHARD JOOS (NATO, The Netherlands), and THOMAS H. KOLBE (Technical University Berlin, Germany).

The local organization was in the hands of HANNA STIGMAR and ARA TOOMANIAN from the GIS-Center of Lund University and LUDVIG EMGÅRD from C3 Technologies AB, Sweden. The workshop proceedings have been published on CD. Selected papers will be reviewed for publication in a special issue of the ISPRS Journal.

42 scientists from 12 different countries participated in the 2-days-workshop: The 20 presentations were subdivided into five sessions and were supplemented by a poster session. A time slot was reserved to form discussion groups.

As an introduction to the workshop, THOMAS KOLBE, director and Dean of Studies of the In-

stitute of Geodesy and Geoinformation Science of Berlin University of Technology, gave an inspiring keynote on the *Assessment of the structural quality of virtual 3D city models*. In his talk, he analyzed different aspects of the data quality of 3D city models with respect to their semantic and geometric structure. He introduced the notion of „structural quality“ as a measure of the coherence between and the richness of semantic and geometric components of a model.

The second keynote was given by KALLE ÅSTRÖM, professor and head of the division of Mathematics and Numerical Analysis at the Centre for Mathematical Sciences of Lund University. In his interesting talk on *Computer Vision and Cognitive Vision* he gave an overview on the history of the mathematics of computer vision, outlined classical problems such as the structure and motion problem of recovering the scene structure and the motion of a camera from a sequence of images, and outlined current problems in cognitive vision such as face understanding and automatic object detection.

The topic of the first session, *geometric reasoning*, is the logical deduction of geometric information from spatial facts employing axiomatic calculi. SANDRA LOCH-DEHBI (Germany) presented a method to develop consistent and non-redundant models of building parts using automatic theorem proving on geometric constraint sets. GWEN WILKE (Austria) proposed a fuzzyfication of Euclidean incidence geometry that can deal with geometric primitives that have an extension in space. YOUNESS DEHBI (Germany) showed how formal grammar rules of 3D building models and their parts can be obtained by the machine-learning technique Inductive Logic Programming.

The second session discussed aspects of *interpretation and enrichment* of city models. HONGCHAO FAN’S (Germany) presentation addressed the visualization of change in spatio-temporal city models. He stressed that the interpretation of changes as events is dependent on the spatial and temporal resolution of the

model and introduced a mathematical tool for event-detection. FREDERIK TACK (Belgium) proposed a method to extract urban surface models in a semi-automatic way from multi-scopical Ikonos imagery. He showed that the proposed method provides an encouraging approach to cope with the high complexity of built-up areas in the context of photogrammetric methods. JONATHAN QUINN and PHILIP SMART (UK) described a novel and robust approach for the combination of 2D and 3D city models and the semantic enrichment of the output.

Scale is a long discussed topic in geographic information science, but the lack of, e.g., sufficient generalization functionality is still an issue. It was therefore very interesting to follow the ideas of scientists in the third session, *scale issues*. It started with the presentation of a conceptual process model for the generalization of hierarchical feature models: RICHARD GUERCKE (Germany) focused on the implementation of generalization as a generic service and proposed to overcome its strong application-dependency by a modularization of the process model. In the following talk, MONIKA SESTER (Germany) gave an overview of the problems that arise from aggregating buildings in city models in conjunction with terrain models. She presented a solution by considering height dependent constraints. JOCHEN SCHIEWE then discussed approaches from the field of visual analytics for the change analysis processes with a special emphasis on considering uncertainty information.

Session four complemented the preceding session on scale issues with a discussion of *technical issues*. BO MAO (Sweden) introduced the CityTree framework which supports the generalization of 3D city models: With an implementation based on CityGML and X3D, CityTree defines a multiple representation data structure, which dramatically reduces the load time of 3D models and thereby allows dynamic zooming in real time. MAHDI FARNAGHI (Iran) looked at different technologies, techniques and standards for 3D mobile GIS applications with the goal to find an integrated solution which reduces the workload of mobile devices and increases the efficiency of applications. As a result of performance tests, a client/server architecture was proposed that utilizes web services technologies and a tiling

mechanism for large datasets. IVAN NOVAKOVIĆ and IVAN BACIC-DEPRATO from the Croatian company Geofoto d.o.o. concluded the session with a very impressive report on the process of creating a virtual 3D model of the Croatian capital Zagreb, which was used to produce a 3x3 meters scale model of Zagreb by utilizing 3D printing technology.

The fifth and last session on *quality and applications* was started by CHRISTOPH KINKELDEY (Germany) who discussed an advanced uncertainty measure for classified remotely sensed scenes based on fuzzy set theory. By considering both, the uncertainties in the classification as well as in the reference data, the proposed measure accounts for the growing requirements on the correctness of models due to the increasing geometric and thematic accuracies of modern sensor systems. FLORENTINA FARCAS (Sweden) reported on the implementation of a GIS-software package for creating 3D road traffic noise maps and presented a case study for the Skåne region in the south of Sweden. The last presentation of the workshop was given by AHMED AL AMOURI (Germany) on the geometric and semantic quality assessment of historic images of the town of Baalbek, an urban heritage in eastern Lebanon. He showed that the 3D features derived from the historic imagery are sufficient to create a 3D city model of Baalbek that is based on CityGML in level of detail 1 and 2.

In addition to the oral presentations, several topics were presented in a poster-session. On the second day of the workshop, discussion groups were formed that focused on five different aspects of city models, and thereby allowed for a stimulating exchange of ideas. Results were reported subsequently to the whole audience.

In the course of the workshop a welcome reception and a workshop dinner was held as official events. The workshop dinner was located at a restaurant in the old town center of Lund and proceeded in a friendly mood, with a speech given by JONAS ANDRÉASSON from the Municipality of Lund.

The ISPRS/COST-workshop on *“Quality, Scale and Analysis Aspects of City Models”* 2009 at Lund University was fruitful and definitely a success.

GWEN WILKE, Vienna

## Neue Mitglieder der DGPF

Als neue Mitglieder begrüßt die DGPF:

ABDALLA ALOBEID, Hannover  
 ROBERT BLASKOW, Dresden  
 Dipl.-Ing. DAVID BORNEMANN, Trebbin OT  
 Blankensee  
 Dipl.-Ing. JONAS BOSTELMANN, Hannover  
 Dipl.-Ing. MARTINA BRAUNE, Potsdam  
 M.Sc. CORINNA BRÜSSHABER, Berlin  
 Dr.-Ing. HARTMUT DIENST, Bad Berleburg  
 B.A. DENNIS EDLER, Bochum  
 Dr. JONAS FRANKE, München  
 CHRISTIAN GÖTZE, Halle  
 PD Dr. GERHARD GRÖGER, Bonn  
 B.Sc. MARTIN HAAG, Berlin  
 Dipl.-Ing. (FH) CHRISTIAN HÖNNIGER, Ham-  
 burg  
 B.Sc. FRIEDRICH KELLER, Hamburg  
 Prof. Dr.-Ing. FREDIE KERN, Mainz  
 Dr. ANGELA LAUSCH, Leipzig

Dipl.-Phys. WOLFRAM LÜHRIG, Braunschweig  
 Dipl.-Ing. MICHAEL NEID, Berlin  
 Dipl.-Geogr. STEFAN NICOLAUS, Osnabrück  
 M.Sc. JARED PABST, Hagen  
 Dipl.-Ing. BETTINA PETZOLD, Wuppertal  
 Prof. Dr. MICHAEL SCHAEPMAN, Zürich,  
 Schweiz  
 Dipl.-Ing. MATTHIAS SCHRAMM, Würzburg  
 B.Sc. KRISTIN SCHREYER, Hamburg  
 Dr.rer.nat. SEBASTIAN VAN DER LINDEN, Berlin  
 Dipl.-Geol. ELKE WETZEL, Potsdam  
 B.Sc. NILS WOLF, Bochum  
 Dr. HEIKO ZUMSPREKEL, Freiburg

Neue Korporative Mitglieder – Firmen:  
 MILAN Geoservice GmbH

Neue Korporative Mitglieder – Hochschulen:  
 TU Bergakademie Freiberg, Institut für Mark-  
 scheidewesen und Geodäsie

## Buchbesprechung

**RAINER SANDAU (Hrsg.), 2010: Digital Air-  
 borne Camera. Springer, Dordrecht, Nie-  
 derlande**

Das beim Springer Verlag im Jahre 2010 neu  
 erschienene Buch „Digital Airborne Camera“,  
 zusammengestellt von RAINER SANDAU, ISBN  
 978-1-402-8877-3 ist das Werk von insgesamt  
 16 spezialisierten Autoren in englischer Spra-  
 che. Es ist eine revidierte und übersetzte Auf-  
 lage der im Jahre 2005 beim Wichmann Ver-  
 lag, Heidelberg, erschienenen Auflage des  
 Buches „Digitale Luftbildkamera – Einfüh-  
 rung und Grundlagen“.

Wegen der Bedeutung des Buches soll hier  
 noch einmal das Gesamtwerk rezensiert wer-  
 den, obwohl prinzipiell nur das Kapitel 7 mit  
 den im Detail behandelten Kamerasystemen  
 ADS40 (ADS80), DMC und Ultracam neu ge-  
 schrieben worden ist.

Das englischsprachige Werk wird einem  
 grösseren Leserkreis zur Verfügung stehen  
 als bisher.

RAINER SANDAU ist mit diesem Werk ein gu-  
 ter Wurf gelungen. Es beinhaltet in seinem  
 multidisziplinär ausgerichteten Text Einzel-  
 heiten, die vielleicht den Kamerakonstrukteu-  
 ren bekannt waren, die aber in dieser Form in  
 der bisherigen photogrammetrischen Literatur  
 nicht zur Verfügung standen.

Es sei daran erinnert, dass die ersten hoch-  
 auflösenden digitalen Kameras für den Ein-  
 satz im Weltraum gebaut wurden. Hier war in  
 erster Linie das DLR mit RAINER SANDAU be-  
 teiligt. Es wäre schön gewesen, wenn die  
 Übertragung dieser Technologie in die euro-  
 päische kameraherstellende Industrie, z.B.  
 durch Leica und Carl Zeiss als gemeinsames  
 Vorhaben möglich gewesen wäre. Die europä-  
 ische Kartellbehörde hat diesem seinerzeiti-

gen Vorhaben einen Riegel vorgeschoben. Sie ist letztlich dafür verantwortlich, dass die heute am weitesten entwickelten hochauflösenden digitalen Kameras von Hexagon, Intergraph und Microsoft, zwar mit den bewährten Entwicklungsteams, aber von einer globalisierten und nicht europäischen Szene weiterentwickelt werden.

RAINER SANDAU war in den Jahren einer angestrebten Kooperation zwischen DLR und Leica in der kritischen Entwicklungszeit in Heerbrugg in der Schweiz. Insofern ist das erschienene Buch ein Zeugnis für diese Tätigkeit.

Das Buch mit 331 Seiten und 7 Kapiteln beginnt mit einer Einleitung in Kapitel 1, in der die historischen Entwicklungen und die Bedeutung digitaler Kamerasysteme von SANDAU aufgezeigt werden. Den Abschluss des Buches mit Kapitel 7 bilden die von den Herstellerfirmen Leica Geosystems (FRICKER über ADS40 und ADS80), Intergraph Z/I (NEUMANN über die DMC) und Microsoft-Vexcel (GRUBER über die Ultracam) verfassten Detailbeschreibungen ihrer Kamerasysteme.

Die dazwischenliegenden Kapitel 2 bis 6 behandeln alle wichtigen Detailfragen, die beim Kamerabau berücksichtigt werden müssen und die zum Verständnis des Kamerabaus notwendig sind:

Kapitel 2 stellt die physikalisch-nachrichtentechnischen Grundlagen der optischen Abbildung in der Fernerkundung dar, wobei Autoren des DLR (JAHN), von Leica (BEIL) und von deutschen Hochschulinstituten (CRAMER, JACOBSEN) zu Wort kommen. Im Text enthalten sind: Abbildung durch Linsen, Eigenschaften des Lichts, die Fouriertransformation, die physikalische Leistungsfähigkeit optischer Systeme, Auflösung und Noise, die Modulationsübertragungsfunktion und die analytische Darstellung des Farbraums, die geometrische Sensororientierung und die indirekte und die direkte Georeferenzierung.

Kapitel 3 (VON SCHÖNERMARK, Uni Stuttgart) behandelt die Einflüsse der Atmosphäre, den Objektkontrast und die bidirektionale Reflexionsfunktion.

In Kapitel 4 (SANDAU, DLR) werden die Designkriterien für die Komponenten einer digi-

talen Kamera besprochen (CCD-Eigenschaften, Vorwärtsbewegungskompensation, die Pupille und deren Einflüsse auf die Modulationsübertragungsfunktion). Schließlich werden die Eigenschaften der Filter, des optoelektronischen Konverters (HILBERT, DLR), der CCD Architekturen in Form von Linien und Matrizen, der Fokalebene (DRIESCHER, DLR) und der benötigten elektronischen Komponenten abgehandelt. Auch die GPS/INS Synchronisierung, der Strombedarf und die Möglichkeiten der Datenkompression werden diskutiert.

Kapitel 5 (TEMPELMANN, Leica) betrifft die geometrische und die radiometrische Kalibrierung der Kameras.

Kapitel 6 (TEMPELMANN, Leica) behandelt die Datenverarbeitungs- und Archivierungsaufgaben.

Es ist nicht zu verkennen, dass die Erfahrungen von Rainer Sandau hauptsächlich die Zeilensensoren betreffen, denen das Buch gegenüber den Matrix basierten CCD Kameras den Vorzug gibt:

- sie haben die gleiche Auflösung für alle Spektralbereiche
- sie ermöglichen eine komplette spektrale Trennung aller Spektralbereiche
- sie ergeben eine erhöhte Farbkontinuität in der Mosaikbildung
- sie haben keine Pixelfehler
- sie ermöglichen ein günstiges Basis-Höhenverhältnis für die Stereoerfassung
- sie benötigen keine Verschlussmechanismen
- sie haben nur ein einziges temperatur- und druckkontrolliertes Linsensystem in einer Fokalebene (siehe Kapitel 7).

Die Hersteller der Matrix basierten CCD Kameras kommen aber in Kapitel 7 selbst zu Wort.

Das Buch stellt eine heute notwendige Bereicherung der photogrammetrischen Literatur dar und kann deshalb dem interessierten Leserkreis bestens empfohlen werden.

Besonders hervorzuheben ist, dass es RAINER SANDAU, wie schon früher für Kleinsatellitenmissionen, gelungen ist, eine kompetente Autorenrunde für das Thema zu verpflichten und erfolgreich zu vereinigen.

GOTTFRIED KONECNY, Hannover

## Veranstaltungskalender

### 2010

6.–7. Mai: **InterGeo-East 2010** – Trade Fair & Conference for Landmanagement, Geoinformation, Building Industry, Environment in **Istanbul**, Türkei. [www.intergeo-east.com/](http://www.intergeo-east.com/)

26.–28. Mai: **ISPRS Commission II Symposium “Theory & Concepts of Spatial Information Science”** in **Hong Kong**, China. [isgis.lsgi.polyu.edu.hk/](http://isgis.lsgi.polyu.edu.hk/)

2.–4. Juni: **ISPRS Commission VI Symposium “Education & Outreach”** in **Enschede**, Niederlande. [www.itc.nl/isprscom6/symposium2010](http://www.itc.nl/isprscom6/symposium2010)

8.–10. Juni: 58. **Deutscher Kartographentag** in **Berlin/Potsdam**. [dkt2010.dgfk.net/](http://dkt2010.dgfk.net/)

9.–10. Juni: 6. **Hamburger Forum für Geomatik** – Aktuelle Entwicklungen aus Forschung und Praxis in **Hamburg**. [www.geomatik-hamburg.de/forum-geomatik/2010](http://www.geomatik-hamburg.de/forum-geomatik/2010)

10.–11. Juni: 6. **GIS-Ausbildungstagung 2010** in **Potsdam**. [gis.gfz-potsdam.de](http://gis.gfz-potsdam.de)

12.–14. Juni: **ISDE 2010 Digital Earth Summit “Digital Earth in the Service of Society: Sharing Information, Building Knowledge”** in **Nessebar**, Bulgaria. [ww.cartography-gis.com/digitalearth/](http://ww.cartography-gis.com/digitalearth/)

16.–18. Juni: **GIS/SIT 2010** – Schweizer Forum für Geoinformation an der Universität **Zürich-Irchel**, Schweiz. [www.gis-sit.ch/](http://www.gis-sit.ch/)

16.–18. Juni: **ISPRS Commission I Symposium “Image Data Acquisition – Sensors & Platforms”** in **Calgary**, Kanada. [www.geo-conf.ca](http://www.geo-conf.ca)

16.–18. Juni: **IEEE Conference on Computer Vision and Pattern Recognition** in **San Francisco**, USA. [www.cvpr2010.org/](http://www.cvpr2010.org/)

22.–24. Juni: **ISPRS Commission V Symposium “Close-Range Sensing: Analysis & Applications”** in **Newcastle upon Tyne**, Großbritannien. [www.isprs-newcastle2010.org/](http://www.isprs-newcastle2010.org/)

29. Juni–2. Juli: **GEOBIA 2010 - GEOgraphic Object-Based Image Analysis** in **Ghent**, Belgien. [geobia.ugent.be](http://geobia.ugent.be)

1.–3. Juli: 30. **Wissenschaftlich-technische Jahrestagung der DGPF** im Rahmen der Dreiländertagung in **Wien**. [www.dgpf.de/neu/jahrestagung/informationen.htm](http://www.dgpf.de/neu/jahrestagung/informationen.htm)

5.–7. Juli: **ISPRS Commission VII Symposium “100 Years ISPRS – Advancing Remote Sensing Science”** in **Wien**, Österreich. [www.isprs100vienna.org/](http://www.isprs100vienna.org/)

6.–9. Juli: **GI\_Forum2010: Symposium & Exhibit “Applied Geoinformatics”** in **Salzburg**, Österreich. [www.gi-forum.org/](http://www.gi-forum.org/)

7.–9. Juli: **AGIT 2010 Symposium und Fachmesse für Angewandte Geoinformatik** in **Salzburg**, Österreich. [www.agit.at/](http://www.agit.at/)

20.–23. Juli: **ISARA 9<sup>th</sup> International Symposium on Spatial Accuracy Assessment in Natural Resources & Environmental Sciences** in **Leicester**, Großbritannien. [www.le.ac.uk/geography/accuracy/index.html](http://www.le.ac.uk/geography/accuracy/index.html)

1.–5. August: **SPIE Optical Engineering + Applications** in **San Diego**, USA. [spie.org/optical-engineering.xml](http://spie.org/optical-engineering.xml)

9.–13. August: **ISPRS Commission VIII Symposium “Remote Sensing Applications & Policies”** in **Kyoto**, Japan. [www.isprscom8.org/](http://www.isprscom8.org/)

1.–3. September: **ISPRS Commission III Symposium “Photogrammetric Computer Vision & Image Analysis”** in **Paris**, Frankreich. [pcv2010.ign.fr/](http://pcv2010.ign.fr/)

- 1.–5. September: **7<sup>th</sup> ICA Mountain Cartography Workshop** in **Borsa**, Rumänien. [www.mountaincartography.org/activities/workshops/](http://www.mountaincartography.org/activities/workshops/)
- 5.–11. September: **European Conference on Computer Vision** in **Heraklion**, Kreta, Griechenland, [www.ics.forth.gr/eccv2010](http://www.ics.forth.gr/eccv2010)
- 14.–17. September: **GIScience 2010 – 6<sup>th</sup> International Conference on Geographic Information Science** in **Zürich**, Schweiz. [www.giscience2010.org/](http://www.giscience2010.org/)
- 20.–23. September: **SPIE Remote Sensing in Toulouse**, Frankreich. [spie.org/remote-sensing-europe.xml](http://spie.org/remote-sensing-europe.xml)
- 22.–24. September: **DAGM 2010 – 32<sup>nd</sup> Annual Pattern Recognition Symposium** in **Darmstadt**. [www.dagm2010.org/](http://www.dagm2010.org/)
- 27.–28. September: **AgA-Tagung: Automation in Kartographie, Photogrammetrie und GIS** in **Dresden**. [www.ikg.uni-hannover.de/aga](http://www.ikg.uni-hannover.de/aga)
- 5.–7. Oktober: **INTERGEO®** – Kongress und Fachmesse für Geodäsie, Geoinformation und Landmanagement in **Köln**. [www.intergeo.de/de/deutsch/index.php](http://www.intergeo.de/de/deutsch/index.php)
- 11.–13. Oktober: **ISPRS WG I/4 Workshop on Modeling of Optical Airborne & Space Borne Sensors** in **Istanbul**, Türkei.
- 27.–29. Oktober: **12. Seminar “GIS & Internet”** – Integration von GIS-Funktionalitäten in Lösungen an der UniBw München, in **Neubiberg**. [www.agis.unibw.de/gis&internet/](http://www.agis.unibw.de/gis&internet/)
- 16.–18. November: **ISPRS Commission IV Symposium “Geodatabases & Digital Mapping”** in **Orlando**, USA. [www.commission4.isprs.org/](http://www.commission4.isprs.org/)

## Neuerscheinungen

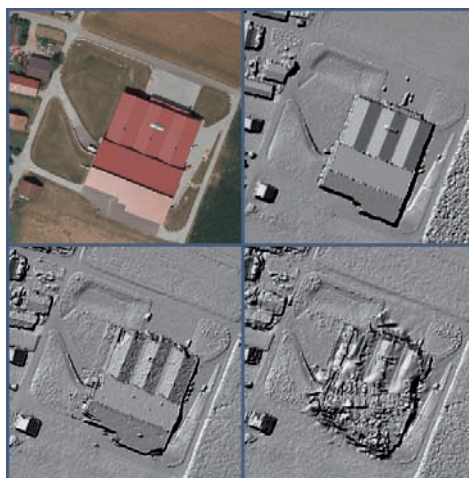
- BENNING, W. 2009. Statistik in Geodäsie, Geoinformation und Bauwesen. 3., überarbeitete und erweiterte Auflage, XIV, 314 S., kartoniert mit CD-ROM, ISBN 978-3-87907-499-0, Wichmann, Verlagsgruppe Hüthig Jehle Rehm.
- KUMMER K. & FRANKENBERGER, J. (Hrsg.) 2009. Das deutsche Vermessungs- und Geoinformationswesen 2010. XXV, 878 S., kartoniert, ISBN 978-3-87907-487-7, Wichmann, Verlagsgruppe Hüthig Jehle Rehm.
- MEINEL, G. & SCHUMACHER, U. (Hrsg.) 2009. Flächennutzungsmonitoring, Konzepte – Indikatoren – Statistik. 202 S., ISBN 978-3-8322-8740-5, Shaker Verlag GmbH, Aachen.
- SCHMIDT, A., KARRASCH, P. & NEUBERT, M. 2009. Vergleichende Untersuchung der Atmosphärenkorrekturprogramme ATCOR und FLAASH auf der Datengrundlage des Satellitensystems IKONOS. Fernerkundung und angewandte Geoinformatik, Band 5, ISBN 978-3-941216-07-5, Rhombos-Verlag, Berlin, 132 S.

## Zum Titelbild

### The DGPF-Project on Digital Photogrammetric Airborne Camera Evaluation

The project on Digital Photogrammetric Airborne Camera Evaluation is one of the most important both scientific and user driven activities run in the framework of the German Society for Photogrammetry and Remote Sensing (DGPF). Initiated at the end of the year 2007, comprehensive empirical data sets have been acquired in the summer of 2008. By now, major parts of the analysis have been completed and this PFG issue is dedicated to give an overview of the latest findings of the different evaluation teams.

The figure on the title page exemplarily shows results of the evaluation team “Digital Elevation Models”. Based on the available data sets, the current state-of-the-art of photogrammetric 3D data generation by automatic image matching was documented and evaluated. By means of these investigations, the benefits of digital image recording as compared to scanning analogue images for elevation data generation could clearly be demonstrated. As shown in the figure, this is especially true for regions with limited surface texture. The bottom left picture shows a shaded DSM from image matching based on the Z/I Imaging DMC 8 cm GSD (ground sample distance) block. The corresponding result for the scanned analogue Zeiss RMK data is depicted on the bottom right. These two examples of the test are especially interesting, since both image blocks were captured simultaneously at identical atmospheric and illumination conditions using a double-hole aircraft. Both depicted DSM grids of 0.2 m raster width were generated from the 8 cm GSD imagery using the software MATCH-T DSM. For comparison, the top left image of the figure shows the corresponding ortho image. The shaded DSM derived from the Leica Geosystems ALS



50 LiDAR point cloud is depicted in the top right.

Obviously, the higher radiometric quality of digital images allows for much better matching while scanned analogue imagery is not suitable for the automatic derivation of highly accurate surface models. This supremacy was verified for all investigated digital camera systems of the DGPF test. Thus, recent developments in sensor and software technology facilitate the automatic image based generation of elevation data at a quality, which in the past was only feasible by LiDAR measurements. The results clearly indicate, that a considerable number of applications will be feasible based on height data from image matching, if digital airborne cameras are used.

More details on the DGPF-project are given in this issue's papers.

MICHAEL CRAMER (project leader) and NORBERT HAALA (team leader Digital Elevation Models) Universität Stuttgart, Institut für Photogrammetrie (ifp), Geschwister-Scholl-Str. 24D 70174 Stuttgart, michael.cramer@ifp.uni-stuttgart.de, norbert.haala@ifp.uni-stuttgart.de

## Korporative Mitglieder

### Firmen

AEROWEST GmbH  
 AICON 3D Systems GmbH  
 aphos Leipzig AG  
 Applanix Corporation  
 Becker GeoInfo GmbH  
 Bernhard Harzer Verlag GmbH  
 Blom Deutschland GmbH  
 Brockmann Consult  
 bsf swissphoto GmbH  
 Büro Immekus  
 CGI Systems GmbH  
 con terra GmbH  
 Creaso GmbH  
 DEFINIENS AG  
 DELPHI IMM GmbH  
 Deutsches Bergbau-Museum  
 EFTAS Fernerkundung Technologietransfer GmbH  
 ESG Elektroniksystem- und Logistik-GmbH  
 ESRI Geoinformatik GmbH  
 EUROPEAN SPACE IMAGING  
 Eurosense GmbH  
 fokus GmbH  
 fpi Fuchs Ingenieure GmbH  
 g.on experience gmbh  
 GAF Gesellschaft f. Angewandte Fernerkundung mbH  
 GeoCad GmbH  
 GeoCart Herten GmbH  
 GeoContent GmbH  
 Geoinform. & Photogr. Engin. Dr. Kruck & Co. GbR  
 geoplana Ingenieurgesellschaft mbH  
 GEOSYSTEMS GmbH  
 GGS - Büro für Geotechnik, Geoinformatik, Service  
 Hansa Luftbild AG  
 IGI - Ingenieur-Gesellschaft für Interfaces mbH  
 ILV Ing.-büro für Luftbildausw. und Vermessung  
 Imetric 3D GmbH  
 INVERS - Industrievermessung & Systeme  
 J. Linsinger ZT-GmbH  
 Jena-Optronik GmbH  
 KAZ Bildmess GmbH  
 Leica Geosystems GmbH  
 Luftbild Brandenburg GmbH Planer + Ingenieure  
 Luftbilddatenbank-Würzburg  
 Messbildstelle GmbH  
 Microsoft Photogrammetry  
 MILAN Geoservice GmbH  
 PHOENICS GmbH  
 PMS - Photo Mess Systeme AG  
 RWE Power AG, Geobasisdaten/Photogrammetrie  
 technet GmbH  
 TERRA-Bildmessflug GmbH & Co.  
 TerraVista Umweltdaten GmbH  
 TRIGIS Vermessung + Geoinformatik GmbH  
 Trimble Germany GmbH  
 trimetric 3D Service GmbH, Garbsen  
 Verlaggruppe Hüthig Jehle Rehm GmbH  
 Z/I Imaging Ltd.

### Behörden

Amt für Geoinformationswesen der Bundeswehr  
 Bayerische Landesanstalt für Wald und Forstwirtschaft  
 Bundesamt für Kartographie und Geodäsie  
 Bundesmin. für Ernäh., Landw. u. Verbraucherschutz  
 DB Netz AG  
 Hess. LA für Bodenmanagement und Geoinformation  
 Innenministerium NRW, Gruppe Vermessungswesen  
 Inst. für Umwelt- und Zukunftsforschung  
 LA für Geoinformation u. Landentw., Baden-Württem.  
 LA für Vermessung und Geoinformation, Bayern  
 LB Geoinformation und Vermessung, Hamburg  
 LB f. Küstenschutz, Nationalpark u. Meeresschutz, SH  
 Landesvermessung und Geobasisinformation Nieders.  
 Märkischer Kreis, Vermessungs- und Katasteramt  
 Regierungsprä. Tübingen, Abt. 8 Forstdirektion  
 Regionalverband Ruhr  
 Staatsbetrieb Sachsenforst Pirna  
 Stadt Bocholt, Fachbereich 31  
 Stadt Düsseldorf, Vermessungs- und Katasteramt  
 Stadt Köln, Amt für Liegensch., Verm. und Kataster  
 Stadt Wuppertal, Verm., Katasteramt und Geodaten  
 Thüringer LA für Vermessung und Geoinformation

### Hochschulen

BTU Cottbus, Lehrstuhl für Vermessungskunde  
 FH Frankfurt a.M., FB 1, Studiengang Geoinformation  
 FH Mainz, Inst. f. Raumbez. Inform.- und Messtechn.  
 FH Oldenburg, Inst. für Angew. Photogr. und Geoinf.  
 HCU HafenCity Universität Hamburg, Geomatik  
 HfT Stuttgart, Vermessung und Geoinformatik  
 HS Bochum, FB Vermessung und Geoinformatik  
 FS Karlsruhe, FB Geoinformationswesen  
 HTW Dresden, FB Vermessungswesen/Kartographie  
 Ruhr-Uni Bochum, Geographisches Institut  
 RWTH Aachen, Geodätisches Institut  
 TU Bergak. Freiberg, Inst. f. Markscheid. u. Geodäsie  
 TU Bergak. Freiberg, Inst. für Geologie, RSG  
 TU Berlin, Computer Vision & Remote Sensing  
 TU Braunschweig, Inst. für Geodäsie und Photogr.  
 TU Clausthal, Inst. für Geotechnik und Markscheidew.  
 TU Darmstadt, Inst. für Photogrammetrie und Kartogr.  
 TU Dresden, Inst. für Photogrammetrie und Fernerk.  
 TU München, FG Photogrammetrie und Fernerk.  
 TU Wien, Inst. für Photogrammetrie und Fernerk.  
 Uni Bonn, Inst. für Photogrammetrie  
 Uni Göttingen, Inst. für Waldinv. und Waldwachstum  
 Uni Hannover, Inst. für Kartogr. und Geoinformatik  
 Uni Hannover, Inst. für Photogrammetrie und GeoInf.  
 Uni Heidelberg, IWR Interdis. Zentr. f. Wiss. Rechnen  
 Uni Karlsruhe, Inst. für Photogrammetrie und Fernerk.  
 Uni Kassel, FB Ökologische Agrarwissenschaften  
 Uni Kiel, Geographisches Institut  
 Uni Stuttgart, Inst. für Photogrammetrie  
 Uni Würzburg, Geographisches Institut  
 Uni zu Köln, Geographisches Institut



## Rheinische Friedrich-Wilhelms-Universität Bonn

### Landwirtschaftliche Fakultät

An der Rheinischen Friedrich-Wilhelms-Universität ist an der Landwirtschaftlichen Fakultät im Institut für Geodäsie und Geoinformation (IGG) zum 01.10.2011 eine

#### **Professur für Photogrammetrie (W3)** (Nachfolge Prof. Dr.-Ing. W. Förstner)

zu besetzen. Wir suchen eine/einen im Bereich der photogrammetrischen Bildanalyse international methodisch ausgewiesene/n Wissenschaftlerin/Wissenschaftler, die/der in der Lösung von komplexen Problemen in zukunftsweisenden klassischen und nichtklassischen Anwendungsfeldern der Photogrammetrie eine Herausforderung sieht.

Bewerberinnen/Bewerber sollten über Erfahrungen auf mindestens einem der folgenden Gebiete verfügen:

- Methodenentwicklung in der Bildmessung und des maschinellen Sehens
- Bildverarbeitung, Mustererkennung, Bildinterpretation und Bildfolgenanalyse
- Anwendungen der Photogrammetrie (3D-Stadtmodelle, Agrar- und Geowissenschaften, Robotik)

Als Institut der Landwirtschaftlichen Fakultät wirkt das IGG an dem DFG - Graduiertenkolleg "Precision Farming" und dem BMBF-Forschungsverbund "Cropsense" mit und forciert den Einsatz bildgebender Verfahren in den Agrarwissenschaften. Im Bereich der Methodenentwicklung sucht und verstärkt das IGG die Zusammenarbeit mit der Bonner Informatik (Computer Vision, Computergrafik, Robotik, angewandte Informatik) und Mathematik (Hausdorff Centre for Mathematics). Es beteiligt sich darüber hinaus am Geoverbund ABC/J der Aachen-Bonn-Köln-Jülicher Region und am Zentrum für Fernerkundung der Landoberfläche (ZFL). Von der Bewerberin/dem Bewerber erwarten wir eine aktive Mitarbeit bei der Umsetzung dieses Zukunftskonzepts.

In der Lehre ist das Fach Photogrammetrie im Studiengang Geodäsie und Geoinformation (Bachelor und Master) sowie in Nebenfächern zu vertreten.

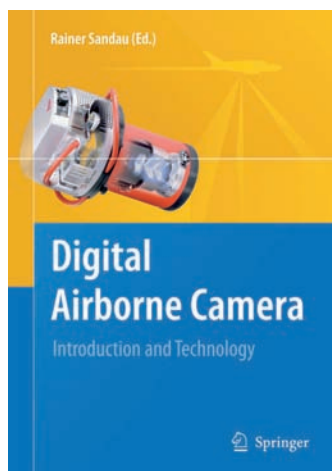
Die Bewerberinnen/Bewerber müssen die allgemeinen Einstellungsvoraussetzungen nach § 36 des Hochschulgesetzes für das Land Nordrhein-Westfalen erfüllen.

Frauen werden nach Maßgabe des Landesgleichstellungsgesetzes bei gleicher Qualifikation bevorzugt berücksichtigt.

Schwerbehinderte Bewerberinnen/Bewerber werden bei gleicher Eignung bevorzugt eingestellt.

Aussagekräftige Unterlagen mit Darstellung der bisherigen Lehr- und Forschungsleistungen sowie fünf Sonderdrucke der wichtigsten Publikationen der letzten Jahre werden bis zum **21.06.2010** erbeten an den

Dekan der Landwirtschaftlichen Fakultät  
Rheinische Friedrich-Wilhelms-Universität  
Meckenheimer Allee 174  
53115 Bonn



R. Sandau, DLR, Berlin, Germany (Ed.)

## Digital Airborne Camera

### Introduction and Technology

Digital airborne cameras are now penetrating the fields of photogrammetry and remote sensing. Due to the last decade's results in research and development in the fields of for instance detector technology, computing power, memory capacity position and orientation measurement it is now possible to generate with this new generation of airborne cameras different sets of geometric and spectral data with high geometric and radiometric resolutions within a single flight. This is a decisive advantage as compared to film based airborne cameras. The linear characteristic of the opto-electronic converters is the basis for the transition from an imaging camera to an images generating measuring instrument. Because of the direct digital processing chain from the airborne camera to the data products there is no need for the processes of chemical film development and digitising the film information. Failure sources as well as investments and staff costs are avoided. But the effective use of this new technology requires the knowledge of the features of the image and information generation, its possibilities and its restrictions. This book describes all components of a digital airborne camera from the object to be imaged to the mass memory device. So... *more on <http://springer.com/978-1-4020-8877-3>*

2010. XII, 343 p. 215 illus. Hardcover

- ▶ **129,95 €**
- ▶ **\$169.00**
- ▶ **SFr. 202.00**
- ▶ **£117.00**

ISBN 978-1-4020-8877-3

- ▶ Provides the information of this new technology to a wide audience
- ▶ The first title dedicated to digital airborne cameras

## Order Now!

Yes, please send me \_\_\_\_\_ copies

"Digital Airborne Camera"  
ISBN 978-1-4020-8877-3

Methods of Payment     Check/Money Order enclosed     AmEx     MasterCard     VISA

Card No.

Exp. Date

Please send orders to:

Outside the Americas:

Springer  
Order Department  
PO Box 2485  
Secaucus, NJ 07096-2485  
USA

Springer  
Customer Service Center GmbH  
Haberstrasse 7  
69126 Heidelberg  
Germany

- ▶ **Call toll-free** 1-800-SPRINGER  
8:30 am – 5:30 pm ET
- ▶ **Fax your order to** (201) 348-4505
- ▶ **Web** [springer.com](http://springer.com)
- ▶ **Email** [orders-ny@springer.com](mailto:orders-ny@springer.com)

- ▶ **Call:** + 49 (0) 6221-345-4301
- ▶ **Fax:** +49 (0) 6221-345-4229
- ▶ **Web:** [springer.com](http://springer.com)
- ▶ **Email:** [orders-hd-individuals@springer.com](mailto:orders-hd-individuals@springer.com)

Name
Address
Street Address
(Sorry, we cannot deliver to P.O. boxes)
City / State / ZIP-Code
Country
Telephone / Email
Date ✕
Signature ✕

CA, MA, NJ, NY, and PA residents, please add sales tax. Canadian residents, please add 5% GST. Please add \$5.00 for shipping one book and \$1.00 for each additional book. Outside the US and Canada add \$10.00 for first book, \$5.00 for each additional book. All orders are processed upon receipt. If an order cannot be fulfilled within 90 days, payment will be refunded upon request. Prices are payable in US currency or its equivalent. Remember, your 30-day return privilege is always guaranteed. Pre-publication pricing: Unless otherwise stated, pre-pub prices are valid through the end of the third month following publication, and therefore are subject to change.

All € and £ prices are net prices subject to local VAT, e.g. in Germany 7% VAT for books and 19% VAT for electronic products. Pre-publication pricing: Unless otherwise stated, pre-pub prices are valid through the end of the third month following publication, and therefore are subject to change. All prices exclusive of carriage charges. Prices and other details are subject to change without notice. All errors and omissions excepted. Please consult [springer.com](http://springer.com) for information on postage.